# Block Copolymer-Based Ion Gels as Solid Polymer Electrolytes

A DISSERTATION
SUBMITTED TO THE FACULTY OF THE GRADUATE SCHOOL
OF THE UNIVERSITY OF MINNESOTA
BY

Sipei Zhang

IN PARTIAL FULFILLMENT OF THE REQUIREMENTS
FOR THE DEGREE OF
DOCTOR OF PHILOSOPHY

Advisers: C. Daniel Frisbie and Timothy P. Lodge

October 2012

## Acknowledgements

First and foremost, I would like to express my greatest gratitude to my advisors, Prof. Dan Frisbie and Prof. Tim Lodge, for their invaluable guidance and support throughout my PhD career. They both have been great sources of ideas and knowledge during the past several years and taught me how to become a better materials scientist. Dan's enthusiasms about my thesis project, and research in general, have influenced my research attitude profoundly. His encouragement has always been a solid support to help me look forward. Tim's patience and thoroughness in conducting research have set a benchmark that I constantly strive to reach. Despite his extremely busy schedule, I can always rely on him for a prompt response to any issue. This thesis would not be possible without them.

I am also indebted to a lot of people who have helped me throughout my thesis research. In particular, I thank Prof. Philippe Buhlmann for allowing me to use the impedance analyzer in his group; Dr. Zhifeng Bai and Dr. Takeshi Ueki for teaching me polymer synthesis; Dr. David Giles, Dr. Hyunwoo Kim, Dr. Jiyoul Lee, and Yu Lei for getting me started on rheological and impedance measurements; Keun Hyung Lee and Yuanyan Gu for collaborations on multiple projects; Jingru Sun for conducting measurements of ionic conductivity on polymer solutions. Many other people have provided help through instrument training, measurement assistance, helpful discussions, and so on: Salil Bapat, Dr. Bryan Boudouris, Dr. Seongho Choi, Abel Demissie, Chris Frethem, Mingjing Ha, Prof. Marc Hillmyer, Prof. Russell Holmes, Matt Irwin, Dr. Brad Jones, Dr. Vivek Kalihari, Dr. Toshinori Kato, Dr. Hau-Nan Lee, Dr. Chun Liu, Dr. Joe

Lott, Jie Lu, Yuanchi Ma, Luca Martinetti, John McAllister, Lucas McIntosh, Dr. Luciana Meli, Dr. Michelle Mok, Dr. Adam Moughton, Bryan Paulsen, Nichalos Petcovich, Dr. Louis Pitet, Morgan Schulze, Dr. Myungeun Seo, Dr. Peter Simone, Josh Speros, Prof. Andreas Stein, Dr. Derek Stevens, Dr. Rajiv Taribagil, Dr. Shun Wang, Dr. Yu Xia, Wei Xie, Ligeng Yin, and Can Zhou. I am grateful to all Frisbie and Lodge group members, both former and present, for being wonderful learning and discussion sources and maintaining various instruments.

Last but not least, I owe gratitude to my parents, for their love, care, encouragement, support, and sacrifice, without which I would never be who I am. I would never forget that they have allowed me to choose my own desired path in life, which is not very common in the environment I grew up. I thank Yichen for being there whenever needed, and my friends for making life at Minnesota colorful and enjoyable.

*To Mom, Dad, and Yichen*

## Abstract

Block copolymer-based (BCP) ion gels are a class of interesting solid polymer electrolytes (SPEs) in electrochemical applications. This thesis aims to systematically study the mechanical and electrical properties of BCP-based ion gels formed by the self-assembly of ABA triblock copolymers in an ionic liquid, and find ways to enhance the properties of the gels, in order to formulate optimal designs in terms of the triblock for applications to electrochemical devices. Two particular target applications are organic transistors and electrochemical capacitors, due to the very large specific capacitance (on the order of $\mu F/cm^2$) of these electrolytes and therefore low voltage operation and potentially desirable energy storage.

To study the effect of the BCP on the properties of ion gels, BCPs with different mid-blocks and end-block lengths were prepared, and the viscoelastic and electrical properties of the ion gels were investigated over large composition and temperature ranges. The gels were formed by the self-assembly of poly(styrene-*b*-methyl methacrylate-*b*-styrene) (SMS) and poly(styrene-*b*-ethylene oxide-*b*-styrene) (SOS) in the ionic liquid 1-ethyl-3-methylimidazolium bis(trifluoromethylsulfonyl)amide ([EMI][TFSA]). The end-blocks associate into cross-links, while the midblocks are well-solvated by this ionic liquid. In terms of viscoelastic properties, it was found that the plateau modulus of the gels depends primarily on concentration and the molecular weight of the mid-block, while high temperature behavior is controlled by the length of the end-blocks. A body-centered cubic (BCC) structure was observed at elevated temperatures only for gels with short end-

blocks due to end-block pull-out from the cross-linking cores, while the relaxation of the end-blocks are within the cores for gels with long end-blocks. In terms of electrical properties, the double-layer capacitance of the gels was found to be fairly insensitive to polymer content and identity, whereas the ionic conductivity varies significantly especially at polymer concentrations of more than 20 wt%. It was also found that the presence of the end-blocks primarily obstructs the ion paths without much effect on ion number density. In terms of materials design, a flexible, low molecular weight mid-block is desirable. Generally, there is a trade-off between ionic conductivity and shear modulus for this type of gels.

To enhance the mechanical properties of the gels, a novel ion gel based on poly[(styrene-*r*-vinylbenzyl azide)-*b*-ethylene oxide-*b*-(styrene-*r*-vinylbenzyl azide)] (SOS-$N_3$) with chemically cross-linkable end-blocks was prepared. The gel with 10 wt% polymer goes through two transitions as temperature increases: solid (physically cross-linked network) $\rightarrow$ liquid $\rightarrow$ solid (chemically cross-linked network). The modulus and ionic conductivity was found to remain fairly constant after chemical cross-linking, while the toughness is more than 8 times higher. This demonstrates a promising approach to improve the mechanical properties of a moderately dilute gel without interfering with the high ionic conductivity.

Overall, BCP-based ion gels are promising SPEs for transistor and capacitor applications. Through judicious selection of the triblocks, the properties of the gels can be tuned to fulfill different requirements.

# Table of Contents

## List of Tables

## List of Figures

# Chapter 1

# Background

## 1.1 Introduction

This chapter is an overview of previously published work motivating the research described in later chapters of the thesis. Section 1.2 provides an introduction to ionic liquids with an emphasis on their electrochemical properties. Electrochemical stability, ionic conductivity and differential capacitance are discussed, which are crucial properties to consider when selecting ionic liquids for electrochemical applications. Section 1.3 reviews work on ionic liquids gelled with macromolecules, with a particular focus on ion transport and mechanical properties. Section 1.4 describes solid polymer electrolytes (SPEs), with a focus on their response to AC electric fields in the context of applications to capacitors and transistors. Typical classes of SPEs that have been utilized in capacitors and transistors, including PEO/$LiClO_4$, ion gels, and polyelectrolytes are compared and contrasted in terms of their dissipation factor and ionic conductivity. Section 1.5 discusses the motivation of this thesis and provides an outline of what follows in subsequent chapters.

## 1.2 Ionic Liquids

Ionic liquids, also known as low temperature molten salts, are generally defined as ionic compounds with melting points below 100 °C.[1] In fact, most ionic liquids in the literature are also liquid near room temperature. Although it may seem that a matter of

degrees is the only difference between ionic liquids and high temperature molten salts, *e.g.* NaCl, the practical applications enabled by this feature sufficiently justify a separately identified class of material.

The first report of ionic liquid dates back to the preparation of ethylammonium nitrate, $[EtNH_3][NO_3]$, in 1914.[2] In the middle of the 20th century (1948), the first ionic liquid based on chloroaluminate anions was patented.[3–5] However, not until late 1970s did the modern era for ionic liquids truly begin. One example of the pioneering work around this time was the discovery of the 1-butylpyridinium chloride and aluminum chloride mixture.[6] In the following decade, much attention was directed to what is now termed the haloaluminate ionic liquids. Like the work mentioned above, these systems are created by mixing aluminum halides (usually chloride) with the corresponding halide salt of an organic cation, the most common of which are pyridinium and imidazolium. Because these ionic liquid mixtures preclude the solvation and solvolysis phenomena that often corrupt metal halide complexes in molecular liquids, they have been utilized as solvents in quite a few studies of solution electrochemistry, electrodeposition, as well as electrolytes in batteries.[7]

One principal drawback of the haloaluminate ionic liquids is that they are reactive with water, resulting in corrosive products of HX (X = Cl or Br). Consequently, they must be handled under essentially anhydrous conditions, which complicates processing and limits the potential applications of these species. In the early 1990s, the search began for water-stable anions as an alternative. Remarkable examples include tetrafluoroborate ($[BF_4]^-$),[8] hexafluorophosphate ($[PF_6]^-$),[9] and bis(trifluoromethylsulfonyl)amide ([TF-

SA]$^-$).[10] These non-haloaluminate ionic liquids will be the primary focus of discussion here.

As mentioned previously, ionic liquids distinguish themselves from high temperature molten salts by virtue of their low melting points. This is due to the their bulky and often asymmetric component ions, which result in increased ion-ion separation and decreased packing efficiency and order, thus leading to much lower melting points.[11] For instance, changing the $Cl^-$ anion of NaCl to $AlCl_4^-$ reduces the melting point from 801 °C to 185 °C. Examples of component ions employed in common ionic liquids are shown in Figure 1.1.

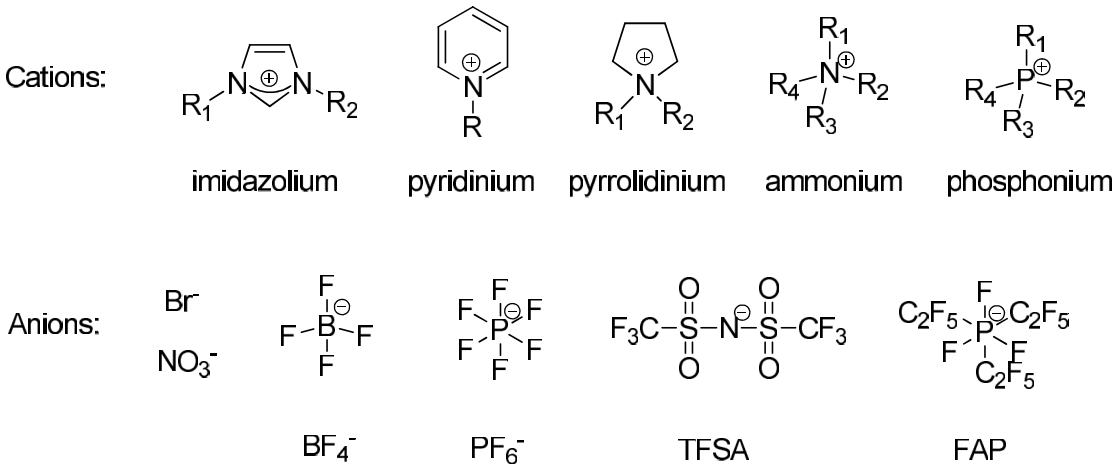


**Figure 1.1** Common cations and anions in ionic liquids.

The availability of numerous cations and anions provides virtually unlimited combinations to tune the properties of ionic liquids.[12] Therefore, a gold rush has been generated over the past decade, as researchers try to synthesize, understand and utilize this exciting class of material. Despite disadvantages such as relatively high cost and the barely addressed issue of toxicity, their negligible volatility, exceptional thermal,

chemical and electrochemical stability, combined with relatively high ionic conductivity[13–15] make ionic liquids promising candidates for a variety of applications, including solvents in organic synthesis and catalysis,[16] matrices for chemical separations,[17] and electrolytes in dye-sensitized solar cells,[18 – 20] electromechanical actuators,[21–23] lithium ion batteries,[24–26] electrochemical capacitors,[27–31] and organic thin film transistors.[32–39] Practically, applications of ionic liquids in synthesis and catalysis have been commercialized, while electrochemical devices employing ionic liquids are still mostly limited to the research community.

In the early days of ionic liquids, research on the application of haloaluminate ionic liquids as electrochemical solvents dominated. After the advent of non-haloaluminate ionic liquids, efforts were first devoted to applications other than electrochemistry, *e.g.* green solvents for synthesis and catalysis.[13] However, the situation was soon changed, as evidenced by the fast growing number of publications over the last decade on both electrochemical properties and applications of ionic liquids. Selected electrochemical properties of neat ionic liquids containing aprotic organic cations are described herein.

### 1.2.1 Electrochemical Stability

Electrochemical stability is a crucial property in selecting solvents for electrochemical applications. For non-haloaluminate ionic liquids, the electrochemical window, given as the voltage range in which the ionic liquid remains stable, is usually determined by the resistance of the cation to reduction and that of the anion to oxidation. Compared to water and organic solvents, the large electrochemical window of ionic

liquids, often in excess of 4 V, makes them attractive candidates for solvents in electrochemical studies.

The electrochemical windows of ionic liquids are most often measured by cyclic voltammetry.[11] In a three-electrode system, the potential of an inert reference electrode is consecutively scanned to positive and negative voltages until the current rises substantially due to either reduction or oxidation at the working electrodes. The potentials at arbitrarily chosen threshold current values give the reduction and oxidation potential limits. This fact, along with the choice of different reference and working electrodes as well as varying scanning rates,[40] induce uncertainties in the measurements and make comparisons between different ionic liquids more involved than one might expect.

The electrochemical windows of various ionic liquids have been reported.[14,40] Nevertheless, great care must be taken when comparing them, both because of the reasons mentioned above, and of the important issue of sample purity. Residual halide impurities left from synthesis steps shrink the electrochemical window inasmuch as they are less resistive to oxidation than the anions commonly used in ionic liquids. In the presence of oxygen, the reduction potential limit is reduced and the background current is higher than that measured in an inert atmosphere.[41] The impurity that affects the electrochemical window most significantly is water. Almost all ionic liquids are hygroscopic, *i.e.*, water-absorbing. Even hydrophobic ionic liquids may take up more than 1 wt% of water under atmospheric conditions.[11] In the case of water, both the cathodic and the anodic stability are diminished. For instance, the electrochemical

potential window of 1-butyl-3-methylimidazolium ([BMI]) [$BF_4$] in the dry state is 4.10 V, while that of the same ionic liquid with 3 wt% water is reduced to only 1.95 V.[42]

Despite the difficulty in the comparison of electrochemical windows among various ionic liquids, some general trends regarding different classes of ions exist. With the same anion, the electrochemical stability of the cations usually follows the order pyridinium < imidazolium < ammonium (see Figure 1.1 for their chemical structures).[14] For imidazolium-based ionic liquids, replacing the 2-position proton on the imidazolium ring by an alkyl substituent increases the cation stability,[10] likely due to the highest acidity and hence activity of the this proton on the ring.[43] The stability of the anions usually does not vary as much as that of the cations. For instance, the oxidation potentials of the [$BF_4$], [$PF_6$], [TFSA], and the more recently developed tris(perfluoroalkyl)trifluorophosphate ([FAP]) ions are all within a 0.5 V range in the dry state.[44,45]

### 1.2.2 Ionic Conductivity

The ionic conductivity of ionic liquids has been extensively studied due to interest in using them as electrolytes in electrochemical applications.[11] The vast majority of ionic conductivity data in the literature were collected employing AC impedance methods. Measurements generally involve a cell structure with ionic liquids sandwiched between two electrodes. The total impedance, which comes from both resistive and capacitive contributions, is recorded. In the frequency range where the resistive contribution dominates, the conductivity can be obtained from the resistance ($R_b$) using the following equation,

$$\sigma = \frac{l}{AR_b} \tag{1.1}$$

where $l$ is the distance between the two electrodes, and $A$ is the area of the electrodes.

It may seem that ionic liquids should have very high conductivities because they are composed almost entirely of ions, and the number density of ions can be as high as ca. $10^{21}$ cm$^{-3}$ at room temperature.[46] However, this overly simplified picture does not take into account every factor that contributes to conductivity, as evidenced by the following relations, the latter of which comes from the Einstein equation ($\mu = qD/(k_B T)$),

$$\sigma = nq\mu = \frac{nq^2 D}{k_B T} \tag{1.2}$$

where $n$ is the effective number density of carriers, $q$ is electric charge, $\mu$ is carrier mobility, $D$ is diffusion coefficient, $k_B$ is Boltzman's constant, and $T$ is absolute temperature. Clearly, conductivity depends both on the available number of charge carriers and their mobilities. It has been reported that the component ions in ionic liquids form ion pairs and/or ion aggregates and hence do not all participate in the conduction process.[47,48] Even if the majority of the ions are charge carriers, the relatively large sizes of the mobile ions reduce their mobility. Indeed, most ionic liquids possess moderately high conductivities, often below 20 mS/cm around room temperature. Comprehensive lists of conductivity data for ionic liquids can be found in several reviews.[11,14]

The ionic conductivity of ionic liquids is a sensitive function of temperature, following the Vogel-Tammann-Fulcher (VTF) equation,

$$\sigma = \sigma_0 \exp[-B/(T-T_0)] \tag{1.3}$$

where $\sigma_0$ is a prefactor, $B$ is a constant related to the entropic barrier of conduction, and $T_0$ is the Vogel temperature. As shown in the equation, $T_0$ is the temperature at which

conductivity goes to zero. The Vogel temperature is often some 50 degrees lower than the calorimetric glass transition temperature, $T_g$ (the temperature at which a solid-like material changes to a liquid-like material).[14] Sometimes, the fitting parameter $B$ is assumed to be weakly temperature dependent.[11] The temperature dependence of conductivity stems from the similar temperature dependence of the diffusion coefficient, which is a measure of the rate of ion movements in a medium, and is related to the ionic conductivity through eq (1.2).

Combining Equation (1.2) and the Stokes-Einstein relation,

$$D = \frac{k_B T}{a \pi r \eta} \tag{1.4}$$

where a is a constant, $r$ is the hydrodynamic radius, and $\eta$ is viscosity, it can be seen that conductivity and viscosity are inversely proportional to each other. Indeed, the conductivity and viscosity of ionic liquids were found to obey Walden's rule,

$$\Lambda\eta = \text{constant} \tag{1.5}$$

where $\Lambda$ is molar conductivity, given by

$$\Lambda = \sigma/c = \sigma M/\rho \tag{1.6}$$

where $c$ is molar concentration, $M$ is molar mass, and $\rho$ is density. The Walden product ($\Lambda\eta$) remains the same for a given ionic liquid at varied temperatures,[11] and depends on the type of ions for different ionic liquids.[27] Based on the Walden's rule, higher conductivities of ionic liquids can be obtained if viscosities are sufficiently reduced. One example is the recently developed fluorohydrogenated ionic liquids that contain the $[(HF)_{2.3}F]$ anions, with conductivities in excess of 100 mS/cm at ambient temperature.[49]

It is well documented that even small amounts of impurities, the most prevalent of which are halides and water, can greatly affect the conductivity of ionic liquids. Halides are usually introduced into ionic liquids during synthesis that involves anion metathesis reactions. As mentioned in the previous section, almost all ionic liquids, even those that are considered hydrophobic, absorb water when left in the atmosphere. It has been shown that the presence of chloride ion reduces conductivity through increasing the viscosity, while water has the opposite effect.[50] Therefore, care must be taken to eliminate these impurities to obtain reliable conductivity data.

Compared to the extensive research on DC conductivity discussed above, there appears to be relatively few reports on the frequency-dependent AC conductivities of ionic liquids. Note that the complex conductivity function is related to the complex impedance, complex permittivity, and complex electric modulus through the following equations

$$\sigma^*(\omega,T) = \frac{l}{Z^*(\omega,T)A} = i\omega\varepsilon_0\varepsilon^*(\omega,T) = \frac{i\omega\varepsilon_0}{M^*(\omega,T)} \tag{1.7}$$

where $\omega$ is the radial frequency, and $\varepsilon_0$ is vacuum permittivity. Therefore, these four parameters are physically equivalent quantities emphasizing different aspects.

Recently, Sangoro et al. reported the complex conductivities of a number of imidazolium-based ionic liquids as a function of frequency.[46,51–53] Data collected at different temperatures were shifted onto master curves that span over fourteen orders of magnitude in frequency. The plateau value on the master curve corresponds to the DC conductivity. The conductivity spectra at high frequencies (low temperatures) were analyzed using the Dyre theory developed for disordered solids, and charge transport was

attributed to the hopping of ions in a random, spatially varying potential. At lower frequencies (or higher temperatures), electrode polarization effects were observed. In this regime, ions migrate to the electrolyte/electrode interfaces and establish electrical double layers (EDLs). Here, the spectra depend on the geometry of the sample and the electrode material used, which renders the underlying physical mechanism more elusive. This will be discussed in more detail in the following section.

### 1.2.3 Differential Capacitance

The differential capacitance, $C$, of an EDL (Figure 1.2) for an ideally polarizable electrode (one where no electrode reactions can occur within a fairly wide electrode potential range and therefore behaves like a capacitor with only capacitive current flow upon a change of potential) at constant temperature $T$, pressure $p$, and chemical composition $\theta$, is defined as[54]

$$C = \left( \frac{\partial Q}{\partial V} \right)_{T,p,\theta} \tag{1.8}$$

where $Q$ is the charge density on the electrode and $V$ is the applied potential.

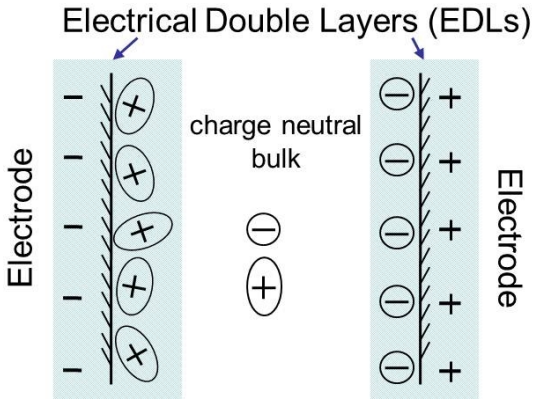


**Figure 1.2** Scheme of electrical double layers (EDLs) at electrode-ionic liquid interfaces.

Compared with the extensive studies on DC conductivity and electrochemical stability of ionic liquids, a lot fewer works have been published on their double-layer capacitance and little is known about the EDL structure at the ionic liquid/electrode interface. In addition, most of these studies focus on measurements of capacitance-potential curves at a fixed frequency. Even so, such experiments still provide insight into possible structures of the EDL and guidance in utilizing ionic liquids as electrolytes in electrochemical devices such as double-layer capacitors.

The pioneering work of Gale and Osteryoung on the mixture of $AlCl_3$ and 1-butyl-pyridinium chloride showed that the differential capacitance of an equimolar mixture is around 20 $\mu F/cm^2$ and is almost independent of the applied voltage.[55] Although this mixture belongs to the haloaluminate class of ionic liquid, it is historically important and will be the only one in this class mentioned here.

Practically no work in this area was published until Nanjundiah et al. reported the differential capacitance for four 1-ethyl-3-methylimidazolium ([EMI])-based ionic liquids. The measurements were conducted at a fixed frequency of 1 kHz at ambient temperature, in contact with carbon yarn, glassy carbon and mercury electrodes.[56] Differential capacitance of the ionic liquids were found to be in the range of 7.0 to 15.1 $\mu F/cm^2$, which is higher than non-aqueous solutions but lower than concentrated aqueous solutions.

Baldelli et al. reported differential capacitance for two ionic liquids with the [BMI] cation and $[BF_4]$ and $[N(CN)_2]$ anions in contact with platinum electrodes.[57,58] The shapes of the capacitance-voltage curves were found to be near parabolic in both cases, with

differential capacitance ranging from 12 to 17 μF/cm$^2$ for [BMI][$BF_4$] and from 36 to 48 μF/cm$^2$ for [BMI][$N(CN)_2$]. Assuming correspondence of the capacitance minimum with the potential of zero charge (PZC, the value of the electric potential of an electrode at which one of the charges defined is zero), multi- and single-layer structures at the electrode interface were assigned to the ionic liquids, respectively.

Recently, more reports on the differential capacitance-potential curves of ionic liquids appeared, the shapes of which generally include the near parabola mentioned above, albeit varied if considered in more detail.[59−65] Various simulations emphasizing different factors that might affect the EDL, such as ion specific adsorption, surface topography, electrode material, etc., have been performed for ionic liquids in an attempt to better model the data acquired on different electrodes.[66−73] However, to date, no single theory on the EDLs at ionic liquid/electrode interfaces exists that satisfactorily explains all the experimental data.

Among the published works on the differential capacitance of ionic liquids, only a few explicitly address the frequency dependence of capacitance. Ono et al. reported capacitance as a function of frequency for two ionic liquids composed of [EMI] cation and [TFSA] and [$(SO_2F)_2N$] anions.[34] The values of capacitance increase with decreasing frequency, reaching 11 and 5.4 F/cm$^2$ at 0.1 Hz in the former and latter case, respectively. Literature on the differential capacitance of ionic liquids only dabbles in the capacitance frequency relationship, or the so-called capacitance dispersion phenomenon, which is in fact quite universal among electrolytes. A common explanation involves specific ion adsorption, and possibly broad distributions of time constants associated with these

processes. Therefore, instead of having only one resistive and one capacitive contribution over the entire interface, microscopically the EDL can be broken down to very small areas, each having its own resistance and capacitance associated with a particular adsorption/desorption rate. On the macroscopic scale, this is usually manifested as different *C-f* relationships for different electrode materials and roughness, or equivalently, a difference in the slope of complex conductivity versus frequency plot, as mentioned in the last section. As far as data processing is concerned, researchers have either reported capacitance values at fixed frequencies, or modeled capacitance dispersion over a range of frequencies using a constant phase element (CPE).[74] The concept of CPE will be discussed in more detail in Section 1.4.

## 1.3 Ion Gels

From an applications standpoint, it is desirable to utilize ionic liquids with structural support. The mechanical integrity that ionic liquids lack can be supplied by mixing them with low molecular weight gelators[75−78] or more often macromolecules,[12,79] forming what is referred to as an ion gel. The term "gel" has been used somewhat loosely in the literature, and often a solid polymer solution is referred to as a gel. Here it is defined as a material that contains a network structure and lots of solvent. Gelation using low molecular weight gelators is often of a physical nature, *e.g.* intermolecular hydrogen bonding between the gelator and the ionic liquid,[75−77] colloidal dispersion of nanoparticles within the ionic liquid,[78] etc. The following discussions will be focused on ion gels formed with macromolecules.

In recent years, there has been a growing interest to study systems containing polymers and ionic liquids. Most studies in this area utilize ionic liquids as "designer solvents" inasmuch as their component ions can be designed to fulfill specific tasks.[79] Examples include reaction media for various kinds of polymerization,[80] solubilization of poorly soluble bio-polymers such as silk[81] and wool keratin,[82] and components in polymer electrolytes.[83] Polymeric ion gels are but one niche area among different possibilities involving the combination of polymers and ionic liquids.

Polymeric ion gels can be formed by either chemical or physical cross-linking. Chemical cross-linking can be realized through polymerization of vinyl monomers in the presence of a cross-linker,[84,85] or polyaddition reaction of (macro)monomers with multifunctional reactive groups.[86–89] In the former case, the Watanabe group conducted the pioneering work on ion gels prepared via in situ polymerization of methyl methacrylate (MMA) in the ionic liquid [EMI][TFSA] using ethylene glycol dimethacrylate as a cross-linker.[84] The ionic conductivity of the ion gels increases with decreasing mole fraction of MMA, reaching almost 6 mS/cm at the lowest polymer concentration (MMA:[EMI][TFSA] = 3:7 in mole) at ambient temperature, with a temperature dependence following the VTF equation, as described in Section 1.2.2. The authors also performed dynamic mechanical analysis on a gel with 80 mol% MMA. The storage modulus was found to be on the order of 0.1 GPa at ambient temperature. In the latter case, a representative work of the Rogers group reported gelation of 1-hexyl-3-methylimidazolium ([HMI]) [TFSA] by the cross-linking reaction of poly(ethylene glycol) (PEG) macromonomers with four-arm tetra-amine PEG cross-linkers.[86] The gels

showed conductivities on the order of $10^{-3}$ S/cm and physical properties comparable to PEG hydrogels (cross-linked in aqueous media). No mechanical properties were reported in this work. More recently, Matsumoto and Endo prepared epoxy-based ion gel films containing ammonium/imidazolium [TFSA], and measured ionic conductivity as well as tensile properties for different compositions at room temperature.[88,89] At the lowest polymer concentration explored (50%), it was found that the Young's modulus of the network was 45 MPa, and the ionic conductivity was appoximately $10^{-5}$ S/cm at room temperature.

In the case of physical cross-linking, block copolymers (BCPs) are especially versatile candidates due to the ease in tuning morphologies and properties through variations of block length and sequence.[90–93] BCPs are macromolecules containing two or more different repeat units that are covalently linked in contiguous sequences (blocks).[12] Using an ABA triblock copolymer with ionic liquid incompatible A blocks and an ionic liquid compatible B block, segregation on the A block length scale can be achieved,

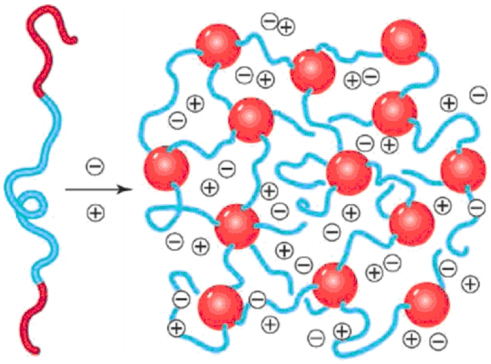

**Figure 1.3** An ABA triblock copolymer with soluble B block (blue) and insoluble A blocks (red) self-assembles in the presence of an ionic liquid (+ and − symbols) to form an ion gel.[12]

thereby forming ion gels with the addition of only a few percent polymer (Figure 1.3). The triblock copolymer can be viewed as a network swollen with ions, thus providing mechanical integrity without much loss of the ionic liquid's desirable electrical properties.

Our group was the first to report BCP-based ion gels. The gels were formed through the self-assembly of poly(styrene-*b*-ethylene oxide-*b*-styrene) (SOS) in the ionic liquid [BMI][$PF_6$].[90] The gel point was found to be only about 4 wt% SOS, lower than the cases of chemical cross-linking mentioned above. The ionic conductivity of gels with 5 and 10 wt% SOS was minimally reduced from the neat ionic liquid over the temperature range of 10 – 90 °C. The storage modulus for the gels is a few kilopascals. Interestingly, the relaxations of both the mid-blocks and end-blocks have been observed under shear, which would be difficult in BCP-based hydrogels due to solvent evaporation at high temperatures. More recently, thermoreversible ion gels have been developed. If the A blocks are designed to be soluble in the ionic liquid at elevated temperatures, a solid-liquid transition will be formed that enables liquid-state processing but solid-state use, hence eliminating the use of a cosolvent. Using poly(*N*-isopropyl acrylamide-*b*-ethylene oxide-*b*-*N*-isopropyl acrylamide) (NON) triblock copolymer and [EMI][TFSA] ionic liquid, a thermoreversible ion gel was prepared.[91] The ion gel with 10 wt% NON is highly conductive (ca. 45% decrease with respect to neat [EMI][TFSA]) and possesses sufficient mechanical strength (several kilopascals, linear region > 70% strain). Nevertheless, the sol-gel transition is around 17 °C, which is impractical for room

temperature usage. This can be overcome by further modifications of the A block to increase the transition temperature.[92]

**1.4 Solid Polymer Electrolytes**

According to IUPAC, a solid polymer electrolyte (SPE) is defined as an electrically conducting solution of a salt in a polymer. Here the term SPE refers to electrolytes that contain a polymeric structure. Since the first report of SPE in the early 1970's,[94] SPEs have found their applications in various electrochemical devices, such as lithium batteries,[95] fuel cells,[96] electrochemical sensors,[97] etc. The discussion here focuses on a niche application of utilizing SPEs as "dielectric" materials for capacitors and transistors. The SPE separates two electrodes in a capacitor, and a gate electrode and a semiconductor in a transistor. In the more complicated case of a transistor, the gate serves as a valve which controls the amount of current flow across the semiconductor through controlling the number of charge carriers induced by the gate dielectric (Figure 1.4). The gate dielectric needs to be electrically insulating, otherwise the valve (gate) will be

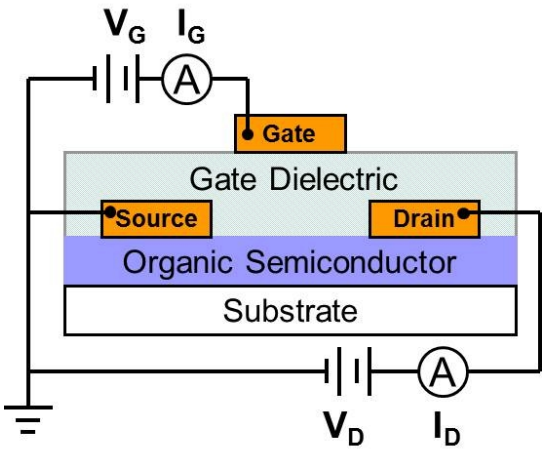


**Figure 1.4** Cross-sectional schematic of a top-gate, top-contact organic transistor.

damaged (shorted). The same applies to a capacitor, where the "dielectric" is used to store energy instead of dissipating it (leakage current through the device).

There are several property requirements that the electrolyte has to fulfill for the device to be practical. First, in order to induce large number of charge carriers at a given voltage/store more charge ($Q = CV$, $U = CV^2/2$), the capacitance ($C$) of the "dielectric" material needs to be large. SPEs are particularly advantageous in this regard due to their high sheet capacitance, typically in the range of 1−10 μF/cm$^2$ depending on the electrode material in contact with them. As a comparison, an 810 nm thick poly(methyl methacrylate) (PMMA) film only has a capacitance of 4 nF/cm$^2$. Additionally, compared to conventional ceramic or bulk polymer dielectrics, the specific capacitance for SPEs do not depend on sample thickness. This is because the capacitance of SPEs comes from the EDLs instead of from polarizing the dipoles in the bulk of the material, thus in the definition of $C = \varepsilon_0\varepsilon_r/d$, where $\varepsilon_r$ is dielectric constant, the $d$ value for SPEs is the thickness of the EDLs, which is only on the order of 1 nm.[98] Another key figure of merit is the amount of electrical energy dissipated versus the energy stored in a system during AC operation (*e.g.*, charging/discharging a capacitor), which can be quantified by the dissipation factor, or loss tangent. In order for the device to be energy efficient, the dissipation factor of the dielectric should be as small as possible. Additionally, the time it takes for the ions in the SPE to move to the electrolyte/electrode interface and establish stable EDLs can be the limiting factor for the switching speed of the device. In order to achieve a short response time, a high ionic conductivity is desirable. Last but not least, the SPE needs to possess sufficient mechanical strength to at least hold the electrode

material on top, or better yet, withstand forces coming from processing (*e.g.*, roll-to-roll printing) and maintain good shapes in more complicated structures (*e.g.*, stacked capacitors). Dissipation factor and ionic conductivity will be discussed in more detail in the following sections.

### 1.4.1 Equivalent Circuit under Small AC Electric Fields

AC impedance spectroscopy can be used to investigate the electrochemical characteristics of a wide variety of materials. Under an alternating voltage over a range of frequencies, the resulting alternating current of a sample can be measured. The impedance describes the sample's opposition to a sinusoidal alternating current, and is thus can be represented in a complex form

$$Z^* = Z' - iZ'' \tag{1.9}$$

where $Z'$ and $Z''$ represent the real and imaginary parts of the total impedance, respectively. As mentioned in Section 1.2.2, complex impedance can be equivalently expressed as complex conductivity, complex permittivity, and complex electric modulus. Graphically, complex impedance is often shown in the form of a Nyquist plot, where the magnitude of the imaginary part is plotted versus the real part on a linear scale.

A representative Nyquist plot for an ionic conductor sandwiched between a pair of blocking electrodes (no charge transfer across the electrolyte/electrode interfaces) is shown in Figure 1.5. At higher frequencies, the electric field probes the polarization of the dipoles within the material, and the equivalent circuit is comprised of a resistor representing the bulk resistance ($R_b$) in parallel with a capacitor that represents dipole polarization of the material ($C_b$). In terms of the Nyquist plot, $|Z''|$ versus $Z'$ takes on the

shape of a semicircle. At lower frequencies, the electric field probes the ionic motions, or the establishment of EDLs along the interfaces, and the equivalent circuit is composed of the same resistor in series with a capacitor representing the EDLs ($C_{dl}$). This is the frequency regime of interest for dielectric applications due to the very large $C_{dl}$ (1 – 10 μF/cm$^2$). In this case, the Nyquist plot would be a vertical line. However, as discussed in section 1.2.3, the behavior of electrolytes in contact with solid electrodes almost always deviates from that of an ideal capacitor, leading to the so-called capacitance dispersion phenomenon, which can usually be approximated using a CPE. In this case, the vertical line becomes tilted, as shown by the dashed line in Figure 1.5. This is because current leads voltage by a constant phase, whose angle is approximately fixed at a value less than that of an ideal capacitor (90°), hence the name CPE. Equivalently, if one uses complex conductivity ($\sigma^*$) to express the results, then an ideal *RC* series circuit gives a plot of

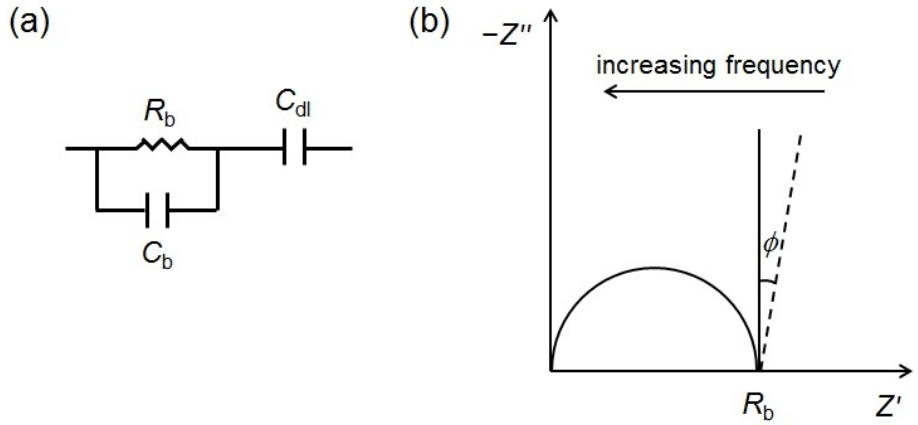


**Figure 1.5** (a) Equivalent circuit and (b) Nyquist plot of an ionic conductor sandwiched between two blocking electrodes. The dashed line shows the situation where a constant phase element (CPE) is present instead of an ideal double-layer capacitor.

log$\sigma^*$ versus log$f$ very similar to that of a Maxwell element in rheology. In the regime

where contribution from $C_{dl}$ dominates (lower frequencies), $\log\sigma'$ and $\log\sigma''$ have slopes of 2 and 1 versus $\log f$. In the region where resistive contribution dominates (higher frequencies), $\sigma'$ becomes flat and $\log\sigma''$ adopts a slope of −1 versus $\log f$. In real cases, the slopes are almost never the precise integers noted above. A specific example will be given in Chapter 4.

### 1.4.2 Dissipation Factor

As mentioned earlier, one of the key figures of merit for electrolytes, and dielectrics in general, is the loss tangent, or dissipation factor, defined as

$$\tan\phi \equiv \frac{\varepsilon''}{\varepsilon'} = \frac{Z'}{Z''} = \frac{\sigma'}{\sigma''} = \frac{M''}{M'} \tag{1.10}$$

where $\varepsilon'$, $\varepsilon''$, $Z'$, $Z''$, $\sigma'$, $\sigma''$, $M'$, and $M''$ are the real and imaginary parts of complex permittivity, impedance, conductivity, and electric modulus, respectively, and $\pi/2 - \phi$ is the phase angle between the resulting current and the applied voltage, which equals the angle between the measured values of $Z'$ and $Z''$ on the complex impedance plane (Figure 1.5).[99] In the ideal case that the equivalent circuit is a resistor and a capacitor in series,

$$\tan\phi = \frac{R}{1/(\omega C)} = \omega RC \tag{1.11}$$

Therefore, a smaller $RC$ time constant is not only desirable for faster switching speed, as eluted to previously (large $\sigma$), but reduces the dissipation factor as well. Unfortunately, usually the equivalent circuit is represented by RCPE in series, and therefore eq 1.11 is not an accurate prediction for the actual dissipation factor.[100] In terms of a Nyquist plot, the phase angle, or $\pi/2 - \phi$, between the measured values of $Z''$ and $Z'$ is less than 90°. In this case, tan $\phi$ exhibits values typically in the range of 10-15%. In this regard, electrolyte

"dielectrics" do not store energy as efficiently as more conventional dielectrics, and it becomes particularly problematic for devices operating at high frequencies. Table 1.1 provides a summary of specific capacitance and dissipation factors for several polymers and SPEs used as dielectrics in capacitors.[101] It is obvious that the dissipation factor values for SPEs exceed those for bulk polymers. However, it is also clear that the specific capacitances of SPEs are far larger, as mentioned earlier. The choice on which class of material to use thus depends on the most crucial requirement for a particular application.[102]

**Table 1.1** Summary of Dielectric Properties ($C$: specific capacitance, $d$: thickness, $\varepsilon_r$: dielectric constant, tan $\phi$: dissipation factor) for Typical Polymers and SPEs.[101]

| Dielectric | | ref | $C$ (μF/cm$^2$) | $d$ (nm) | $\varepsilon_r$ | tan $\phi$ |
|---|---|---|---|---|---|---|
| Polymers | PMMA | 103 | 0.0051 | 560 | 3.2 | |
| | | 110 | | | 3.0 | 0.055 (1 kHz) |
| | PS | 104 | 0.002 | | 2.6 | 0.002 (1 kHz) |
| | | 110 | | | 2.61 | 0.003 (1 kHz) |
| | PVA | 105 | | | | 0.005 (1 kHz) |
| | | 106 | 0.0178 | 500 | 10 | |
| SPEs | PEO/LiClO4 | 107 | 250 | $5 \times 10^4$–$5 \times 10^5$ | | 0.16 (10 mHz) |
| | | 108 | 5 | 400 | | |
| | Ion gels | 39 | 11 [a] | $1 \times 10^4$ | | 0.11 (1 kHz) |
| | | 120 | 12 [a] | $2 \times 10^3$ | | 0.09 (1 kHz) |
| | P(VPA-AA) | 109 | 10 [b] | 54 | | 0.23 (1 kHz) |

[a] capacitance value at 1 Hz, [b] capacitance value at 100 Hz, PS: poly(styrene), PVA: poly(vinyl alcohol), PEO: poly(ethylene oxide), P(VPA-AA): poly(vinyl phosphonic acid-*co*-acrylic acid).

### 1.4.3 Ionic Conductivity

One of the earliest and most extensively studied SPEs consists of poly(ethylene oxide) (PEO) doped with a lithium salt (*e.g.* $LiClO_4$). In these electrolytes, the oxygen lone pairs on the PEO chains coordinate with the $Li^+$ cation, resulting in coupled ionic motion with the polymer backbone. The reason that ions can move in the solid state stems from the flexibility of the PEO chain. Due to the low glass transition temperature ($T_g$) of PEO (ca. −60 °C),[110] ionic motion is boosted by the relaxation of PEO chains at temperatures far above $T_g$. Therefore, ion transport in these electrolytes depends greatly on both temperature and the $T_g$ of the polymer. Additionally, ionic conductivity in these electrolytes displays a maximum versus salt concentration. The strong Lewis acid-base interactions between $Li^+$ cations and PEO chains serves as transient cross-linking points, thereby increasing the $T_g$ of the system with the addition of lithium salt.[79] As a result, the ion mobility in these electrolytes peaks at a certain salt concentration, leading to decreased ionic conductivity upon further increases in salt concentration, even though the number density of ions keeps increasing.

Extensive modifications to the initial PEO/lithium salt system have been reported. Crosslinked polymer networks, random, block or graft copolymers containing short chains of PEO have been used to replace PEO homopolymer, in order to minimize crystallization and enhance ion transport.[111−114] Various inorganic and/or organic ad-

ditives have been utilized, including $Al_2O_3$, $TiO_2$, $SiO_2$, $LiAlO_2$, zeolites, and clay, to better understand and control mechanical properties and crystallinity of the electrolytes.[115–119] Despite these efforts, the ionic conductivity of these systems generally remains in the range of $10^{-4}$ to $10^{-5}$ S/cm at room temperature (Figure 1.6).

More recently, polymeric ion gels that exhibit higher ionic conductivity have been utilized as alternative gate dielectrics for faster switching organic transistors.[32,33,38,39] In contrast to PEO/lithium salt electrolytes, the ionic motions in polymeric ion gels can be decoupled from the segmental motion of the polymers, especially at low polymer concentrations or with flexible polymers, therefore resulting in relatively high ionic conductivity (ca. $10^{-3}$ S/cm at room temperature).[120] Notably, these electrolytes exhibit an order of magnitude increase in ionic conductivity over PEO/$LiClO_4$ based ones. Figure 1.6 compares the ionic conductivity range at room temperature for ion gel electrolytes with those of the other electrolytes described in this section. The ionic conductivity of a 0.01 molar NaCl aqueous solution is also shown as a reference. Figure 1.7 shows an optical image of an SOS ion gel with 10 wt% polymer whose properties will be discussed in Chapters 2 and 4. As seen in the image, the gel is a transparent and flexible.

Another interesting class of SPEs is polyelectrolytes, or polymers having backbones with pendant substituents containing ionic functionalities. The motivation for utilizing these materials lies in transistor applications, where ion penetration into the semiconductor can be avoided due to the long polymer chains. The ionic conductivity for conventional polyelectrolytes such as poly(acrylic acid) and sodium poly(styrene sulfonate) in the solid state depends greatly on humidity due to their water-soluble nature,

and is usually below $10^{-5}$ S/cm at room temperature.[95] More recently, poly(ionic liquid)s (PILs), or polyelectrolytes synthesized with ionic liquid monomers instead of solid salt monomers, have been developed as novel polyelectrolytes.[121,122] Because the counter-ions for PILs are often hydrophobic, most PILs do not dissolve in water. As with conventional polyelectrolytes, the ionic conductivity of PILs in the solid state depends on several factors such as chemical nature of the polymer backbone, the counter-ion, $T_g$, and

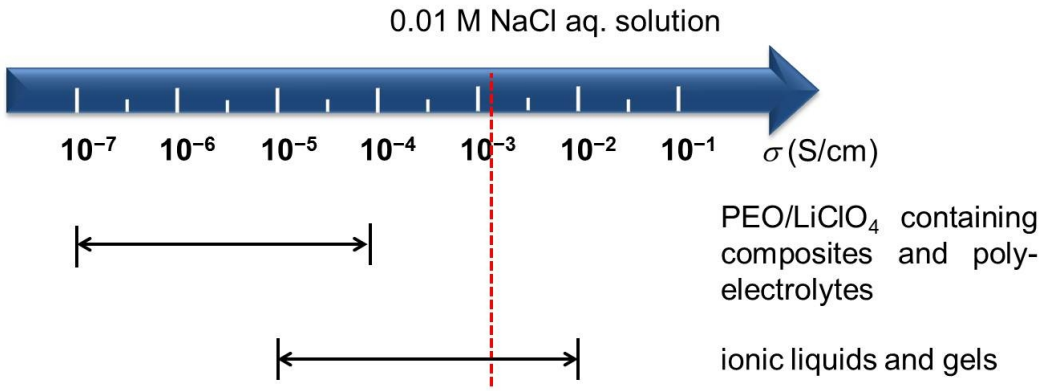


**Figure 1.6** Ionic conductivity ranges of ionic liquids and ion gels versus other SPEs discussed in this section.

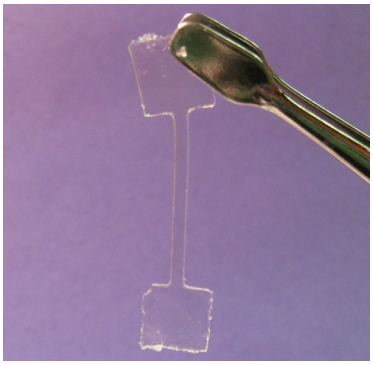

**Figure 1.7** Optical image of a solvent-cast SOS/[EMI][TFSA] ion gel bar with 10 wt% SOS. The bar was shaped with a dog-bone punch and peeled off from a petri dish. The length, width, and thickness of the gauge area are 40 mm, 2 mm, and 0.9 mm, respectively. Taken by Lucas McIntosh.

humidity. Generally, because the ions are incorporated in the polymer backbone, the lower the $T_g$, the higher the ionic conductivity. For instance, PILs with very low $T_g$'s of ca. −60 °C exhibit ionic conductivity above $10^{-4}$ S/cm at room temperature.[122] Another trend is that PILs with polyanions often show higher ionic conductivity than those with polycations. In most cases, the ionic conductivity of PILs is still too low for application in devices. Therefore, efforts have been devoted to blending PILs and ionic liquids to enhance ionic conductivity without losing the mechanical integrity provided by the PIL. The ionic conductivity of these tailored blends is usually in the range of $10^{-3}$ to $10^{-5}$ S/cm at room temperature. Additionally, random and block copolymers based on PILs have been synthesized to fine tune their properties.[123,124]

## 1.5 Thesis Overview

As can be seen from Section 1.3, the pioneering works describing both mechanical properties and ionic conductivity of BCP-based ion gels focus on the relatively dilute regime with the addition of 10 wt% or less polymer, and report ionic conductivity at two polymer concentrations at most. Therefore, the goal of this thesis project is to 1) study the mechanical and electrical properties of these electrolytes more systematically, and 2) try to enhance the properties of the gels, in order to formulate optimal designs in terms of the triblock for applications ranging from electrochemical capacitors to organic transistors. [EMI][TFSA] was chosen because it has been widely used in electrochemical applications due to its thermal stability, low viscosity (hence high ionic conductivity) and large electrochemical window.

Chapter 2 describes the viscoelastic properties of SOS/[EMI][TFSA] ion gels over wide temperature and composition ranges. Qualitatively different behaviors and structures are observed for the gels with S blocks having different lengths. This can be attributed to whether or not a significant amount of end-block chain exchange can happen at elevated temperatures, which depends on the energy barrier of chain pull-out. Time-temperature superposition (tTS) master curves are obtained. Characteristics such as the plateau modulus, longest relaxation time, cross-linking core radius, aggregation numbers, etc., are extracted.

Chapter 3 discusses the same properties of a poly(styrene-*b*-methyl methacrylate-*b*-styrene) (SMS)/[EMI][TFSA] ion gel. A notable feature that is discussed in detail is that in the event when end-block pull-out is highly unlikely to happen, the relaxation of the end-blocks within the cores and of the cores moving within a disordered medium can be observed rheologically, which would be difficult in BCP-based hydrogels due to solvent evaporation at high temperatures. Also, despite the huge difference in $T_g$, the SMS gel and SOS gel having long S blocks exhibit qualitatively similar behaviors under shear, which re-emphasizes the important effect of end-block length on viscoelastic properties.

Chapter 4 reviews and compares the electrical properties of both SOS- and SMS-based ion gels. Key parameters such as ionic conductivity ($\sigma$), specific capacitance ($C$), and $RC$ time constant are extracted and discussed. It turns out that $C$ is fairly insensitive to the addition of polymer, whereas $\sigma$ is greatly affected by polymer concentration. One important conclusion in this chapter is that the presence of S insulating cores serves only as obstructions to the ion paths, and has a moderate effect on ionic conductivity.

Chapter 5 examines a route to enhance the mechanical properties of the ion gels. A novel ion gel composed of poly[(styrene-*r*-vinylbenzyl azide)-*b*-ethylene oxide-*b*-(styrene-*r*-vinylbenzyl azide)] (SOS-$N_3$)/[EMI][TFSA] is studied. The azide groups can be chemically cross-linked at elevated temperatures, thereby locking the PS blocks in the cores. As temperature increases, the gel with 10 wt% polymer goes through the following structural transitions: solid (physical network) $\rightarrow$ liquid $\rightarrow$ solid (chemically cross-linked network). This is the first time that both physical and chemical crosslinking have been realized on the same BCP-based ion gel. The mechanical properties and ionic conductivity of the gel are investigated before and after chemical crosslinking. The shear modulus and ionic conductivity with 10 wt% polymer remain the same, whereas the toughness is more than 8 times higher. This demonstrates that the simple act of chemically cross-linking the cores yields a much tougher gel without interfering with ion transport.

Chapter 6 summarizes the works presented, and provides recommendations for future research.

## 1.6 References

(1) Wilkes, J. S. *Green Chem.* **2002**, *4*, 73-80.

(2) Walden, P. *Bull. Sci. Acad. Imp. Sci. St. Petersb.* **1914**, 405-422.

(3) Hurley, F. H. US2446331, 1948.

(4) Wier, T. P., Jr.; Hurley, F. H. US2446349, 1948.

(5) Wier, T. P., Jr. US2446350, 1948.

(6) Gale, R. J.; Gilbert, B.; Osteryoung, R. A. *Inorg. Chem.* **1978**, *17*, 2728-2729.

(7) Hussey, C. L. *Pure Appl. Chem.* **1988**, *60*, 1763-1772.

(8) Wilkes, J. S.; Zaworotko, M. J. *J Chem. Soc.,Chem.Commun.* **1992**, 965-967.

(9) Fuller, J.; Carlin, R. T.; De Long, H. C.; Haworth, D. *J Chem. Soc. Chem.Commun.* **1994**, 299-300.

(10) Bonhote, P.; Dias, A.-P.; Papageorgiou, N.; Kalyanasundaram, K.; Graetzel, M. *Inorg. Chem.* **1996**, *35*, 1168-1178.

(11) Wasserscheid, P.; Welton, T. *Ionic Liquids in Synthesis*, 2nd ed.; Wiley-VCH, 2008.

(12) Lodge, T. P. *Science* **2008**, *321*, 50-51.

(13) Welton, T.; *Chem. Rev.* **1999**, *99*, 2071-2083.

(14) Galinski, M.; Lewandowski, A.; Stepniak, I. *Electrochim. Acta* **2006**, *51*, 5567-5580.

(15) MacFarlane, D. R.; Forsyth, M.; Howlett, P. C.; Pringle, J. M.; Sun, J.; Annat, G.; Neil, W.; Izgorodina, E. I. *Acc. Chem. Res.* **2007**, *40*, 1165-1173.

(16) Dyson, P. J.; Geldbach, T. J. *Electrochem. Soc. Interface* **2007**, *16*, 50-53.

(17) Pandey, S. *Anal. Chim. Acta* **2006**, *556*, 38-45.

(18) Gorlov, M.; Kloo, L. *Dalton Trans.* **2008**, 2655-2666.

(19) Zakeeruddin, S. M.; Graetzel, M. *Adv. Funct. Mater.* **2009**, *19*, 2187-2202.

(20) Papageorgiou, N.; Athanassov, Y.; Armand, M.; Bonhote, P.; Pettersson, H.; Azam,

A.; Grätzel, M. *J. Electrochem. Soc.* **1996**, *143*, 3099-3108.

(21) Lu, W.; Fadeev, A. G.; Qi, B.; Smela, E.; Mattes, B. R.; Ding, J.; Spinks, G. M.; Mazurkiewicz, J.; Zhou, D.; Wallace, G. G.; MacFarlane, D. R.; Forsyth, S. A.; Forsyth, M. *Science* **2002**, *297*, 983-987.

(22) J. Ding, D. Zhou, G. Spinks, G. Wallace, S. Forsyth, M. Forsyth, D. MacFarlane, *Chem. Mater.* **2003**, *15*, 2392.

(23) Zhou, D.; Spinks, G. M.; Wallace, G. G.; Tiyapiboonchaiya, C.; MacFarlane, D. R.; Forsyth, M.; Sun, J. *Electrochim. Acta* **2003**, *48*, 2355-2359.

(24) Lewandowski, A.; Swiderska-Mocek, A. *J. Power Sources* **2009**, *194*, 601-609.

(25) Ishikawa, M.; Sugimoto, T.; Kikuta, M.; Ishiko, E.; Kono, M. *J. Power Sources* **2006**, *162*, 658.

(26) Kim, G. T.; Jeong, S. S.; Joost, M.; Rocca, E.; Winter, M.; Passerini, S.; Balducci, A. *J. Power Sources* **2011**, *196*, 2187-2194.

(27) McEwen, Alan B.; Ngo, Elen L.; LeCompte, Karen; Goldman, Jay L. *J. Electrochem. Soc.* **1999**, *146*, 1687-1695.

(28) Sato, T.; Masuda, G.; Takagi, K. *Electrochim. Acta* **2004**, *49*, 3603-3611.

(29) Ue, M.; Takeda, M.; Toriumi, A.; Kominato, A.; Hagiwara, R.; Ito, Y. *J Electrochem. Soc.* **2003**, *150*, A499-A502.

(30) Katakabe, T.; Kaneko, T.; Watanabe, M.; Fukushima, T.; Aida, T. *J. Electrochem. Soc.* **2005**, *152*, A1913-A1916.

(31) Balducci, A.; Henderson, W. A.; Mastragostino, M.; Passerini, S.; Simon, P.; Soavi,

F. *Electrochim. Acta* **2005**, *50*, 2233-2237.

(32) Lee, J.; Panzer, M. J.; He, Y.; Lodge, T. P.; Frisbie, C. D. *J. Am. Chem. Soc.* **2007**, *129*, 4532-4533.

(33) Cho, J. H.; Lee, J.; Xia, Y.; Kim, B.; He, Y.; Renn, M. J.; Lodge, T. P.; Frisbie, C. D. *Nat. Mater.* **2008**, *7*, 900-906.

(34) Ono, S.; Seki, S.; Hirahara, R.; Tominari, Y.; Takeya, J. *Appl. Phys. Lett.* **2008**, *92*, 103313/1-103313/3.

(35) Yuan, H.; Shimotani, H.; Tsukazaki, A.; Ohtomo, A.; Kawasaki, M.; Iwasa, Y. *Adv. Funct. Mater.* **2009**, *19*, 1046-1053.

(36) Chen, F.; Qing, Q.; Xia, J.; Li, J.; Tao, N. *J. Am. Chem. Soc.* **2009**, *131*, 9908-9909.

(37) Ye, J. T.; Inoue, S.; Kobayashi, K.; Kasahara, Y.; Yuan, H. T.; Shimotani, H.; Iwasa, Y. *Nat. Mater.* **2010**, *9*, 125-128.

(38) Lee, S. W.; Lee, H. J.; Choi, J. H.; Koh, W. G.; Myoung, J. M.; Hur, J. H.; Park, J. J.; Cho, J. H.; Jeong, U. *Nano Lett.* **2010**, *10*, 347-351.

(39) Lee, K. H.; Kang, M. Sung; Zhang, S.; Gu, Y.; Lodge, T. P.; Frisbie, C. D. *Adv. Mater.* 2012, *24*, 4457-4462.

(40) Ohno, H. *Electrochemical Aspects of Ionic Liquids*; John Wiley & Sons, Inc., 2005.

(41) Randstroem, S.; Appetecchi, G. B.; Lagergren, C.; Moreno, A.; Passerini, S. *Electrochim. Acta* **2007**, *53*, 1837-1842.

(42) Schroder, U.; Wadhawan, J. D.; Compton, R. G.; Marken, F.; Suarez, P. A. Z.; Consorti, C. S.; de Souza, R. F.; Dupont, J. *New J. Chem.* **2000**, *24*, 1009-1015.

(43) Hermann, W.; *Angew. Chem.* **2008**, *47*, 654-670.

(44) Buzzeo, M. C; Evans, R. G; Compton, R. G. *Chem. Phys. Chem.* **2004**, *5*, 1106-1120.

(45) Ignat'ev, N. V.; Welz-Biermann, U.; Kucheryna, A.; Bissky, G.; Willner, H. *J. Fluorine Chem.* **2005**, *126*, 1150-1159.

(46) Sangoro, J. R.; Serghei, A.; Naumov, S.; Galvosas, P.; Karger, J.; Wespe, C.; Bordusa, F.; Kremer, F. *Phys. Rev. E* **2008**, *77*, 051202.

(47) Noda, A.; Hayamizu, K.; Watanabe, M. *J. Phys. Chem. B* **2001**, *105*, 4603-4610.

(48) Tokuda, H.; Tsuzuki, S.; Susan, M. A. B. H.; Hayamizu, K.; Watanabe, M. *J. Phys. Chem. B* **2006**, *110*, 19593-19600.

(49) Matsumoto, K.; Hagiwara, R.; Ito, Y. *Electrochem. Solid-State Lett.* **2004**, *7*, E41-E44.

(50) Seddon, K. R.; Stark, A.; Torres, M.-J. *Pure Appl. Chem.* **2000**, *72*, 2275-2287.

(51) Sangoro, J.; Iacob, C.; Serghei, A.; Naumov, S.; Galvosas, P.; Karger, J.; Wespe, C.; Bordusa, F.; Stoppa, A.; Hunger, J.; Buchner, R.; Kremer, F. *J. Chem. Phys.* **2008**, *128*, 214509/1-214509/5.

(52) Sangoro, J. R.; Iacob, C.; Serghei, A.; Friedrich, C.; Kremer, F. *Phys. Chem. Chem. Phys.* **2009**, *11*, 913-916.

(53) Sangoro, J. R.; Iacob, C.; Naumov, S.; Valiullin, R.; Rexhausen, H.; Hunger, J.; Buchner, R.; Strehmel, V.; Kaerger, J.; Kremer, F. *Soft Matter* **2011**, *7*, 1678-1681.

(54) Grahame, D. C. *Chem. Rev.* **1947**, *41*, 441-501.

(55) Gale, R. J.; Osteryoung, R. A. *Electrochim. Acta* **1980**, *25*, 1527-1529.

(56) Nanjundiah, C.; McDevitt, S. F.; Koch, V. R. *J. Electrochem. Soc.* **1997**, *144*, 3392-3397.

(57) Baldelli, S. *J. Phys. Chem. B* **2005**, *109*, 13049-13051.

(58) Aliaga, C.; Baldelli, S. *J. Phys. Chem. B* **2006**, *110*, 18481-18491.

(59) Alam, M. T.; Islam, M. M.; Okajima, T.; Ohsaka, T. *J. Phys. Chem. C* **2007**, *111*, 18326-18333.

(60) Lockett, V.; Sedev, R.; Ralston, J.; Horne, M.; Rodopoulos, T. *J. Phys. Chem. C* **2008**, *112*, 7486-7495.

(61) Alam, M. T.; Islam, M. M.; Okajima, T.; Ohsaka, T. *J. Phys. Chem. C* **2008**, *112*, 2601-2606.

(62) Alam, M. T.; Islam, M. M.; Okajima, T.; Ohsaka, T. *J. Phys. Chem. C* **2008**, *112*, 16600-16608.

(63) Silva, F.; Gomes, C.; Figueiredo, M.; Costa, R.; Martins, A.; Pereira, C. M. *J. Electroanal. Chem.* **2008**, *622*, 153-160.

(64) Costa, R.; Pereira, C. M.; Silva, F. *Phys. Chem. Chem. Phys.* **2010**, *12*, 11125-11132.

(65) Lockett, V.; Horne, M.; Sedev, R.; Rodopoulos, T.; Ralston, J. *Phys. Chem. Chem. Phys.* **2010**, *12*, 12499-12512.

(66) Lauw, Y.; Horne, M. D.; Rodopoulos, T.; Nelson, A.; Leermakers, F. A. M. *J. Phys. Chem. B* **2010**, *114*, 11149-11154.

(67) Georgi, N.; Kornyshev, A. A.; Fedorov, M. V. *J. Electroanal. Chem.* **2010**, *649*, 261-267.

(68) Loth, M. S.; Skinner, Brian; Shklovskii, B. I. *Phys. Rev. E* **2010**, *82*, 056102/1-056102/7.

(69) Bazant, M. Z.; Storey, B. D.; Kornyshev, A. A. *Physical Rev. Lett.* **2011**, *106*, 046102/1-046102/4.

(70) Jiang, D.; Meng, D.; Wu, J. *Chem. Phys. Lett.* **2011**, *504*, 153-158.

(71) Feng, G.; Huang, J.; Sumpter, B. G.; Meunier, V.; Qiao, R. *Phys. Chem. Chem. Phys.* **2011**, *13*, 14723-14734.

(72) Vatamanu, J.; Cao, L.-L.; Borodin, O.; Bedrov, D.; Smith, G. D. *J. Phys. Chem. Lett.* **2011**, *2*, 2267-2272.

(73) Si, X.; Li, S.; Wang, Y.; Ye, S.; Yan, T. *Chem. Phys. Chem.* **2012**, *13*, 1671-1676.

(74) Brug, G. J.; Van den Eeden, A. L. G.; Sluyters-Rehbach, M.; Sluyters, J. H. *J. Electroanal. Chem.* **1984**, *176*, 275-295.

(75) Kimizuka, N.; Nakashima, T. *Langmuir* **2001**, *17*, 6759-6761.

(76) Hanabusa, K.; Fukui, H.; Suzuki, M.; Shirai, H. Langmuir 2005, 21, 10383-10390.

(77) Mohmeyer, N.; Kuang, D.; Wang, P.; Schmidt, H.-W.; Zakeeruddin, S. M.; Graetzel, M. *J. Mater. Chem.* **2006**, *16*, 2978-2983.

(78) Ueno, K.; Hata, K.; Katakabe, T.; Kondoh, M.; Watanabe, M. *J. Phys. Chem. B* **2008**, *112*, 9013-9019.

(79) Ueki, T.; Watanabe, M. *Macromolecules* **2008**, *41*, 3739-3749.

(80) Winterton, N. *J. Mater. Chem.* **2006**, *16*, 4281-4293.

(81) Phillips, D. M.; Drummy, L. F.; Conrady, D. G.; Fox, D. M.; Naik, R. R.; Stone, M. O.; Trulove, P. C.; De Long, H. C.; Mantz, R. A. *J. Am. Chem. Soc.* **2004**, *126*, 14350-14351.

(82) Xie, H.; Zhang, S.; Li, S. *Green Chem.* **2006**, *8*, 630-633.

(83) Armand, M.; Endres, F.; MacFarlane, D. R.; Ohno, H.; Scrosati, B. *Nat. Mater.* **2009**, *8*, 621-629.

(84) Susan, M. A. B. H.; Kaneko, T.; Noda, A.; Watanabe, M. *J. Am. Chem. Soc.* **2005**, *127*, 4976-4983.

(85) Jana, S.; Parthiban, A.; Chai, C. L. L. *Chem. Commun.* **2010**, *46*, 1488-1490.

(86) Klingshirn, M. A.; Spear, S. K.; Subramanian, R.; Holbrey, J. D.; Huddleston, J. G.; Rogers, Robin, D. *Chem. Mater.* **2004**, *16*, 3091-3097.

(87) Neouze, M.-A.; Le Bideau, J.; Gaveau, P.; Bellayer, S.; Vioux, A. *Chem. Mater.* **2006**, *18*, 3931-3936.

(88) Matsumoto, K.; Endo, T. *Macromolecules* **2008**, *41*, 6981-6986.

(89) Matsumoto, K.; Endo, T. *Macromolecules* **2009**, *42*, 4580-4584.

(90) He, Y.; Boswell, P. G.; Buehlmann, P.; Lodge, T. P. *J. Phys. Chem. B* **2007**, *111*, 4645-4652.

(91) He, Y.; Lodge, T. P. *Chem. Commun.* **2007**, 2732-2734.

(92) He, Y.; Lodge, T. P. *Macromolecules* **2008**, *41*, 167-174.

(93) Noro, A.; Matsushita, Y.; Lodge, T. P. *Macromolecules* **2008**, *41*, 5839-5844.

(94) Fenton, D. E.; Parker, J. M.; Wright, P. V. *Polymer* **1973**, *14*, 589-589.

(95) Meyer, W. H. *Adv. Mater.* **1998**, *10*, 439-448.

(96) Smitha, B.; Sridhar, S.; Khan, A. A. *J. Membr. Sci.* **2005**, *259*, 10-26.

(97) Opekar, F.; Stulik, K. *Anal. Chim. Acta* **1999**, *385*, 151-162.

(98) Fedorov, M. V.; Kornyshev, A. A. *Electrochim. Acta* **2008**, *53*, 6835-6840.

(99) Daniel, V. V. *Dielectric Relaxation*; Academic Press: London and New York, 1965.

(100) Levie, R. D. *Electrochim. Acta* **1965**, *10*, 113-130.

(101) Kim, S. H.; Hong, K.; Xie, W.; Lee, K. H.; Zhang, S.; Lodge, T. P.; Frisbie, C. D. *Adv. Mater.*, accepted.

(102) Sarjeant, W. J.; Zirnheld, J.; MacDougall, F. W. *IEEE Trans. Plasma Sci.* **1998**, *26*, 1368-1392.

(103) Yan, H.; Chen, Z.; Zheng, Y.; Newman, C.; Quinn, J. R.; Dotz, F.; Kastler, M.; Facchetti, A. *Nature* **2009**, *457*, 679-686.

(104) Jackson, N. F. *Phys. Educ.* **1968**, *3*, 253-259.

(105) Singh, K. P.; Gupta, P. N. *Eur. Polym. J.* **1998**, *34*, 1023-1029.

(106) Parashkov, R.; Becker, E.; Ginev, G.; Riedl, T.; Johannes, H.-H.; Kowalsky, W. *J. Appl. Phys.* **2004**, *95*, 1594-1596.

(107) Liu, X.; Osaka, T. *J. Electrochem. Soc.* **1996**, *143*, 3982-3986.

(108) Panzer, M. J.; Newman, C. R.; Frisbie, C. D. *Appl. Phys. Lett.* **2005**, *86*, 103503/1-103503/3.

(109) Herlogsson, L.; Crispin, X.; Robinson, N. D.; Sandberg, M.; Hagel, O.-J.;

Gustafsson, G.; Berggren, M. *Adv. Mater.* **2007**, *19*, 97-101.

(110) Brandrup, J.; Immergut, E. H.; Grulke, E. A. *Polymer Handbook*, 4th ed.; Wiley-Interscience: New York, 1999.

(111) Kaskhedikar, N.; Burjanadze, M.; Karatas, Y.; Wiemhoefer, H.-D. *Solid State Ionics* **2006**, *177*, 3129-3134.

(112) Uno, T.; Kawaguchi, S.; Kubo, M.; Itoh, T. *J. Power Sources* **2008**, *178*, 716-722.

(113)Guilherme, L. A.; Borges, R. S.; Moraes, E. Mara S.; Silva, G. Goulart; Pimenta, M. A.; Marletta, A.; Silva, R. A. *Electrochim. Acta* **2007**, *53*, 1503-1511.

(114) Gavelin, P.; Jannasch, P.; Wesslen, B. *J. Polym. Sci., Part A: Polym. Chem.* **2001**, *39*, 2223-2232.

(115) Weston, J. E.; Steele, B. C. H. *Solid State Ionics* **1982**, *7*, 75-79.

(116) Adebahr, J.; Best, A. S.; Byrne, N.; Jacobsson, P.; MacFarlane, D. R.; Forsyth, M. *Phys. Chem. Chem. Phys.* **2003**, *5*, 720.

(117) Cheung, I. W.; Chin, K. B.; Greene, E. R.; Smart, M. C.; Abbrent, S.; Greenbaum, S. G.; Prakash, G. K. S.; Surampudi, S. *Electrochim. Acta* **2003**, *48*, 2149-2154.

(118) Scrosati, B.; Croce, F. *Polym. Adv. Technol.* **1993**, *4*, 198-204.

(119) Sandi, G.; Carrado, K. A.; Joachin, H.; Lu, W.; Prakash, J. *J. Power Sources* **2003**, *119-121*, 492-496.

(120) Lee, K. H.; Zhang, S.; Lodge, T. P.; Frisbie, C. D. *J. Phys. Chem. B* **2011**, *115*, 3315-3321.

(121) Lu, J.; Yan, F.; Texter, J. *Prog. Polym. Sci.* **2009**, *34*, 431-448.

(122) Mecerreyes, D. *Prog. Polym. Sci.* **2011**, *36*, 1629-1648.

(123) Vijayakrishna, K.; Jewrajka, S. K.; Ruiz, A.; Marcilla, R.; Pomposo, J. A.; Mecerreyes, D.; Taton, D.; Gnanou, Y. *Macromolecules* **2008**, *41*, 6299-6308.

(124) Chen, H.; Choi, J.-H.; Salas-de la Cruz, D.; Winey, K. I.; Elabd, Y. A. *Macromolecules* **2009**, *42*, 4809-4816.

# Chapter 2

# Viscoelastic Properties of Ion Gels with a Flexible Midblock*

## 2.1 Introduction

As discussed in Chapter 1, the pioneering works describing both mechanical properties and ionic conductivity of block copolymer-based ion gels focus on the relatively dilute regime with the addition of 10 wt% or less polymer, and more systematic studies on these versatile electrolytes are desirable. In this chapter, the viscoelastic properties of ion gels based on the self-assembly of a poly(styrene-*b*-ethylene oxide-*b*-styrene) (SOS) triblock copolymer in the ionic liquid 1-ethyl-3-methylimidazolium bis(trifluoromethylsulfonyl)amide ([EMI][TFSA]) were investigated in the ionic-liquid-rich composition regime over a wide temperature range. The poly(styrene) (PS) end-blocks associate into micelles, whereas the poly(ethylene oxide) (PEO) mid-blocks are well-solvated by [EMI][TFSA] and have the lowest glass transition temperature ($T_g \sim -60$ °C)[1] among all the polymers that are known to be compatible with [EMI][TFSA]. The midblock molecular weight of the triblock was kept the same, while two different end-block lengths were examined to demonstrate different relaxation processes in the gels. The overall goal is to understand the viscoelastic motions so as to provide insight into the rational design of these high performance microstructured electrolyte materials.

---

* Reproduced in part with permission from Zhang, S.; Lee, K. H.; Sun, J.; Frisbie, C. D.; Lodge, T. P. *Macromolecules* **2011**, *44*, 8981-8989. Copyright 2011 American Chemical Society.

## 2.2 Experimental

### 2.2.1 Polymer Synthesis and Characterization

All reagents were used as received unless otherwise noted. Styrene was passed through an activated alumina column prior to use. The SOS triblock copolymer was synthesized via reversible addition-fragmentation chain transfer polymerization (RAFT) from a poly(ethylene glycol) (PEG) precursor following a previously reported procedure (Figure 2.1).[2] The PEG precursor was purchased from Aldrich ($M_n$ = 35 kDa, $Đ$ = 1.04). The polymer was purified by precipitation of a $CH_2Cl_2$ solution in *n*-hexane, followed by drying in a vacuum oven overnight. The chain transfer agent (CTA), (*S*)-1-dococyl-(*S*′)-(α,α′-dimethyl-α″-acetic acid) trithiocarbonate, was synthesized by Yiyong He following a reported protocol.[3]

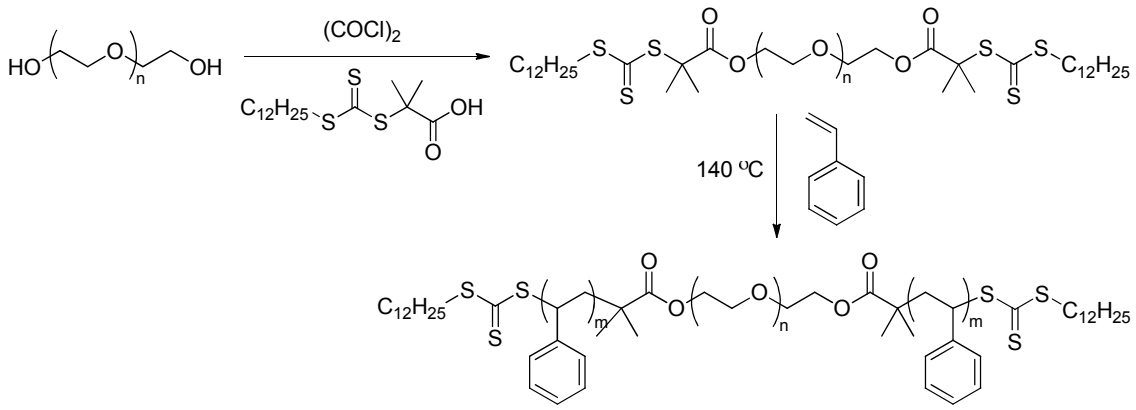


**Figure 2.1** Synthetic scheme of SOS triblock copolymer.

A telechelic PEO macroinitiator (CTA-PEO-CTA) was first prepared. CTA (1.06 g, $2.86 \times 10^{-3}$ mol) was dissolved in dry $CH_2Cl_2$ (5 mL) under argon atmosphere. The solution was bubbled with Ar for ca. 10 min, followed by the addition of excess oxalyl chloride (5 g, 0.039 mol). The mixture was stirred at room temperature until gas

evolution stopped (ca. 2 h). Excess reagents were removed under vacuum, and the product was redissolved in dry $CH_2Cl_2$ (ca. 60 mL), followed by the addition of PEO (9.8 g, $2.8 \times 10^{-4}$ mol). After bubbling with Ar for ca. 10 min, the reaction was allowed to proceed for 24 h at room temperature. The content was precipitated four times in *n*-hexane (ca. 1 L) and dried in a vacuum oven at ca. 60 °C for two days. The CTA-PEO-CTA macroinitiator was then used to grow the S endblocks. CTA-PEO-CTA (8.7 g) and styrene (13.6 mL) were mixed in a high-pressure glass reactor, bubbled with argon for 15 min, sealed, and placed in an oil bath at 140 °C. After 50 min, the reaction was stopped by quenching the content with an ice bath. Most of the unreacted styrene was removed under vacuum. The resulting mixture was dissolved in ca. 100 mL $CH_2Cl_2$ and precipitated three times in *n*-hexane, and the final product was dried in a vacuum oven at ca. 50 °C for two days. Each step of the synthesis was followed by $^1$H NMR spectroscopy (Figure 2.2). The PS blocks have an $M_n$ of 2.8 kDa as determined from peak integration of $^1$H NMR spectrum assuming the endblocks are symmetric, and a dispersity of 1.03 as determined by SEC (Figure 2.3). Another SOS polymer with longer PS endblocks ($M_{n,\,PS}$ = 6 kDa, $Đ$ = 1.05) synthesized and characterized using the same procedures was graciously provided by Yuanyan Gu. For convenience, these polymers are denoted as SOS(3-35-3) and SOS(6-35-6), respectively.

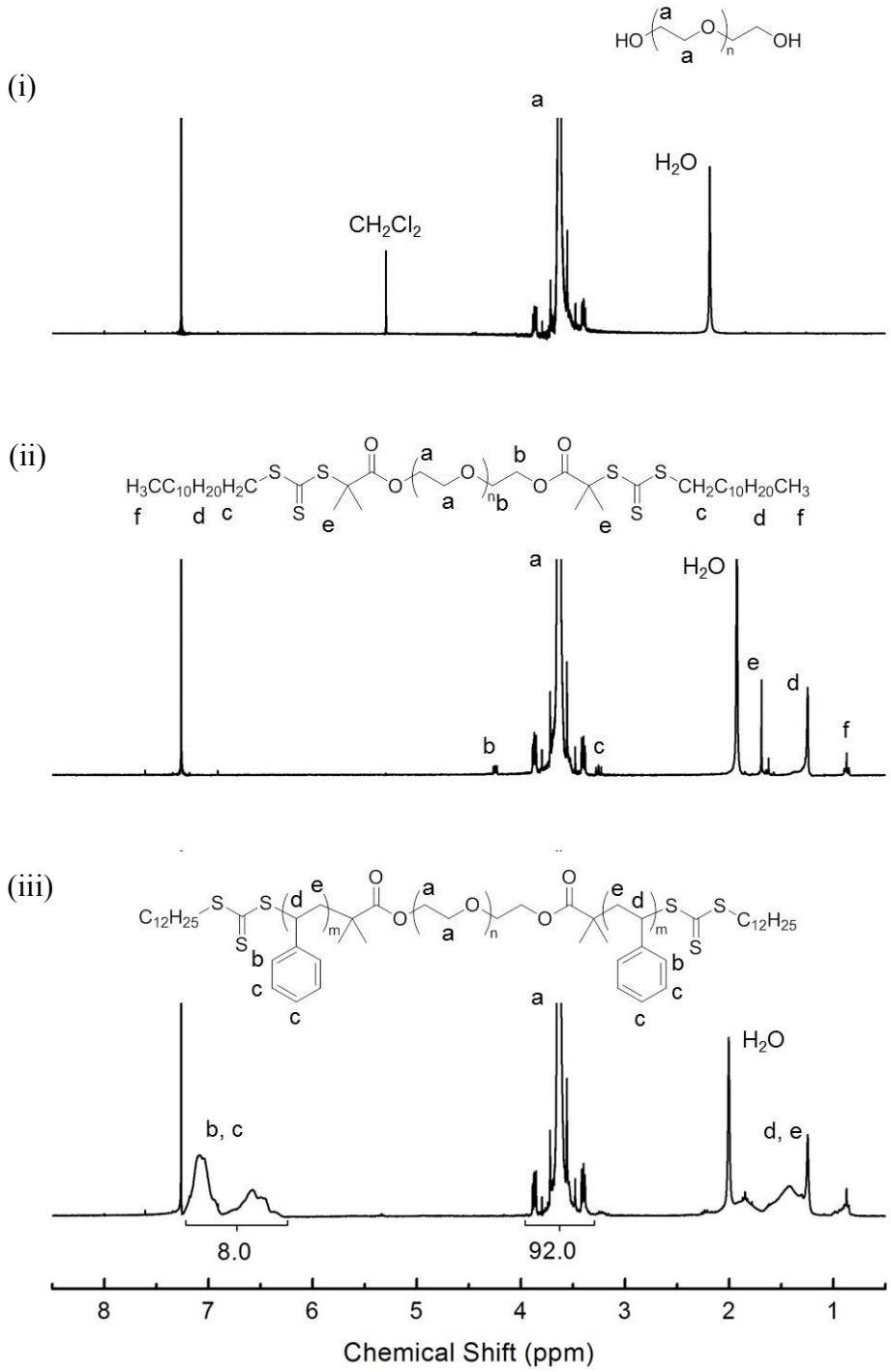


**Figure 2.2** $^1$H NMR spectra (300 MHz, in $CDCl_3$) of (i) PEO (precursor), (ii) CTA-PEO-CTA, and (iii) SOS polymers.

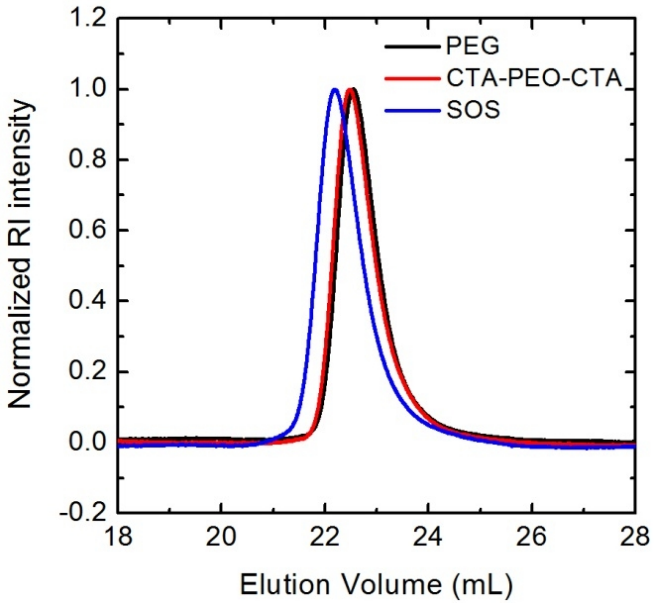


**Figure 2.3** SEC traces of PEO (precursor), CTA-PEO-CTA, and SOS polymers.

### 2.2.2 Ionic Liquid and Ion Gel Preparation

The [EMI][TFSA] ionic liquid was synthesized through an anion exchange reaction following a previously reported protocol.[4] Equal moles of [EMI] bromide ([Br]) (IoLiTec, 99%) (75.7 g) and lithium ([Li]) [TFSA] (3M, HQ-115) (113.8 g) were mixed with 200 mL distilled water, and the reaction was carried out at 70 °C with vigorous stirring for 1 day. The hydrophobic ionic liquid phase was separated and then washed five times with distilled water. Then, the ionic liquid was dissolved in ca. 150 mL $CH_2Cl_2$ and passed through a neutral alumina column. The solvent was subsequently removed in a rotary evaporator and the product was dried in a vacuum oven at 70 °C for 2 days. The ionic liquid was clear and colorless, and was stored in a glovebox to avoid water absorption. The $^1$H NMR spectrum of the product compares well with that previously reported (Figure 2.4).

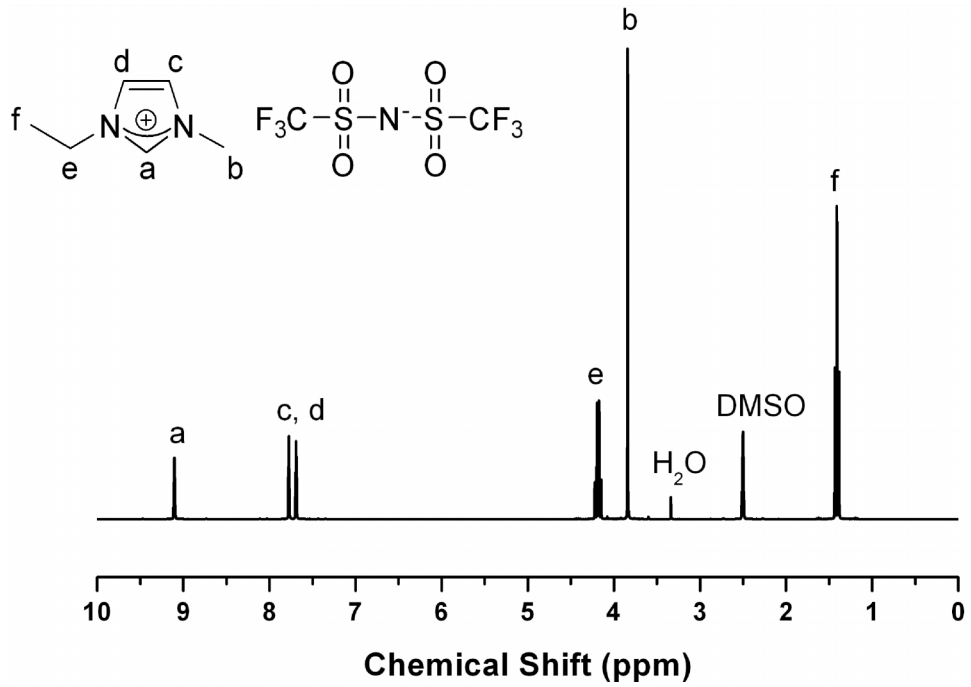


**Figure 2.4** $^{1}$H NMR spectrum (300 MHz, in DMSO-$d_6$) of [EMIM][TFSA].

All ion gels were prepared by mixing weighed amounts of the respective polymer and the ionic liquid in $CH_2Cl_2$ cosolvent. After stirring for 2 hours, the mixtures were purged with nitrogen gas for a day to evaporate most of the cosolvent. Then, the samples were placed in a vacuum oven at ca. 70 °C for 2 days to completely remove the cosolvent. To avoid any effects of moisture, all samples were kept in a vacuum desiccator and were dried in a vacuum oven at ca. 70 °C for a day before any measurements were carried out.

### 2.2.3 Rheology

Rheological measurements were conducted on an ARES rheometer (Rheometric Scientific) using parallel plate geometry. Depending on the modulus, both 50 and 25 mm diameter plates were employed, with a gap spacing of ca. 1 mm. At each temperature, the sample was thermally equilibrated for 15 – 20 min and the gap was adjusted to compensate for the thermal expansion of the tool set. Then, strain sweeps were conducted

to determine the linear viscoelastic regime, followed by measurements of the dynamic shear moduli. Temperatures were controlled to within 0.2 °C of the set points with an environmental control circulator under a nitrogen atmosphere. Measurements were taken at a series of decreasing temperatures.

### 2.2.4 Small Angle X-ray Scattering

Small-angle x-ray scattering (SAXS) experiments were performed at the DuPont-Northwestern-Dow collaborative access team (DND-CAT) beamline at the Advanced Photon Source, Argonne National Laboratories by Brad Jones and Lucas McIntosh. Samples were sealed in hermetic DSC pans, which were heated in a Linkam DSC sample holder during scattering experiments. For the gel with 40 wt% SOS(3-35-3), measurements were performed with an annealing time of 5 min at each temperature. For gels with 20, 30 and 50 wt% SOS(3-35-3), samples were pre-annealed at ca. 140 °C for 1 hour, and annealed for 5 min on the beamline before measurements were taken. For gels with SOS(6-35-6), samples were pre-annealed at ca. 140 °C for 2 hrs, and annealed for 5 min on the beamline before measurements were taken. Two-dimensional scattering patterns were recorded by a Mar-CCD area detector, and then azimuthally integrated to give one-dimensional scattering data in the form of intensity ($I$) versus wave vector ($q$). The x-ray wavelength was 0.7293 Å, and the sample-to-detector distance was 6.12 m.

## 2.3 Results and Discussion

### 2.3.1 Gelation of SOS Triblock Copolymers in [EMI][TFSA]

The dynamic storage ($G'$) and loss ($G''$) moduli for the ion gel with 10 wt% SOS(3-

35-3) were measured over the temperature range from 30 °C to 160 °C. The loss tangent (tan $\delta$) spectra were shifted horizontally using time-temperature superposition (tTS), and the same shift factors were applied to the dynamic moduli to obtain master curves as a function of reduced frequency, as shown in Figure 2.5. A liquid-like behavior is observed at temperatures above 50 °C, as evidenced by the crossover between $G'$ and $G''$, and the power law exponents of two and one for $G'$ and $G''$ versus $\omega$, respectively. This result is qualitatively similar to that reported previously for a similar ion gel with 10 wt% SOS(3.3-20-3.3).[2]

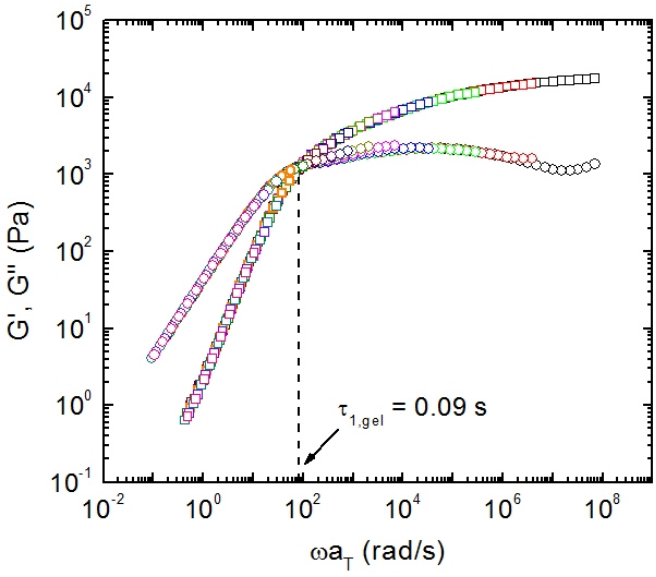


**Figure 2.5** tTS master curves of dynamic storage and loss moduli referenced to 120 °C for the ion gel with 10 wt% SOS(3-35-3).

The terminal flow behavior of this ion gel can be explained by transient network theory.[5] The rheological behavior of transient networks formed by swelling an ABA triblock copolymer in a B-selective solvent has been extensively studied.[6-9] Under conditions where the association strength of the A chains is weak enough to allow them to

reversibly associate/dissociate from the cross-linking points, either by thermal motion or by tension, a transient ABA network is formed. Its viscoelastic properties depend strongly on the terminal relaxation time, $\tau_{1,gel}$. With 10 wt% SOS(3-35-3), the end-blocks are short enough to enable access to the terminal flow regime of the ion gel within the experimental timescale. At the reference temperature of 120 °C, $\tau_{1,gel}$ is 0.09 s, as determined by the crossover frequency ($\omega_c$) at which $G'$ and $G''$ values are equal (Figure 2.5).

To further examine the exchange dynamics of the PS blocks, the values of $\tau_{1,gel}$ at various temperatures were calculated from the horizontal shift factors ($a_T$) used to superpose tan $\delta$, and plotted in Figure 2.6 (left axis). The temperature-dependent viscosity of bulk PS(3.4) taken from ref 10 is also shown for comparison (right axis). It is evident that the temperature dependence of $\tau_{1,gel}$ closely tracks that of the bulk PS viscosity, suggesting that the terminal relaxation of the gel reflects the motion of the PS chains. Note that in Figure 2.6 the bulk PS(3.4) ($T_g$ = 70 °C) viscosity data taken from ref 10 were shifted to lower temperatures by 56 K, suggesting that the $T_g$ of the PS cores is reduced to about 14 °C. This transition was not observed in the DSC thermogram (Chapter 4), likely due to the very small amount of the cross-linking cores. However, such a reduction in $T_g$ is not unexpected considering the nanoscopic PS domains[11] and the possible plasticizing effect of the PEO/[EMI][TFSA] matrix on the PS cores.[12,13]

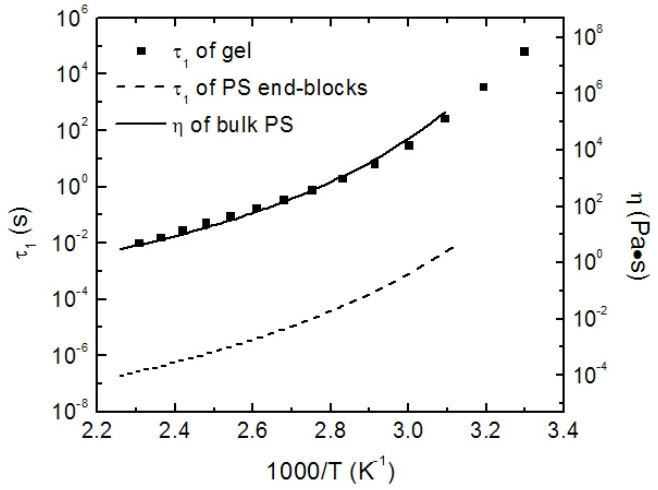


**Figure 2.6** Temperature dependent terminal relaxation times ($\tau_{1,gel}$) of the ion gel with 10 wt% SOS(3-35-3). The viscosity data of a bulk PS sample ($\eta$) and the estimated longest relaxation time of the PS end-blocks in the SOS chains ($\tau_{1,PS}$) are presented for comparison. The bulk PS viscosity data were shifted to lower temperatures by 56 K, assuming a reduction in $T_g$ of the micellar PS cores from bulk PS.

The terminal relaxation of the transient gel depends both on the intrinsic mobility of PS chains and on the thermodynamic penalty of pulling the PS blocks through the PEO/[EMI][TFSA] matrix. The intrinsic mobility of the chains was determined as the terminal relaxation time of bulk PS ($\tau_{1,PS}$) with a $T_g$ of 14 °C (equivalent to that expected of the micellar cores). $\tau_{1,PS}$ was calculated from the segmental relaxation time of bulk PS[14] ($\tau_{seg}$) and the empirical relationship $\tau_{1,PS}/\tau_{seg} \sim N_{PS}^2$, where $N_{PS}$ is the degree of polymerization for the PS blocks, which is 27 for the SOS in this case.[15] In Figure 2.6, $\tau_{1,PS}$ was plotted together with $\tau_{1,gel}$ for comparison. As expected, the temperature dependences of $\tau_{1,PS}$ and $\tau_{1,gel}$ are similar. However, $\tau_{1,gel}$ is more than four orders of magnitude larger than $\tau_{1,PS}$. This dynamic difference can be attributed to the energy barrier for the PS blocks to dissociate and diffuse into the PEO/[EMI][TFSA] matrix,

which depends on the incompatibility $\chi N_{PS}$ between PS and the matrix, where $\chi$ is the Flory-Huggins interaction parameter.[13] According to this "hindered diffusion" mechanism, the diffusion coefficient is given by[16–19]

$$D \sim D_0 \exp(-\alpha\chi N_{PS}) \tag{2.1}$$

where $D_0$ is the diffusion coefficient in the absence of any interactions and $\alpha$ is a constant of order unity. From eq 2.1, the terminal relaxation time of the gel can be expressed as

$$\tau_{1,gel} \sim \tau_{1,PS} \exp(\alpha\chi N_{PS}) \tag{2.2}$$

The inferred value of $\alpha\chi$ is about 0.39, which agrees with that reported previously (0.38) for the ion gel with 10 wt% SOS(3.3-20-3.3).[2] Strictly speaking, for a polymer solution, $\alpha\chi$ in equation 2.2 should be $\alpha(\chi - 0.5)$ or $\alpha(\chi - 1)$.

### 2.3.2 Rheology of SOS Gels with a Body-Centered Cubic (BCC) Structure

As the SOS content is increased to 20 wt%, terminal relaxation behavior is no longer observed. Instead, the system remains an elastic solid ($G' > G''$) over the entire measured temperature and frequency ranges, as shown by the tTS master curves in Figure 2.7a. Further increases in the SOS content up to 50 wt% yield similar master curves, with two plateaus evident in the storage modulus (Figure 2.7). The crossover frequency from one plateau to the other appears to be concentration independent, and agrees with $\omega_c$ for the gel with 10 wt% SOS(3-35-3) (corresponding to $\tau_{1,gel} \sim 0.09$ s at 120 °C). This suggests that the rate at which PS blocks can be reversibly pulled out or inserted into the micellar cores does not vary much with polymer content over the composition range examined. This is reasonable, since the rate of chain exchange for the end-blocks depends only on $\chi N_{PS}$. These features are qualitatively similar to those observed in transient hydrogels

formed by PEO based triblock copolymers.[20]

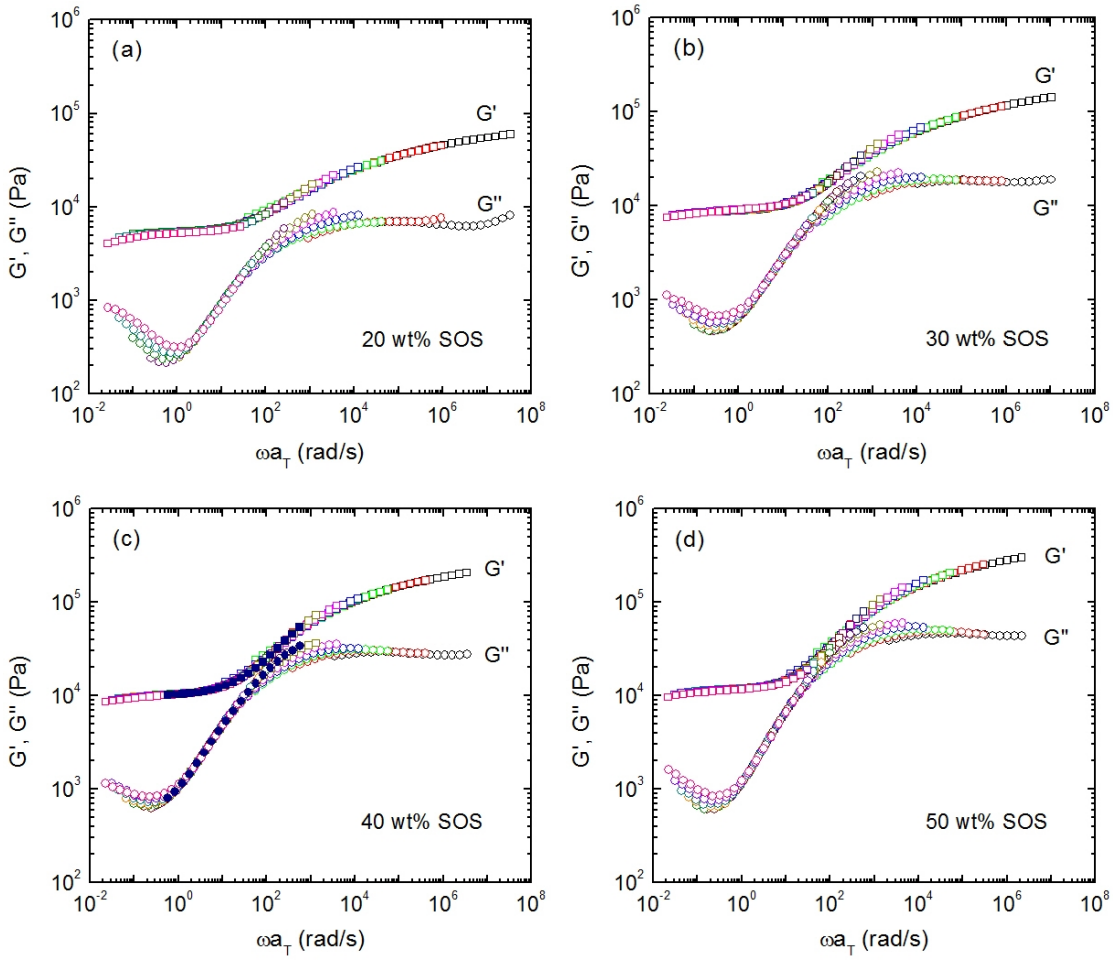


**Figure 2.7** tTS master curves of dynamic storage and loss moduli referenced to 120 °C for ion gels with (a) 20 wt%, (b) 30 wt%, (c) 40 wt% and (d) 50 wt% SOS(3-35-3). Filled symbols in (c) denote the moduli measured at 90 °C.

At frequencies greater than $\omega_c$, the PS chains cannot overcome the energy barrier to diffuse into the PEO/[EMI][TFSA] matrix, and $G'$ exhibits the rubbery plateau of the cross-linked network. Since $G'$ in the plateau region cannot be strictly horizontal, different methods have been developed to define the plateau modulus ($G_N$).[21,22] Here $G_N$ was determined as the value of $G'$ at the frequency where the corresponding curve of tan

$\delta$ (Figure 2.8) has a minimum or smallest value above $\omega_c$. The results are plotted versus SOS weight fraction on a logarithmic scale in Figure 2.9. A power law fit gives a slope of 2.0 ± 0.1, which agrees very well with the value of 2 reported previously for PEG-based hydrogels with polymer concentrations ≤ 17 wt%.[23] Experimentally determined exponents for other polymer solutions range from 2 to 2.5.[21,24] Theory anticipates a value of 2.3 for entangled solutions of neutral polymers in good solvents.[25]

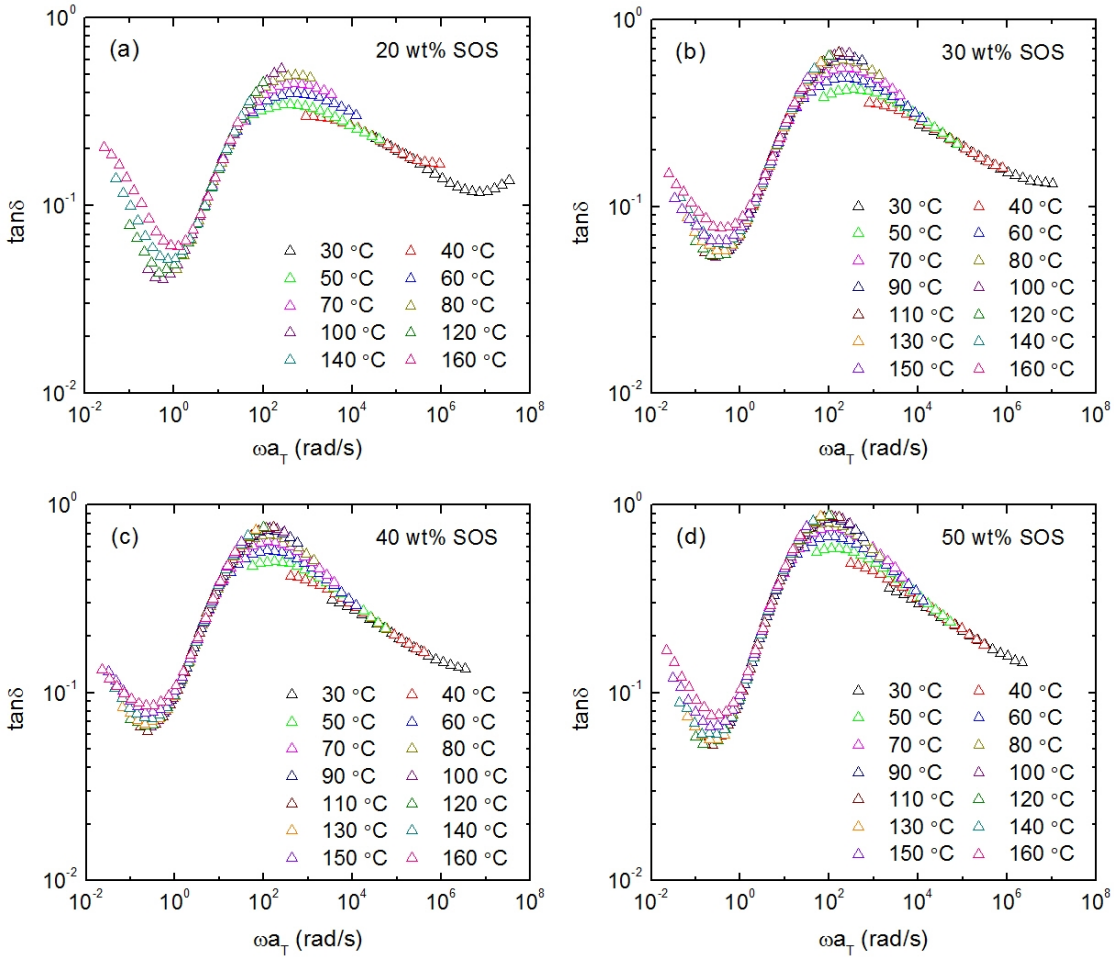


**Figure 2.8** tTS master curves of loss tangent referenced to 120 °C for SOS/[EMI][TFSA] ion gels with (a) 20 wt%, (b) 30 wt%, (c) 40 wt% and (d) 50 wt% SOS(3-35-3).

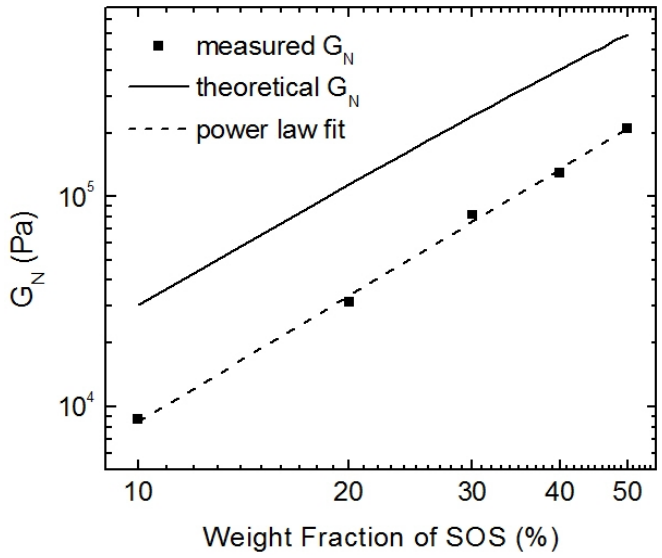


**Figure 2.9** Concentration dependence of plateau modulus ($G_N$) for ion gels with 10 – 50 wt% SOS(3-35-3). The solid line displays the storage modulus calculated from eq 2.4 for ideal gels. The dashed line indicates a power law fit to the measured data.

According to linear viscoelastic theory, $G_N$ can be expressed as[15]

$$G_N = \nu k_B T \tag{2.3}$$

where $\nu$ is the number density of network strands, $k_B$ is the Boltzmann constant, and $T$ is absolute temperature. For an ideal gel where every mid-block is elastically effective, $\nu = cN_A/M_x$, where $c$ is the concentration of the block copolymer in w/v, $N_A$ is Avogadro's number, and $M_x$ is the molecular weight between cross-links. Therefore, eq 2.3 can be written as

$$G_N = \frac{cfRT}{M_x} \tag{2.4}$$

where $f$ is the fraction of bridging or effective mid-blocks inside the copolymer and $R$ is the ideal gas constant. For the SOS gels, $M_x$ is the molecular weight between entanglements along the PEO chains. Therefore, we estimate $M_x = M_{e,\,PEO}/w_{PEO}$, where

$M_{e,\,PEO}$ is the entanglement molecular weight of melt PEO, which is 1.6 kDa at 140 °C,[26] and $w_{PEO}$ is the weight fraction of PEO in the gel. Assuming all PEO chains bridge two cross-linking cores instead of looping back to the same one ($f = 1$), the values of $G_N$ at 40 °C (the temperature at which the measured plateau modulus was extracted) were calculated and plotted as a solid line in Figure 2.9. The bridging fractions can thus be calculated as 29%, 28%, 34%, 32%, and 36% for gels with 10, 20, 30, 40, and 50 wt% SOS(3-35-3). At the low concentration end, this difference is reasonable and is comparable to previously reported transient gels.[23,27,28] At the high concentration end, however, this difference is perhaps more surprising: in the limit of many entanglements, *e.g.* ca. 11 entanglements per PEO chain with 50 wt% SOS(3-35-3), looped mid-blocks should contribute to the modulus almost the same as bridging mid-blocks, and the measured modulus would be expected be closer to that of the ideal gel. This might be caused by incomplete conversion of PEO into CTA-PEO-CTA, which would render the actual cross-linking density less than expected based on 100% conversion. Unfortunately, the integrations of the CTA end-groups are less than 1% of the main peak of PEO, which is below the precision of the measurement itself. Therefore, it is nearly impossible to determine the conversion quantitatively and precisely.

At frequencies below $\omega_c$, the time scale is long enough (or the temperature is high enough) for the PS chains to be pulled out from the cross-links, forming a viscoelastic solution of congested micelles with PS cores and PEO coronas. This partially relaxes the stress of the system and thus brings a second, lower value modulus plateau into the measurable frequency window (Figure 2.7). SAXS measurements were performed to

examine the morphology of the micelle solutions and solid-state gels. Figure 2.10a shows the SAXS profiles of the gel with 40 wt% SOS(3-35-3) upon heating. Below 90 °C, no clear ordering of the PS cores is observed. Above 90 °C, well-defined peaks appear at low $q$, which correspond to the Bragg reflections of a BCC structure. Once the arrangement of the micelles reaches the thermodynamically favorable state (in this case a BCC lattice) under certain conditions, such as heating, the system retains this structure after those conditions are removed, as evidenced by Figure 2.10b for the same gel upon cooling. This suggests that kinetics is the limiting factor for the ordering of the PS micelles. The temperature above which ordering can easily occur agrees with the rheology results: at 90 °C the moduli are at the transition between the two plateaus, as

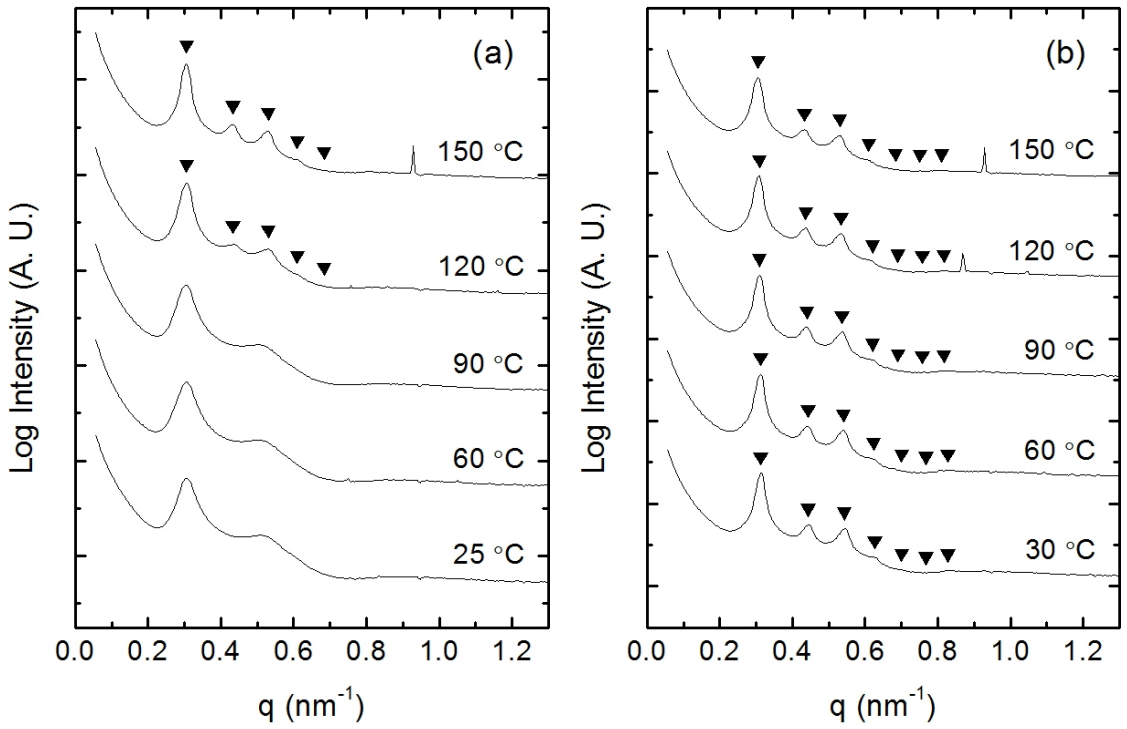


**Figure 2.10** 1D SAXS profiles for the ion gel with 40 wt% SOS(3-35-3) measured upon (a) heating and (b) cooling. Filled triangles correspond to expected intensity maxima for BCC at $q/q^*$ values of 1: √2: √3: √4: √5: √6: √7.

shown by the filled symbols in Figure 2.7c.

Since the SOS(3-35-3) polymers have very long mid-blocks relative to the core, it is reasonable that they pack on a BCC lattice.[12,13,29] Quantities related to the length scale and structure of the gels can be extracted from the scattering profiles. The domain spacing ($d_{110}$) of all gels can be calculated using the profiles measured at 140 °C (Figure 2.11) as $d_{110} = 2\pi/q^*$; values are listed in Table 2.1. This gives a lattice constant of $a = \sqrt{2}d_{110}$. The aggregation number ($N_{agg}$), defined here as the number of end-blocks inside a micelle, is therefore

$$N_{agg} = \nu_c a^3 = \frac{cN_A}{M_n}\left(\frac{2\sqrt{2}\pi}{q^*}\right)^3 \tag{2.5}$$

where $\nu_c$ is the number density of the triblock copolymer and $M_n$ is the number average molecular weight of the triblock, which is 40.6 kDa for the SOS polymer. Note that eq 2.5 assumes that all micelles pack on a BCC lattice, which is not the case as indicated by the contribution of the liquid order to the peaks in the SAXS profiles. However, the average number densities of micelles in ordered versus disordered regions are expected to be similar, and thus the extracted values are still useful. It was found that $d_{110}$ decreases with polymer concentration and $N_{agg}$ increases, over the whole composition range studied (Table 2.1). This suggests that as more polymer is added, more chains aggregate in each micelle, and the number of bridging PEO strands increases, leading to a contracted BCC lattice.

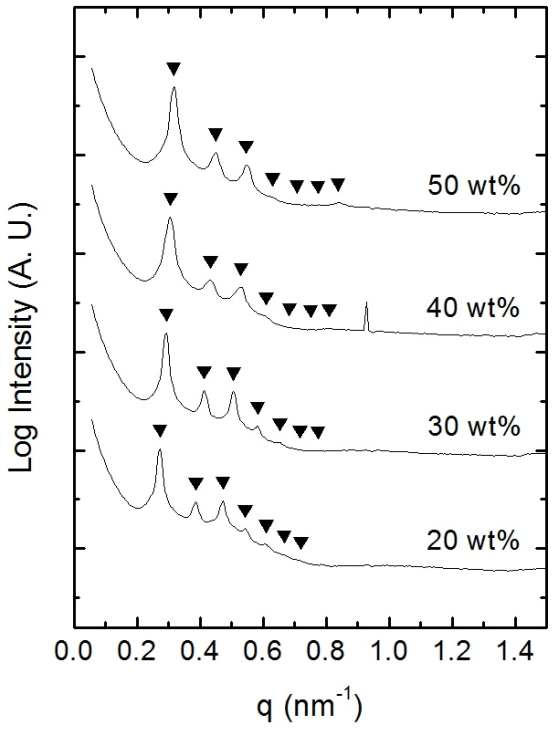


**Figure 2.11** 1D SAXS profiles for ion gels with 20, 30, and 50 wt% SOS(3-35-3) at 140 °C, and ion gel with 40 wt% SOS(3-35-3) at 150 °C. Filled triangles correspond to expected intensity maxima for BCC at $q/q^*$ values of 1: √2: √3: √4: √5: √6: √7.

The distance between the centers of two nearest PS cores, $d_{nn}$, can also be computed,

$$d_{nn} = \frac{\sqrt{6}}{2}\frac{2\pi}{q^*} = \frac{\sqrt{3}a}{2} \tag{2.6}$$

which has the same concentration dependence as $d_{110}$ (Table 2.1). Because core scattering is not very strong at 140 °C (Figure 2.11), the core radius, $R_c$, was estimated from the volume of the core assuming no solvent penetration (Table 2.1):

$$\frac{4\pi R_c^3}{3} = \frac{2M_{n,PS}N_{agg}}{N_A\rho_{PS}} \tag{2.7}$$

where $M_{n,PS}$ is the number average molecular weight of the PS block, which is 2.8 kDa for the polymer in question, and $\rho_{PS}$ is the density of PS, which is taken to be 1.05 g/cm$^3$.

**Table 2.1** Extracted Parameters from the SAXS Profiles of the SOS Ion Gels at 140 °C.

| SOS Content (wt%) | $d_{110}$ (nm) | $N_{agg}$ | $d_{nn}$ (nm) | $R_c$ (nm) |
|---|---|---|---|---|
| 20 | 22.9 ± 0.2 | 143 ± 4 | 28.0 ± 0.2 | 5.3 ± 0.1 |
| 30 | 21.5 ± 0.2 | 171 ± 4 | 26.3 ± 0.2 | 5.6 ± 0.1 |
| 40* | 20.5 ± 0.2 | 193 ± 4 | 25.1 ± 0.2 | 5.9 ± 0.1 |
| 50 | 19.8 ± 0.2 | 209 ± 5 | 24.2 ± 0.2 | 6.0 ± 0.1 |

* Measured at 150 °C.

The viscoelastic behavior of the congested micelles below $\omega_c$ (Figure 2.7) is similar to that of block copolymer/molecular solvent mixtures that adopt a cubic micellar phase, *i.e.*, $G'$ is essentially independent of frequency, while $G''$ passes through a minimum.[30] This characteristic plateau modulus associated with cubic phases ($G_{cubic}$) has also been suggested to be a universal feature for diblock copolymer melts.[31] Furthermore, the same report found that $G_{cubic}$ of the melts with a BCC lattice depends on domain spacing as $G_{cubic}/RT \sim d_{110}^{-3.14}$. A similar correlation between $G_{cubic}$ and $d_{110}$ for block copolymer melts and concentrated micelle solutions has also been proposed, with each sphere per unit volume contributing $18k_BT$ to the modulus at the order-disorder transition temperature ($T_{ODT}$).[32] The power law relation in ref 31 is plotted in Figure 2.12, along with the experimentally measured values for the SOS gels at three temperatures at which the system can be considered a micellar solution. By analogy to $G_N$, the measured $G_{cubic}$ was determined as the value of $G'$ at the frequency where the corresponding curve of tan $\delta$ has a minimum at the indicated temperatures (Figure 2.8). For a particular concentration, the value of $G_{cubic}/RT$ only decreases slightly with increasing temperature

(< 15% over 40 °C). Even though the measured range of $d_{110}$ is too small to compare the power law dependence, the corresponding $G_{cubic}/RT$ values of the SOS system agree very well with those of the diblock copolymer melts with the same $d_{110}$. This indicates that the incorporation of [EMI][TFSA] into the PEO domain can be qualitatively regarded as increasing the volume fraction of the PEO chains, which makes the micellar solution similar to a hypothetical SO diblock melt having the measured domain spacing values.

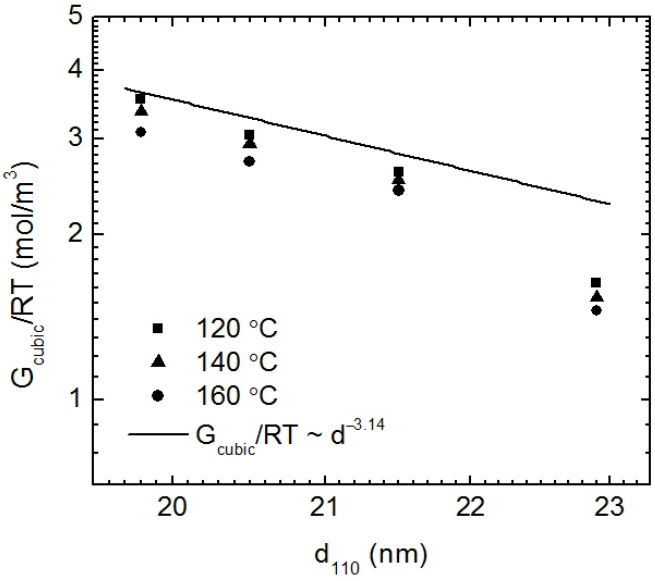


**Figure 2.12** $G_{cubic}/RT$ versus domain spacing ($d_{110}$) for ion gels with 20 – 50 wt% SOS(3-35-3) at selected temperatures. The solid line displays the relationship between $G_{cubic}/RT$ and $d_{110}$ for diblock copolymer melts with a BCC structure reproduced from ref 31.

### 2.3.3 Rheology of SOS Gels with a Longer S Block

For gels with SOS(6-35-6), the viscoelastic properties are expected to be qualitatively different from gels with SOS(3-35-3), with $M_n$ = 6 kDa, $N_{PS}$ = 58, and $\alpha\chi N_{PS}$ = 23. Therefore, an estimate using eq 2.2 yields $\tau_{1,gel} \sim 10^{10}\tau_{1,PS}$, which is well outside of the experimental timescale. As a result, pull-out of the end-block is highly

unlikely to occur. This is evidenced in Figure 2.13, where the gel with 10 wt% SOS(6-35-6) remains an elastic solid ($G' > G''$) over the entire measured temperature and frequency ranges. Moreover, both a fast and a slow relaxation can be observed, as indicated by the increase of $G''$ in Figure 2.13b and the $G''$ peak in Figure 2.13a. These results agree qualitatively well with previously reported SOS ion gels based on relatively long S blocks.[2,27] More detailed discussion on the associated relaxation processes are deferred to Chapter 3.

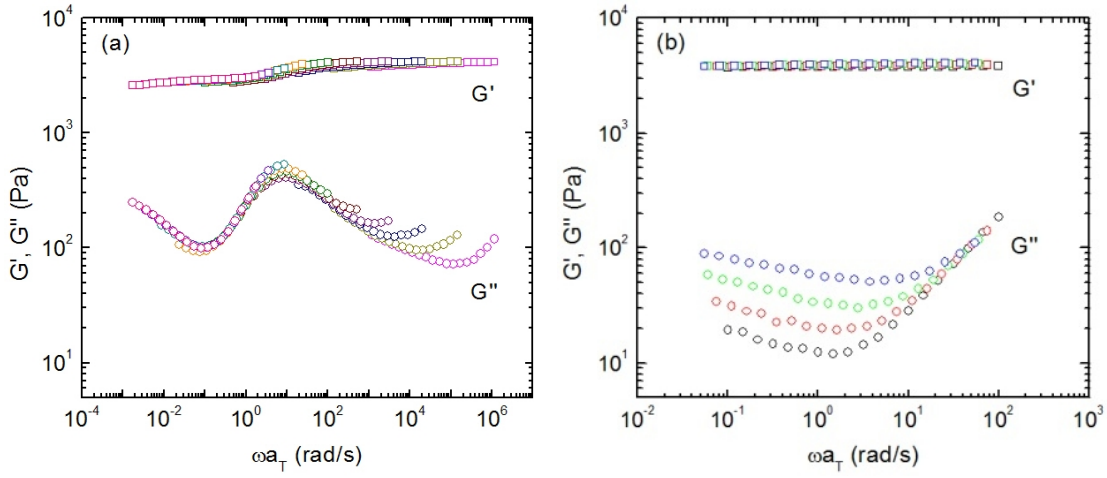


**Figure 2.13** Master curves of storage and loss moduli for the ion gel with 10 wt% SOS(6-35-6) measured at (a) 70 – 160 °C referenced to 120 °C and (b) 30 – 60 °C referenced to 30 °C.

For the gel with 40 wt% SOS(6-35-6), over the temperature range of 110 – 160 °C, the slow relaxation process is dominant, and tTS master curves can be obtained, as shown in Figure 2.14a. Notably, in this temperature region, $G'$ decreases gradually with increasing temperature, which contrasts with the well-defined plateau region present in the SOS(3-35-3) gel with the same polymer concentration (Figure 2.7c). This is further evidence that the relaxation accounting for the storage modulus drop is associated with

internal adjustment rather than end-block pull-out. In the temperature range of 30 – 100 °C, both the fast and the slow relaxation are present, resulting in different temperature dependences of time constants at different temperatures, and tTS master curves cannot be obtained with horizontal shifts of the moduli. The moduli without any shifts are plotted in Figure 2.14b.

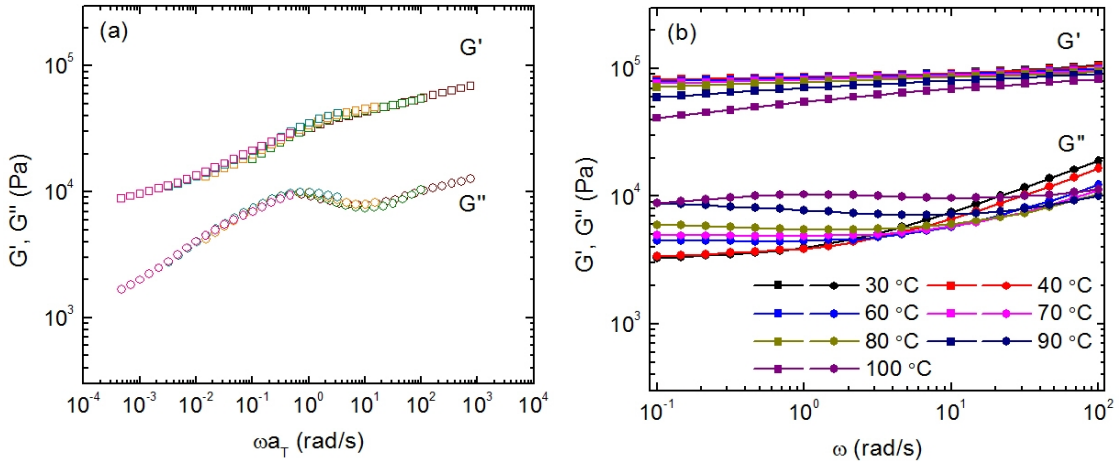


**Figure 2.14** (a) Master curves of storage and loss moduli referenced to 120 °C for the ion gel with 40 wt% SOS(6-35-6) measured at 110 – 160 °C, and (b) storage and loss moduli for the same ion gel measured at 30 – 100 °C without shift.

Another evidence that the relaxation accounting for the modulus drop in gels with longer S end-blocks is not chain pull-out is shown by the SAXS profiles in Figure 2.15. Gels with SOS(3-35-3) display well-defined scattering peaks corresponding to BCC lattices upon annealing at 140 °C for 1 h (Figure 2.11), while no clear ordering was observed for gels with SOS(6-35-6) upon annealing twice as long at the same temperature. For the gel with 10 wt% SOS(6-35-6), scattering from the PS cores is strong, and the core size can be extracted from the position of the first minimum in the form factor. Applying the characteristic equation of the hard-sphere form factor, $\sin(qR_c)$ –

$qR_c\cos(qR_c) = 0$, $R_c$ at 140 ºC can be estimated as 7.9 nm, with $qR_c = 4.493$ at the first minimum (solid symbol in Figure 2.15). For the gel with 40 wt% SOS(6-35-6), on the other hand, core scattering is not observed. This is likely because the cores are much closer than with the addition of 10 wt% polymer, resulting in more scattering interference among different cores.

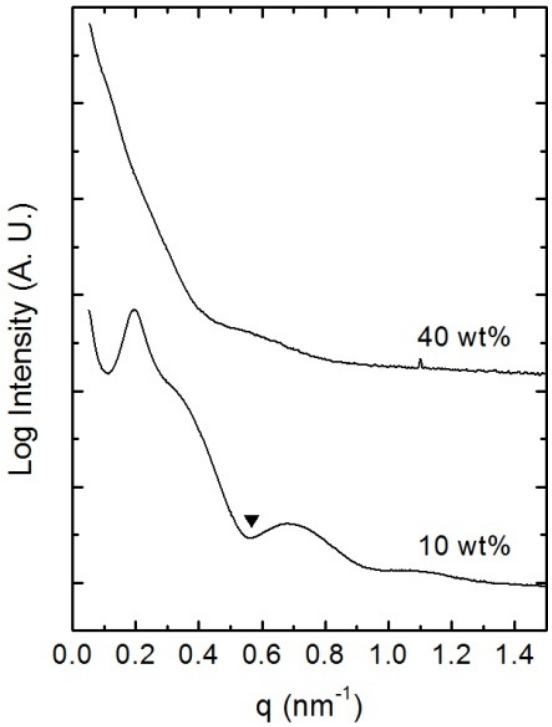


**Figure 2.15** 1D SAXS profiles for ion gels with 10 and 40 wt% SOS(6-35-6) at 140 °C. Solid symbol denotes the position of the first minimum in $q$ used to calculate $R_c$.

## 2.4 Summary

In this chapter, the viscoelastic properties of ion gels based on SOS triblock copolymers and the ionic liquid [EMI][TFSA] were investigated over wide ranges of temperature and composition. The ion gel with 10 wt% SOS(3-35-3) “melts” at high

temperatures; its longest relaxation time tracks the temperature dependence of bulk PS viscosity, while the actual relaxation time values are more than four orders of magnitude higher than those for bulk PS due to the energy barrier of pulling the PS end-blocks through the PEO/[EMI][TFSA] matrix. Gels with 20 – 50 wt% SOS(3-35-3) do not melt and show two plateaus in $G'$. The one above $\omega_c$ is that of the entangled network with PEO strands and PS cross-links; its value depends quadratically on polymer weight fraction and is about half of that predicted from linear viscoelastic theory due to looping. The other plateau below $\omega_c$ is that of the congested micelle solution with PS cores and PEO coronas, the value of which depends on domain spacing in a similar way as diblock melts. For ion gels with SOS(6-35-6), rheology and SAXS results suggest that as temperature increases, stress is released through internal relaxation rather than end-block pull-out.

## 2.5 References

(1) Brandrup, J.; Immergut, E. H.; Grulke, E. A. *Polymer Handbook*, 4th ed.; Wiley-Interscience: New York, 1999.

(2) He, Y.; Lodge, T. P. *Macromolecules* **2008**, *41*, 167-174.

(3) Lai, J. T.; Filla, D.; Shea, R. *Macromolecules* **2002**, *35*, 6754-6756.

(4) Susan, M. A. B. H.; Kaneko, T.; Noda, A.; Watanabe, M. *J. Am. Chem. Soc.* **2005**, *127*, 4976-4983.

(5) Tanaka, F.; Edwards, S. F. *Macromolecules* **1992**, *25*, 1516-1523.

(6) Sato, T.; Watanabe, H.; Osaki, K. *Macromolecules* **2000**, *33*, 1686-1691.

(7) Vega, D. A.; Sebastian, J. M.; Loo, Y.-L.; Register, R. A. *J. Polym. Sci., Part B: Polym. Phys.* **2001**, *39*, 2183-2197.

(8) Inomata, K.; Nakanishi, D.; Banno, A.; Nakanishi, E.; Abe, Y.; Kurihara, R.; Fujimoto, K.; Nose, T. *Polymer* **2003**, *44*, 5303-5310.

(9) Seitz, M. E.; Burghardt, W. R.; Faber, K. T.; Shull, K. R. *Macromolecules* **2007**, *40*, 1218-1226.

(10) Plazek, D. J.; O'Rourke, V. M. *J. Polym. Sci., Polym. Phys. Ed.* **1971**, *9*, 209-243.

(11) Roth, C. B.; Dutcher, J. R. *J. Electroanal. Chem.* **2005**, *584*, 13-22.

(12) Lai, C.; Russel, W. B.; Register, R. A. *Macromolecules* **2002**, *35*, 841-849.

(13) Choi, S.-H.; Bates, F. S.; Lodge, T. P. *J. Phys. Chem. B* **2009**, *113*, 13840-13848.

(14) He, Y.; Lutz, T. R.; Ediger, M. D.; Ayyagari, C.; Bedrov, D.; Smith, G. D. *Macromolecules* **2004**, *37*, 5032-5039.

(15) Hiemenz, P. C.; Lodge, T. P. *Polymer Chemistry*, 2nd ed.; CRC Press: New York, 2007.

(16) Yokoyama, H.; Kramer, E. J. *Macromolecules* **1998**, *31*, 7871-7876.

(17) Cavicchi, K. A.; Lodge, T. P. *Macromolecules* **2003**, *36*, 7158-7164.

(18) Choi, S.-H.; Lodge, T. P.; Bates, F. S. *Phys. Rev. Lett.* **2010**, *104*, 047802/1-047802/4.

(19) Choi, S.-H.; Bates, F. S.; Lodge, T. P. *Macromolecules* **2011**, *44*, 3594-3604.

(20) Renou, F.; Nicolai, T.; Benyahia, L.; Nicol, E. *J. Phys. Chem. B* **2009**, *113*, 3000-3007.

(21) Tao, H.; Huang, C.; Lodge, T. P. *Macromolecules* **1999**, *32*, 1212-1217.

(22) Graessley, W. W. *Adv. Polym. Sci.* **1974**, *16*, 1-179.

(23) Tae, G.; Kornfield, J. A.; Hubbell, J. A.; Lal, J. *Macromolecules* **2002**, *35*, 4448-4457.

(24) Mok, M. M.; Liu, X.; Bai, Z.; Lei, Y.; Lodge, T. P., *Macromolecules* **2011**, *44*, 1016-1025.

(25) Colby, R. H. *Rheol. Acta* **2010**, *49*, 425-442.

(26) Fetters, L. J.; Lohse, D. J.; Richter, D.; Witten, T. A.; Zirkel, A. *Macromolecules* **1994**, *27*, 4639-4647.

(27) He, Y.; Boswell, P. G.; Buhlmann, P.; Lodge, T. P. *J. Phys. Chem. B* **2007**, *111*, 4645-4652.

(28) Annable, T.; Buscall, R.; Ettelaie, R.; Whittlestone, D. *J. Rheol.* **1993**, *37*, 695-726.

(29) McConnell, G. A.; Gast, A. P.; Huang, J. S.; Smith, S. D. *Phys. Rev. Lett.* **1993**, *71*, 2102-2105.

(30) Hamley, I. W. *Phil. Trans. R. Soc. A* **2001**, *359*, 1017-1044.

(31) Kossuth, M. B.; Morse, D. C.; Bates, F. S. *J. Rheol.* **1999**, *43*, 167-196.

(32) Sebastian, J. M.; Lai, C.; Graessley, W. W.; Register, R. A. *Macromolecules* **2002**, *35*, 2707-2713.

# Chapter 3

# Viscoelastic Properties of Ion Gels with a Glassy Midblock*

## 3.1 Introduction

In this chapter, the viscoelastic properties of ion gels based on the self-assembly of a poly(styrene-*b*-methyl methacrylate-*b*-styrene) (SMS) triblock copolymer in the ionic liquid 1-ethyl-3-methylimidazolium bis(trifluoromethylsulfonyl)amide ([EMI][TFSA]) were investigated in the ionic-liquid-rich composition regime over a wide temperature range. The poly(styrene) (PS) end-blocks associate into micelles, whereas the poly(methyl methacrylate) (PMMA) mid-blocks are well-solvated by [EMI][TFSA]. PMMA has the highest glass transition temperature ($T_g$ ~ 110 °C)[1] among all the polymers that are compatible with [EMI][TFSA], thus serving as a stark contrast to the gels composed of poly(styrene-*b*-ethylene oxide-*b*-styrene) (SOS) and this particular ionic liquid. The midblock degree of polymerization was targeted to be similar to that of the SOS polymers discussed in Chapter 2, so as to better compare the behaviors of the corresponding gels. The overall goal is to understand the viscoelastic motions so as to provide insight into the rational design of these high performance microstructured electrolyte materials.

---

* Reproduced in part with permission from Zhang, S.; Lee, K. H.; Frisbie, C. D.; Lodge, T. P. *Macromolecules* **2011**, *44*, 940-949. Copyright 2011 American Chemical Society.

## 3.2 Experimental

### 3.2.1 Polymer Synthesis and Characterization

All reagents were used as received unless otherwise noted. Styrene was passed through an activated alumina column prior to use. The SMS triblock copolymer was synthesized by a two-step atom transfer radical polymerization (ATRP, Figure 3.1).[2–5] CuBr and $CuBr_2$ were stored in the glovebox to avoid water absorption. MMA and styrene monomers were passed through active alumina columns prior to use.

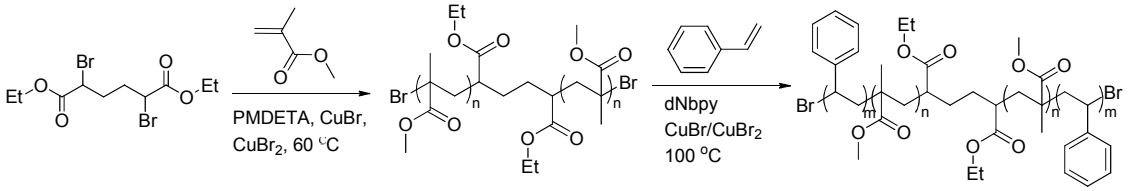


**Figure 3.1** Synthetic scheme of SMS triblock copolymer.

In the first step, a difunctional PMMA macroinitiator was prepared. The initiator diethyl *meso*-2,5-dibromoadipate (0.253 g, $7.0\times10^{-4}$ mol) and $CuBr_2$ (0.008 g, $3.6\times10^{-5}$ mol) were mixed with 80 mL anisole and stirred at 60 °C to ensure complete dissolution, followed by cooling to room temperature and then with an ice bath. MMA (120 mL, 1.12 mol), *N*,*N*,*N*′,*N*″,*N*″-pentamethyldiethylenetriamine (PMDETA, 0.095 mL, $4.6\times10^{-4}$ mol) and CuBr (0.051 g, $3.6\times10^{-4}$ mol) were then added and dissolved. The solution was freeze-pump-thaw degassed three cycles, and polymerization was carried out at 60 °C for 6 hours. The contents were poured into 5 L methanol and stirred vigorously to remove most of the copper, and the resulting precipitate was dissolved in ethyl acetate. The solution was then passed through a neutral alumina column and precipitated in *n*-hexane. The product was dried in a vacuum oven for a day. In the second step, the PMMA

macroinitiator (28.0 g, 0.28 mol), mixed powder of CuBr and $CuBr_2$ (97:3 in mole, 0.182 g, $1.25\times10^{-3}$ mol) and 4,4′-dinonyl-2,2′-bipyridine (1.067 g, $2.61\times10^{-3}$ mol) were dissolved in styrene (80 mL, 0.7 mol). The solution was degassed via five freeze-pump-thaw cycles, after which polymerization was carried out for 64 hours at 100 °C. Purification was the same as in the first step, with an additional precipitation in cyclohexane to remove PS homopolymer. The final product was dried at room temperature in a vacuum oven for two days. The product of each reaction step was confirmed by $^1$H NMR spectroscopy (Figure 3.2) and characterized by size exclusion chromatography (SEC, Figure 3.3). For the PMMA macroinitiator, $M_n$ = 86 kDa, $Đ$ = 1.20. The SMS triblock has PS blocks with an $M_n$ of 17 kDa as determined from peak integration of $^1$H NMR spectrum assuming the endblocks are symmetric, and a dispersity of 1.21 as determined by SEC. Another PMMA polymer previously synthesized by Ilan Zeroni using anionic polymerization ($M_n$ = 126 kDa, $Đ$ = 1.07)[6] was used to prepare the homopolymer solutions. For convenience, the triblock and the homopolymer are denoted as SMS(17-86-17) and PMMA(126), respectively.

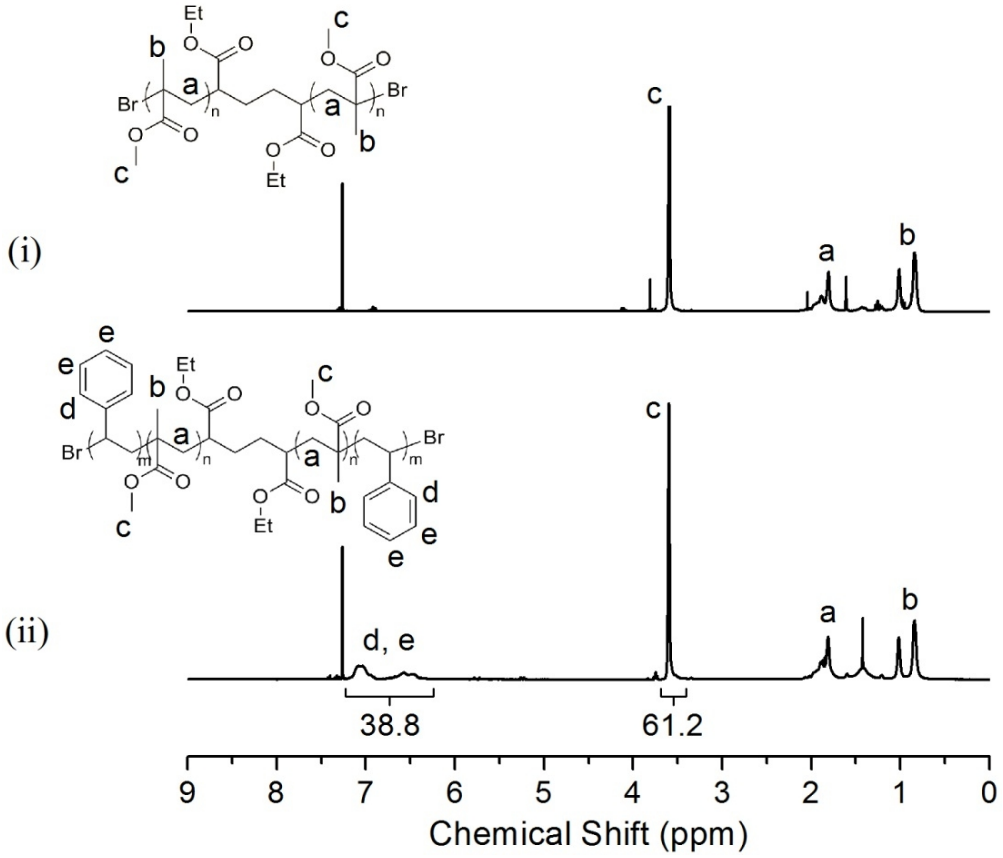


**Figure 3.2** $^{1}$H NMR spectra (300 MHz, in $CDCl_3$) of (i) PMMA macroinitiator and (ii) SMS triblock copolymer.

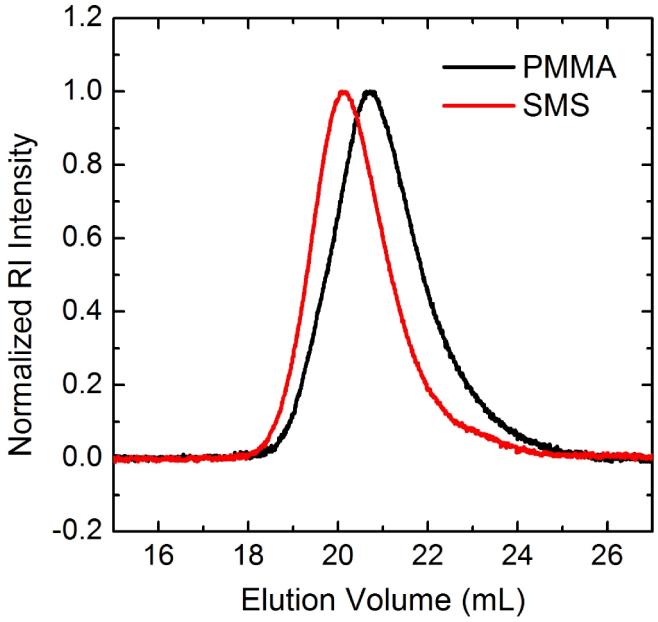


**Figure 3.3** SEC traces of PMMA macroinitiator and SMS triblock copolymer.

### 3.2.2 Ionic Liquid, Polymer Solution and Ion Gel Preparation

The [EMI][TFSA] ionic liquid was synthesized through an anion exchange reaction following a previously reported protocol as described in Chapter 2,[7] and was stored in a glovebox to avoid water absorption. The PMMA/[EMI][TFSA] solutions and all ion gels were prepared by mixing weighed amounts of the respective polymer and the ionic liquid in $CH_2Cl_2$ cosolvent. After stirring for 2 hours, the mixtures were blown with nitrogen gas for a day to evaporate most of the cosolvent. Finally, the samples were placed in a vacuum oven at 70 °C for 2 days to completely remove the cosolvent. To avoid any effects of moisture, all samples were kept in a vacuum desiccator and were dried in a vacuum oven at 70 °C for a day before any measurements were carried out.

### 3.2.3 Rheology

Rheological measurements were conducted on an ARES rheometer (Rheometric

Scientific) using parallel plate geometry. Depending on the modulus, both 50 and 25 mm diameter plates were employed, with a gap spacing of ca. 1 mm. At each temperature, the sample was thermally equilibrated for 15 – 20 min and the gap was adjusted to compensate for the thermal expansion of the tool set. Then, strain sweeps were conducted to determine the linear viscoelastic regime, followed by measurements of the dynamic shear moduli. Temperatures were controlled to within 0.2 °C of the set points with an environmental control circulator under a nitrogen atmosphere. Measurements were taken at a series of decreasing temperatures.

### 3.2.4 Small Angle X-ray Scattering

Small-angle x-ray scattering (SAXS) experiments were performed at the DuPont-Northwestern-Dow collaborative access team (DND-CAT) beamline at the Advanced Photon Source, Argonne National Laboratories by Lucas McIntosh. Samples were sealed in hermetic DSC pans, which were heated in a Linkam DSC sample holder during scattering experiments. The gels were pre-annealed at ca. 140 °C for 2 hrs, and annealed for 5 min on the beamline before measurements were taken. Two-dimensional scattering patterns were recorded by a Mar-CCD area detector, and then azimuthally integrated to give one-dimensional scattering data in the form of intensity ($I$) versus wave vector ($q$). The x-ray wavelength was 0.7293 Å, and the sample-to-detector distance was 6.12 m.

## 3.3 Results and Discussion

### 3.3.1 Rheology of SMS Gels

Figure 3.4 shows the dynamic storage ($G'$) and loss ($G''$) moduli as a function of

frequency for the SMS/[EMM][TFSA] ion gel with 10 wt% SMS(17-86-17) over the temperature range of 30 °C to 200 °C. The results are reversible in the sense that the modulus values are independent of whether the measurements are conducted upon heating or cooling. Rubberlike behavior is observed over the entire investigated temperature and frequency ranges, as indicated by $G' > G''$ and the weakly frequency dependent plateaus in $G'$. Note that in the low temperature region (30 °C – 75 °C), $G'$ is almost independent of temperature at frequencies below 10 rad/s, which is indicative of a network structure that is almost invariant. Increasing the temperature moves a second plateau into the measured frequency window, and by 140 °C two distinct plateaus could be observed. Further increases in temperature reveal the second plateau, as evidenced by the nearly constant $G'$ at low frequencies in the temperature range of 160 °C – 200 °C. These results are qualitatively similar to those observed for SOS-based ion gels with long S end-blocks, as mentioned in Chapter 2. Additionally, it is clear that the plateau modulus decreases with increasing temperature. The plateau modulus of an elastic polymer network ($G_N$) can be written as[8]

$$G_N = \nu k_B T \tag{3.1}$$

where $\nu$ is the number density of network strands, $k_B$ is the Boltzmann constant, and $T$ is absolute temperature. If the structure of the gel does not change, then the modulus should increase with temperature. The opposite observed trend here indicates that the relaxation of the physical cross-links reduces the network stress more than the temperature increase upon heating. Further discussion on the comparison between the measured elastic modulus values and those calculated using eq 3.1 is deferred until later.

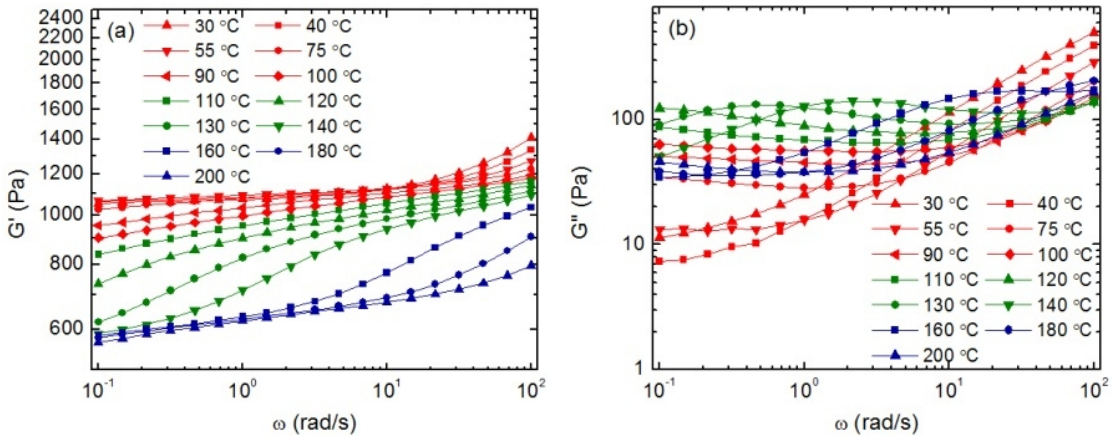


**Figure 3.4** Frequency dependences of (a) dynamic storage and (b) loss moduli for the SMS/[EMI][TFSA] ion gel with 10 wt% SMS(17-86-17).

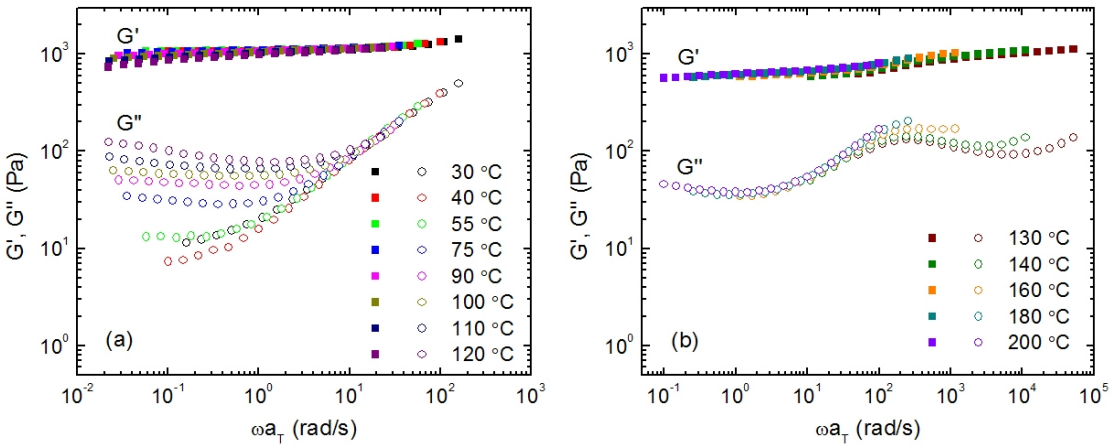


**Figure 3.5** Dynamic storage and loss moduli for SMS/[EMI][TFSA] ion gel with 10 wt% SMS(17-86-17) shifted to (a) 40 °C and (b) 200 °C, corresponding to the fast and slow relaxation modes, respectively.

The observation of two plateaus in $G'$ and the reduced plateau modulus with increasing temperature suggest that two relaxation processes are present in the ion gel, as illustrated by the tTS curves in Figure 3.5. Reasonable superpositions of the moduli were obtained at the high-frequency side of the fast relaxation (Figure 3.5a) and at the low-frequency side of the slow relaxation (Figure 3.5b). In the intermediate

frequency/temperature range, tTS fails because both relaxations are evident.

To understand the relaxation processes better, the horizontal shift factors ($a_T$) used to generate the superpositions in Figure 3.5 are plotted against inverse temperature, as shown in Figure 3.6. The temperature dependences of the viscosity of neat [EMI][TFSA] and bulk PS taken from ref 9 and 10, respectively, are also shown for comparison. It is evident that $a_T$ of the fast relaxation mode follows the temperature dependence of the [EMI][TFSA] viscosity, while $a_T$ of the slow relaxation mode tracks the temperature dependence of the PS viscosity. This suggests that the fast relaxation corresponds to the motion of the bridging PMMA chains in [EMI][TFSA], which tracks the temperature dependence of the solvent viscosity for this moderately dilute system. The slow relaxation, on the other hand, reflects the motion of the PS chains. This relaxation reduces the stretching of the bridging PMMA chains and therefore leads to a lowered stress and plateau modulus of the network upon heating. As discussed in Chapter 2, in order to dissociate and diffuse into the PMMA/[EMI][TFSA] matrix, the PS chains need to overcome an energy barrier.[11] The value of this barrier depends on the incompatibility $\chi N_{PS}$ between PS and [EMI][TFSA], where $\chi$ is the Flory-Huggins interaction parameter and $N_{PS}$ is the degree of polymerization of the PS block.[12] Taking $\chi \sim 0.39$ as inferred in Chapter 2 and $N_{PS} = 168$ for the SMS polymer, the energy barrier is about $65k_BT$. Therefore, end-block pulled-out from the cross-links is highly unlikely to occur. Note that according to eq 3.1, there should not be a decrease in modulus unless the number of elastically effective strands decreases. However, in the ion gels the "crosslinks" are not points, but finite micelles, so passing through the glass transition of these cores is

somewhat analogous to allowing the crosslinks to become mobile, and rearrange to reduce the stress. Note also that in Figure 3.6 the bulk PS ($T_g$ = 95 °C) viscosity data taken from ref 10 were shifted to lower temperatures by 28 K, indicating that the $T_g$ of the PS cores is reduced to about 67 °C. This transition was not observed in the DSC traces (Chapter 4), likely due to the very small amount of the cross-linking cores. However, such a reduction in $T_g$ is not surprising.[12,13]

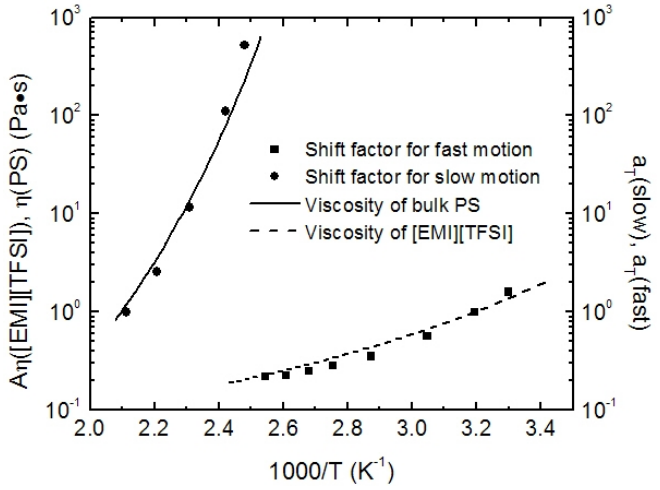


**Figure 3.6** Temperature dependences of the slow and fast relaxation modes of the SMS network in the SMS/[EMI][TFSA] ion gel with 10 wt% SMS(17-86-17). The shift factors were obtained by superposing the fast and slow relaxations in the loss tangent spectrum (Figure 3.10). The viscosity data of bulk PS and bulk [EMI][TFSA] are presented as a comparison.[9,10] A vertical shift ($A$ = 51) was applied to the viscosity of [EMI][TFSA] to compare only the temperature dependence. The bulk PS viscosity data was shifted to lower temperatures by 28 K, indicating a reduction in $T_g$ for the micellar PS cores with respect to the bulk PS.

The effect of SMS content on the temperature dependence of the relaxations is illustrated in Figure 3.7. The shift factors of the slow relaxation for ion gels with 20 wt% to 40 wt% SMS(17-86-17) overlap and track the temperature dependence of PS viscosity,

as is the case with 10 wt% SMS(17-86-17), whereas $a_T$ of the fast relaxation does not follow the temperature dependence of [EMI][TFSA] viscosity any more. This is reasonable, since the concentrations of PMMA chains in these gels are no longer in the moderately dilute regime. In these cases, $a_T$ of the fast relaxation (solid symbols in Figure 3.7) tracks the temperature dependence of $a_T$ of a PMMA/[EMI][TFSA] solution with a similar PMMA(126) concentration to that in the gel (dashed lines in Figure 3.7).[14] This supports the speculation that the fast relaxation is the motion of PMMA chains in [EMI][TFSA].

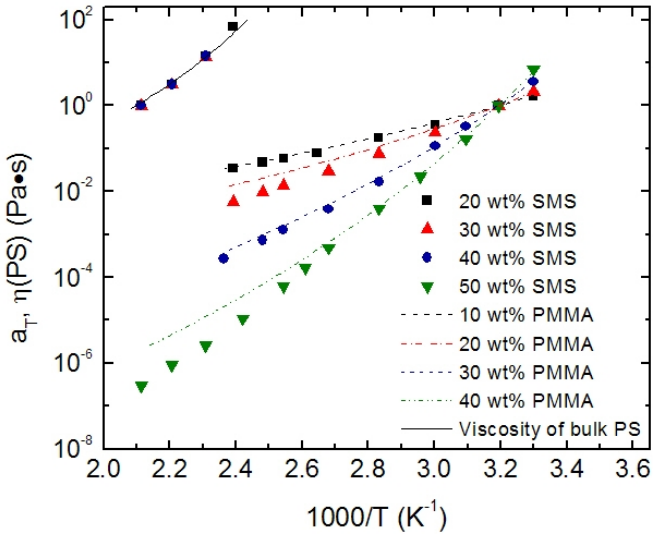


**Figure 3.7** Temperature dependences of the slow and fast relaxation modes of the SMS network in SMS/[EMI][TFSA] ion gels. The viscosity data of bulk PS and the Williams-Landel-Ferry (WLF) fits (see Table 3.1 for the fitting parameters) of shift factors for PMMA/[EMI][TFSA] solutions are presented as comparisons.[10,14] PMMA concentrations in ion gels with 20, 30, 40 and 50 wt% SMS(17-86-17) are 15, 23, 32 and 42 wt%, respectively. The bulk PS viscosity data was shifted to lower temperatures by 28 K, indicating a reduction in $T_g$ for the micellar PS cores with respect to the bulk PS.

**Table 3.1** Williams-Landel-Ferry (WLF) Fitting Parameters of Shift Factors ($a_T$) for PMMA/[EMI][TFSA] Solutions.

$$\log a_T = -C_1(T-T_{ref})/(C_2+T-T_{ref})$$

| PMMA(126) (wt%) | $C_1$ | $C_2$ (°C) | $T_{ref}$ (°C) |
|---|---|---|---|
| 10 | 4.85 ± 0.19 | 126 ± 3 | 0 |
| 20 | 3.68 ± 0.08 | 177 ± 2 | 70 |
| 30 | 4.73 ± 0.20 | 262 ± 6 | 150 |
| 40 | 6.28 ± 0.33 | 242 ± 8 | 140 |

For the ion gel with 50 wt% SMS(17-86-17) (42 wt% PMMA), it can be seen from Figure 3.7 that $a_T$ of this gel follows the temperature dependence of $a_T$ of the homopolymer solution with 40 wt% PMMA(126) below 140 °C. Even more striking than

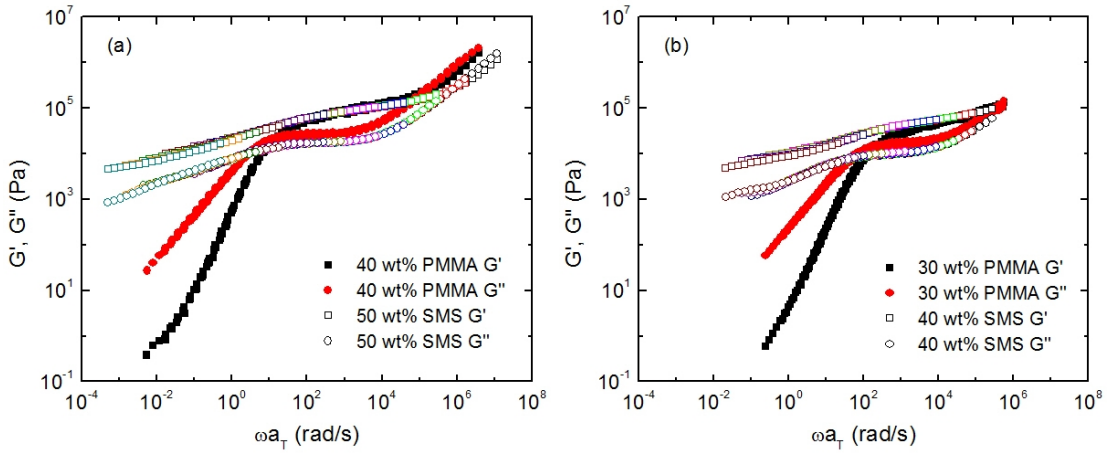


**Figure 3.8** tTS master curves for dynamic storage and loss moduli referenced to 120 °C of (a) PMMA/[EMI][TFSA] solution with 40 wt% PMMA(126)[14] and SMS/[EMI][TFSA] ion gel with 50 wt% SMS(17-86-17). PMMA concentration in the ion gel is 42 wt%. (b) PMMA/[EMI][TFSA] solution with 30 wt% PMMA(126)[14] and SMS/[EMI][TFSA] ion gel with 40 wt% SMS(17-86-17). PMMA concentration in the ion gel is 32 wt%.

the similarity of $a_T$ is the comparable relaxation times, as evidenced by the near-overlap of moduli at high frequencies (> 10 rad/s) shown in Figure 3.8a. This confirms the notion that the PMMA middle blocks in the gel relax in a way similar to free PMMA coils in the solution. The small disparity in moduli is probably due to differences in PMMA concentration (42 wt% in the gel versus 40 wt% in the solution) and molecular weight. This similarity in moduli at high frequencies has also been observed for the ion gel with 40 wt% SMS(17-86-17) (32 wt% PMMA) versus the homopolymer solution with 30 wt% PMMA(126), as shown in Figure 3.8b.

As mentioned before, the entropic elasticity based on eq 3.1 predicts increasing modulus with temperature, whereas the measured values decrease for the gel with 10 wt% SMS(17-86-17) due to faster release of stress by the relaxation of the PS chains. This trend holds for gels with higher SMS concentrations as well, as displayed in Figures 3.8 and 3.9, where lower reduced frequency equals higher temperature. As described in Chapter 2, the plateau modulus representing the network structure ($G_N$) can be determined as the value of $G'$ at the frequency where the corresponding curve of tan $\delta$ (Figure 3.10) has a minimum above the frequency of the fast relaxation peak. Due to the presence of two relaxation processes, the frequency at which a minimum occurs is different at each temperature, yielding slightly different $G_N$ values. Therefore, $G_N$ was extracted from the lowest temperature at which a minimum in tan $\delta$ occurs for gels with 30 – 50 wt% SMS(17-86-17). For gels with 10 and 20 wt% polymer, even the tan $\delta$ curve measured at the lowest temperature (30 °C) is located on the left side of the fast relaxation peak, therefore $G_N$ was arbitrarily chosen to be the value of $G'$ measured at 30

°C and 10 rad/s. The results are displayed in Figure 3.11. For an ideal gel where every mid-block is effective, $\nu = cN_A/M_x$, where $c$ is the concentration of the block copolymer in w/v, $N_A$ is Avogadro's number, and $M_x$ is the molecular weight between cross-links. Therefore, eq 3.1 can be written as

$$G_N = \frac{cfRT}{M_x} \tag{3.2}$$

where $f$ is the fraction of bridging or effective middle blocks inside the copolymer and $R$ is the ideal gas constant. Given the entanglement molecular weight ($M_e$) of 10 kDa for PMMA at 140 °C,[15] the effective PMMA concentration that mid-block entanglement starts to occur can be estimated as $w_{PMMA} = M_e/M_{n,\,PMMA}$ = 12 wt%, which translates into $w_{SMS}$ = 16 wt%. Therefore, at $w_{SMS}$ < 16 wt%, $M_x = M_{n,\,PMMA}$. At $w_{SMS} \geq 16$ wt%, $M_x = M_e/w_{PMMA}$. Assuming all PMMA chains bridge two cross-linking cores instead of looping back to the same one ($f$ = 1), the calculated plateau modulus values using eq 3.2 are shown as stars in Figure 3.11. Comparison of the calculated values to the measured ones yields bridging fractions of 0.26, 0.36, 0.54, 0.71, and 0.73 for gels with 10, 20, 30, 40, and 50 wt% SMS(17-86-17), respectively. At the lower concentration end, the values are comparable to previously reported gels.[16,17] For the gel with 40 and 50 wt% SMS(17-86-17), the fractions become higher. This is also reasonable, because at high polymer concentrations, differences between loops and bridges become diminished due to entanglement (on average 4 and 6 entanglements per chain for 40 and 50 wt% SMS, respectively), and bridging fractions calculated in this regime are not as meaningful as those extracted at the lower concentration end.

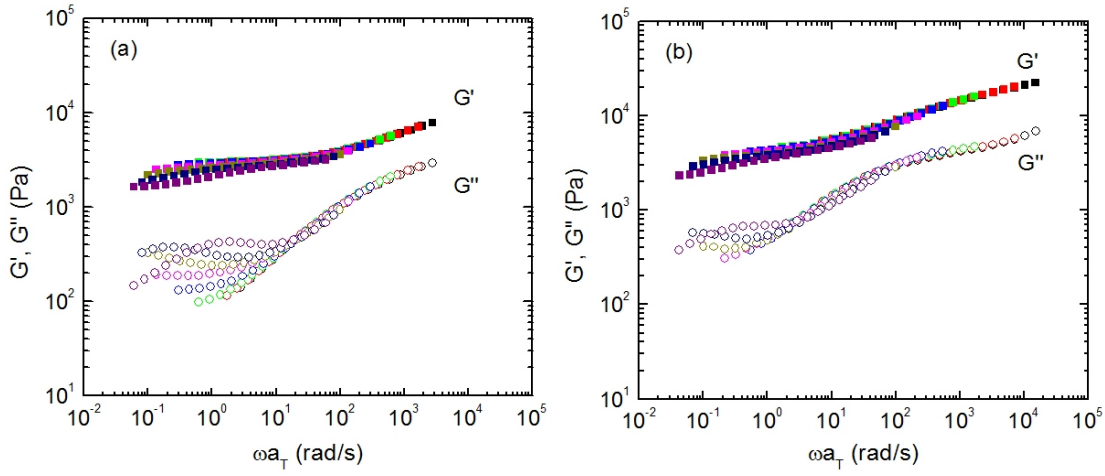


**Figure 3.9** tTS master curves of dynamic storage and loss moduli referenced to 120 °C for ion gels with (a) 20 wt% and (b) 30 wt% SMS(17-86-17) in the fast relaxation regime.

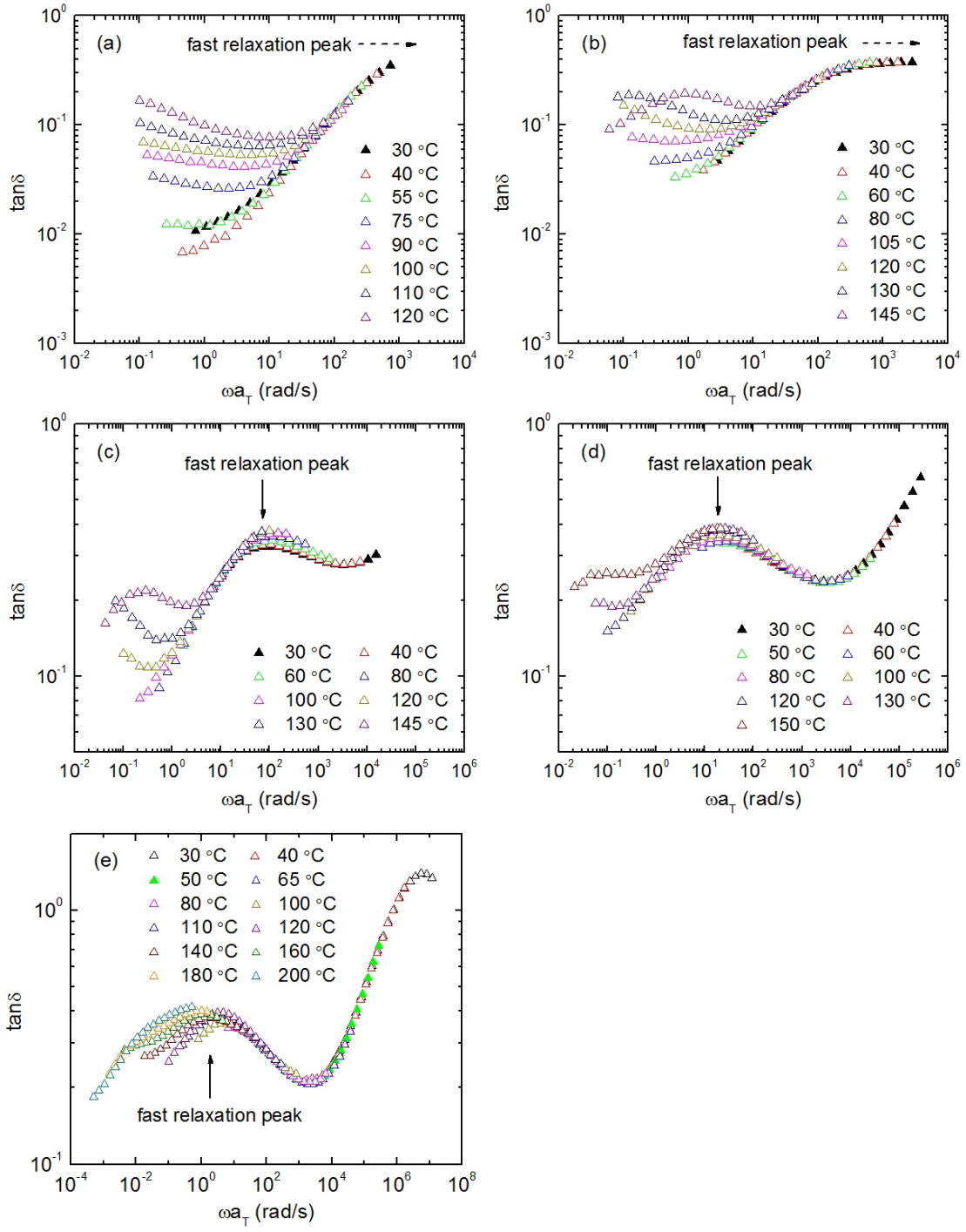


**Figure 3.10** tTS master curves of loss tangent referenced to 120 °C for ion gels with (a) 10 wt%, (b) 20 wt%, (c) 30 wt%, (d) 40 wt% and (e) 50 wt% SMS(17-86-17) in the fast relaxation regime. The color schemes for different temperatures correspond to those used in Figures 3.8 and 3.9. The data at temperatures from which the plateau modulus values were extracted are emphasized in solid symbols.

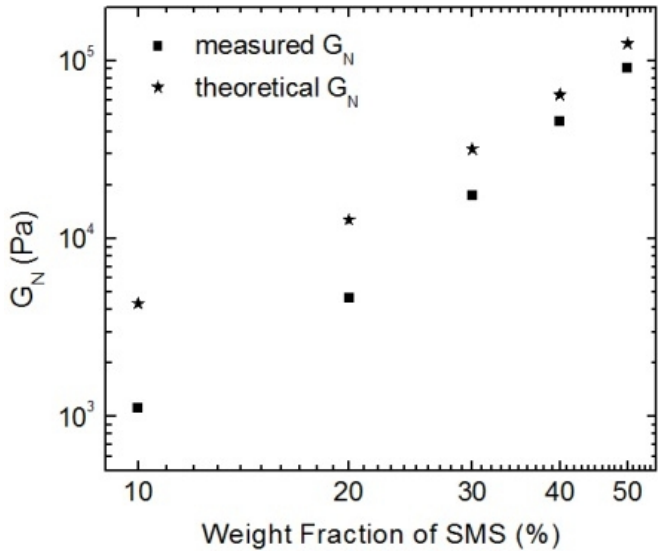


**Figure 3.11** Concentration dependence of plateau modulus ($G_N$) for ion gels with 10 – 50 wt% SMS(17-86-17).

As discussed previously, because of the relatively long S blocks, the large energy barrier associated with pulling the PS chains out of the cores through [EMI][TFSA] makes it highly unlikely for this process to occur even at elevated temperatures. SAXS measurements were performed at 140 °C to examine the morphology of the gels. As evidenced from the 1D profiles (Figure 3.12), no clear ordering occurred for the gels after 2 hours of annealing, consistent with the expectation that the cores cannot move rapidly enough to form an ordered structure without end-block pull-out. With regard to the length scales involved, the position of the structure factor peak at low $q$ shifts toward higher values with increasing SMS concentration (Table 3.2), indicating a decrease of the spacing between cross-links and therefore a "denser" network. The first minimum in $q$ (filled triangles in Figure 3.12), on the other hand, moves toward lower values with increasing SMS concentration, suggesting an increased core size or bigger crosslinks. The core radius can be calculated from the characteristic equation of the hard-sphere form

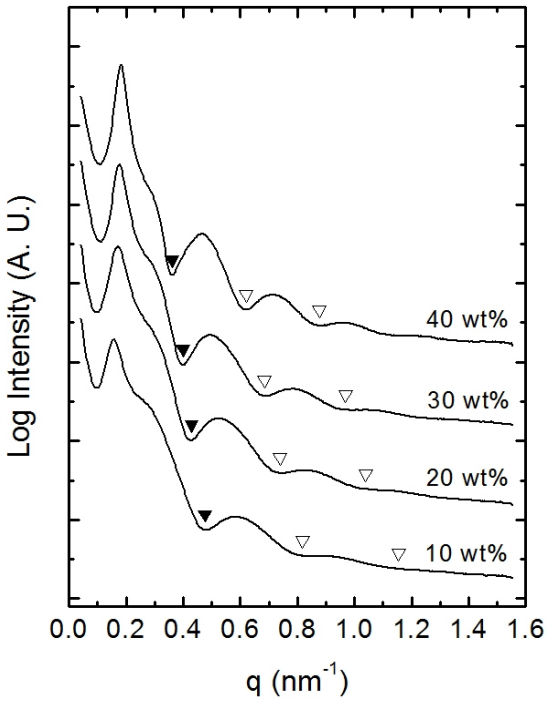


**Figure 3.12** 1D SAXS profiles for ion gels with 10, 20, 30, and 40 wt% SMS(17-86-17) at 140 °C. Filled triangles indicate positions of the 1st minimum in $q$ used to extract core radius. Open indicate positions of the 2nd and 3rd minima in $q$ calculated using the extracted core radius values.

factor, $\sin(qR_c) - qR_c\cos(qR_c) = 0$, with $qR_c = 4.493$ at the first minimum. The values are shown in Table 3.2. Applying the extracted core radius values, the expected second and third minima in $q$ were calculated and displayed as open triangles in Figure 3.12. The expected positions agree very well with the "valleys" observed in the profiles. Assuming no ionic liquid penetration into the cores, the aggregation number of the cores ($N_{agg}$) can be calculated:

$$\frac{4\pi R_c^3}{3} = \frac{2M_{n,PS}N_{agg}}{N_A\rho_{PS}} \tag{3.3}$$

where $M_{n,PS}$ is the number average molecular weight of the PS block, which is 17 kDa

for the polymer in question, and $\rho_{PS}$ is the density of PS, which is taken to be 1.05 g/cm$^3$. The computed values are displayed in Table 3.2.

**Table 3.2** Extracted Parameters from the SAXS Profiles of the SMS Ion Gels at 140 °C.

| SMS Content (wt%) | $q_{peak}$ (nm$^{-1}$) | 1st minimum in $q$ (nm$^{-1}$) | $R_c$ (nm) | $N_{agg}$ |
|---|---|---|---|---|
| 10 | 0.155 ± 0.003 | 0.476 ± 0.003 | 9.4 ± 0.1 | 65 ± 1 |
| 20 | 0.172 ± 0.003 | 0.429 ± 0.003 | 10.5 ± 0.1 | 89 ± 2 |
| 30 | 0.175 ± 0.003 | 0.400 ± 0.003 | 11.2 ± 0.1 | 111 ± 2 |
| 40 | 0.181 ± 0.003 | 0.361 ± 0.003 | 12.4 ± 0.1 | 150 ± 4 |

### 3.3.2 Comparison Between SOS and SMS Gels

Figure 3.13 displays the modulus master curves of the SMS(17-86-17) and SOS(3-35-3) gels with 40 wt% polymer referenced to 120 °C. Qualitatively, both gels exhibit two "plateau" regions: one with larger modulus at high frequencies (low temperatures) and the other with smaller modulus at low frequencies (high temperatures). This feature is universal for gels with polymer concentrations of 20 – 50 wt%. Although $G'$ of both kind of gels decreases by approximately equal amounts (more than an order of magnitude) over the frequency range shown, the relaxations that account for this drop are fundamentally different. For the SMS(17-86-17) gel, the drop in $G'$ is gradual and occurs over the entire frequency range. Comparison of this gel with a PMMA homopolymer solution showed that the decrease in $G'$ from ca. $10^5$ to $3\times10^4$ Pa (corresponding to a frequency range of ca. $3\times10^4$ to 100 rad/s on Figure 3.13a) is mainly due to the relaxation of PMMA strands within the ionic liquid, and further decrease in $G'$ can be attributed to

the relaxation of the PS chains (Figure 3.8b). This is qualitatively similar to the gel with 40 wt% SOS(6-35-6), for which two distinct relaxation modes can be distinguished. On the other hand, the drop in $G'$ for the SOS(3-35-3) gel is much sharper, and occurs mostly within two orders of magnitude in reduced frequency. This can be ascribed to the pull out of the PS chains. The different PS end-block behaviors of the gels are due to the different lengths of the end-blocks. For the SMS(17-86-17) gel, the end-blocks are long, resulting in a large $\chi N_{PS}$. This large thermodynamic barrier makes it unlikely for the PS blocks to be pulled out from the cross-linking cores. Therefore, the system maintains its network structure at elevated temperatures (corresponding to frequencies below 100 rad/s on Figure 3.13a), and the gradual decrease in modulus is due primarily to the motions of PS chains within the cores, and that of the cores within a disordered medium. On the other hand, since the PS blocks of the SOS(3-35-3) are short (small $\chi N_{PS}$), the PS chains can dissociate from the cores and diffuse into the PEO/[EMI][TFSA] matrix at high temperatures, resulting in a viscoelastic micelle solution without a persistent network

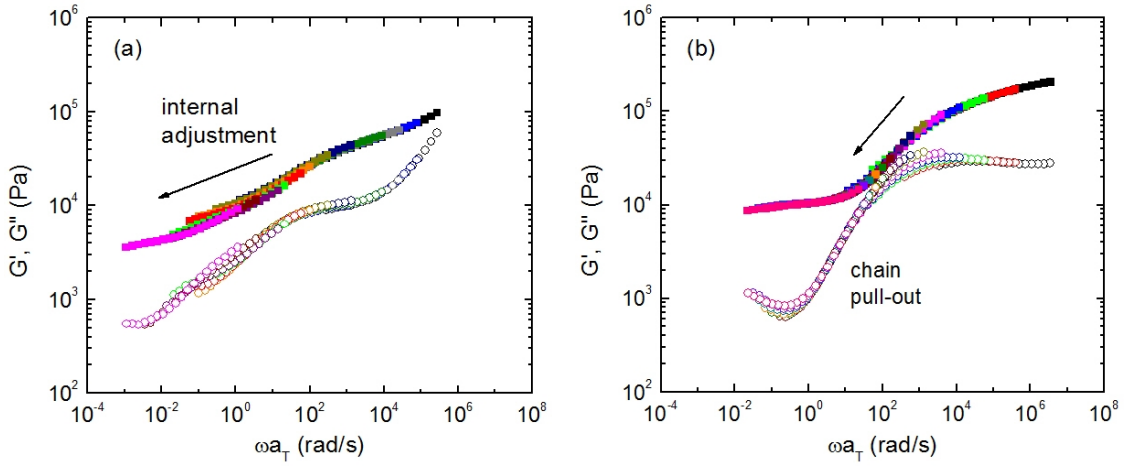


**Figure 3.13** Master curves of storage and loss moduli referenced to 120 °C for ion gels with (a) 40 wt% SMS(17-86-17) and (b) 40 wt% SOS(3-35-3).

structure.

## 3.4 Summary

In this chapter, the viscoelastic properties of ion gels based on SMS triblock copolymers and the ionic liquid [EMI][TFSA] were investigated over wide ranges of temperature and composition. The gels maintain their mechanical integrity up to at least 200 °C. Two relaxation modes were observed. The fast mode is associated with the relaxation of the mid-blocks in the ionic liquid, which is remarkably similar to that of free chains in homopolymer solutions. The slow mode is related to the motion of the end-blocks within their micellar cores, and of the cores within a disordered medium. SAXS results confirm that as temperature increases, stress is released through internal relaxation rather than end-block pull-out, due to the relatively long S end-blocks. Comparison between the SOS and SMS gels shows that the main contributing factor to qualitatively different viscoelastic behaviors is the length of the end-block.

## 3.5 References

(1) Brandrup, J.; Immergut, E. H.; Grulke, E. A. *Polymer Handbook*, 4th ed.; Wiley-Interscience: New York, 1999.

(2) Matyjaszewski, K.; Xia, J. *Chem. Rev.* **2001**, *101*, 2921-2990.

(3) Patten, T. E.; Xia, J.; Abernathy, T.; Matyjaszewski, K. *Science* **1996**, *272*, 866-868.

(4) Xia, J.; Matyjaszewski, K. *Macromolecules* **1997**, *30*, 7697-7700.

(5) Shipp, D. A.; Wang, J.-L.; Matyjaszewski, K. *Macromolecules* **1998**, *31*, 8005-8008.

(6) Zeroni, I.; Ozair, S.; Lodge, T. P. *Macromolecules* **2008**, *41*, 5033-5041.

(7) Susan, M. A. B. H.; Kaneko, T.; Noda, A.; Watanabe, M. *J. Am. Chem. Soc.* **2005**, *127*, 4976-4983.

(8) Hiemenz, P. C.; Lodge, T. P. *Polymer Chemistry*, 2nd ed.; CRC Press: New York, 2007.

(9) Tokuda, H.; Ishii, K.; Susan, M. A. B. H.; Watanabe, M. *J. Phys. Chem. B* **2005**, *109*, 6103-6110.

(10) Chapman, B. R.; Hamersky, M. W.; Milhaupt, J. M.; Kostelecky, C.; Lodge, T. P.; von Meerwall, E. D.; Smith, S. D. *Macromolecules* **1998**, *31*, 4562-4573.

(11) Tanaka, F.; Edwards, S. F. *Macromolecules* **1992**, *25*, 1516-1523.

(12) Choi, S.-H.; Bates, F. S.; Lodge, T. P. *J. Phys. Chem. B* **2009**, *113*, 13840-13848.

(13) Lai, C.; Russel, W. B.; Register, R. A. *Macromolecules* **2002**, *35*, 841-849.

(14) Mok, M.; Liu, X.; Bai, Z.; Lei, Y.; Lodge, T. P. *Macromolecules* **2011**, *44*, 1016-1025.

(15) Fetters, L. J.; Lohse, D. J.; Richter, D.; Witten, T. A.; Zirkel, A. *Macromolecules* **1994**, *27*, 4639-4647.

(16) He, Y.; Boswell, P. G.; Buhlmann, P.; Lodge, T. P. *J. Phys. Chem. B* **2007**, *111*, 4645-4652.

(17) Annable, T.; Buscall, R.; Ettelaie, R.; Whittlestone, D. *J. Rheol.* **1993**, *37*, 695-726.

# Chapter 4

# Electrical Properties of Ion Gels and Polymer/Ionic Liquid Solutions*

## 4.1 Introduction

In this chapter, the electrical properties of block copolymer-based ion gels formed by the self-assembly of poly(styrene-*b*-ethylene oxide-*b*-styrene) (SOS) and poly(styrene-b-methyl methacrylate-b-styrene) (SMS) in the ionic liquid 1-ethyl-3-methylimidazolium bis(trifluoromethylsulfonyl)amide ([EMI][TFSA]) were examined in the ionic-liquid-rich composition regime over wide temperature ranges. AC impedance spectroscopy was utilized to measure the response of the gels within the frequency regime of ionic motions. Important parameters including the glass transition temperature, ionic conductivity, specific capacitance, as well as the *RC* time constant of the gels were determined. Additionally, the effect of the cross-links on ionic conduction was investigated by comparing the gels with homopolymer solutions at similar midblock concentrations. As discussed in Chapters 2 and 3, introducing the cross-links leads to very different modulus of the gels from the homopolymer solutions, especially at low reduced frequencies. However, its effect on ionic conduction turns out to be minimal. Combining considerations on modulus, electrical properties, and thermal reversibility, basic design criteria of the triblock can be formulated to meet specific property requirements of the ion

---

* Reproduced in part with permission from Zhang, S.; Lee, K. H.; Frisbie, C. D.; Lodge, T. P. *Macromolecules* **2011**, *44*, 940-949, and Zhang, S.; Lee, K. H.; Sun, J; Frisbie, C. D.; Lodge, T. P. *Macromolecules* **2011**, *44*, 8981-8989. 

gels.

## 4.2 Experimental

### 4.2.1 Materials

The SOS, SMS, poly(methyl methacrylate) (PMMA) polymers and [EMI][TFSA] were synthesized and characterized as described in Chapters 2 and 3. The polymers are denoted as SOS(3-35-3), SMS(17-86-17), and PMMA(126), with the numbers in parentheses indicating the number average molecular weights in kg/mol. The poly(ethylene oxide) (PEO) polymer used to prepare PEO/[EMI][TFSA] solutions was the precursor for the synthesis of SOS(3-35-3), and is thus denoted PEO(35).

All ion gels and homopolymer solutions were prepared by mixing weighed amounts of the respective polymer and the ionic liquid in $CH_2Cl_2$ cosolvent. After stirring for 2 hours, the mixtures were purged with nitrogen gas for a day to evaporate most of the cosolvent. Finally, the samples were placed in a vacuum oven at ca. 70 °C for 2 days to completely remove the cosolvent. To avoid any effects of moisture, all samples were kept in a vacuum desiccator and were dried in a vacuum oven at ca. 70 °C for a day before any measurements were carried out.

### 4.2.2 Impedance Spectroscopy

Impedance measurements were conducted on an ARES rheometer (Rheometric Scientific) connected to an Agilent 4284A LCR bridge (TA instruments) using stainless steel parallel plates with 25 mm diameter. For samples requiring 50 mm diameter plates for rheology, *i.e.*, gels with 10 wt% polymer, the solution with 5 wt% PMMA(126), and

the solution with 8 wt% PEO(35), impedance measurements were conducted on different samples than those used for rheology. Otherwise, all measurements were performed on the same sample with a gap spacing of approximately 1 mm. The parallel plates were used as fabricated without further surface treatment. At each temperature, following rheological measurements, complex impedance was measured at a shear frequency of 10 rad/s using an AC signal of 0.1 V amplitude in the electrical frequency range of 20 – $2\times10^6$ Hz. The shear frequency was set to 10 rad/s because the instrument requires that impedance data be recorded at a finite shear frequency. There was no dependence of impedance on shear frequency between 1 – 100 rad/s. Temperatures were controlled to within 0.2 °C of the set points with an environmental control circulator under a nitrogen atmosphere.

For gels with 10 wt% polymer, the solution with 5 wt% PMMA(126), and the solution with 8 wt% PEO(35), impedance measurements were also performed with a homemade cell using a Solartron 1255B frequency response analyzer connected to a Solartron SI 1287 electrochemical interface. Frequency sweeps were conducted from 1 – $10^6$ Hz with an AC amplitude of 10 mV. The cell is composed of a Teflon spacer with an inner diameter of 4 mm and a thickness of 2 mm sandwiched between two platinum coated stainless steel electrodes. Temperatures were controlled to within 0.5 °C of the set points with a thermostated water bath. The samples were thermally equilibrated for 30 min prior to the measurements. Conductivity of a sample with 20 wt% SMS(17-86-17) was cross-checked; the value obtained from this instrument agrees with that measured on ARES at room temperature.

### 4.2.3 Differential Scanning Calorimetry (DSC)

Thermal transitions were measured using a TA Instruments Q1000 Differential Scanning Calorimeter with liquid $N_2$ cooling capability. Samples weighing ca. 5 – 10 mg were sealed in hermetic aluminum pans, heated up to 180 °C (SMS gels) or 160 °C (SOS gels), and equilibrated for 3 min to remove prior thermal history. They were then cooled rapidly to –150 °C, and heated back up to 180 °C (SMS gels) or 160 °C (SOS gels) at 10 °C/min. The heating rate for the ion gel with 50 wt% SMS was 20 °C/min. Thermograms were taken from the second heating cycle.

## 4.3 Results and Discussion

### 4.3.1 Complex Conductivity Spectra

The impedance of the SMS(17-86-17) and SOS(3-35-3) based gels were measured over the temperature range of 25 °C – 200 °C and 25 °C – 160 °C, respectively. Figure 4.1 displays the normalized complex conductivity spectra ($\sigma'$ and $\sigma''$) of the ion gel with 40 wt% SMS(17-86-17), referenced to 120 °C. The data were horizontally shifted by the ratios of *RC* time constants at other temperatures ($\tau_{RC}$) to that at the reference temperature ($\tau_{RC,\ ref}$), where the *RC* time constant corresponds to the maximum of the $\sigma''$ versus frequency curve which shifts as a function of temperature. Further discussion of $\tau_{RC}$ is deferred until later. In Figure 4.1, the spectra at different temperatures overlay quite well, indicating that time temperature superposition (tTS) holds for the gel with 40 wt% SMS(17-86-17). If the stainless steel electrodes are considered to be ideally polarizable within the electrochemical window of [EMI][TFSA], the cell can be represented by a

resistor with solution resistance $R$ in series with a capacitor with double-layer capacitance $C$.[1] Therefore, the total impedance ($Z^*$) of the system is

$$Z^* = Z' - iZ'' = R + (i\omega C)^{-1} \tag{4.1}$$

Equivalently, the complex conductivity ($\sigma^*$) can be expressed as

$$\sigma^* = \frac{l}{A[R + (i\omega C)^{-1}]} \tag{4.2}$$

where $l$ is the sample thickness and $A$ is the electrode area. The DC conductivity $\sigma$ (or solution resistance $R$) can be obtained from the high frequency plateau in $\sigma'$ where the gel is purely resistive. The capacitance $C$ can be calculated from $Z''$ via eq 4.1. It is known, however, that the electrical behavior of solid electrode interfaces usually deviates from that of an ideal capacitor in the sense that capacitance is frequency dependent.[2] Two common methods have been utilized to account for this capacitance dispersion phenomenon. One is to calculate the capacitance at a selected frequency of interest, and the other is to model it by a constant phase element (CPE) with impedance $Z_{CPE} = Q(i\omega)^{-(1-\alpha)}$, where $Q$ and $\alpha$ are positive constants, in order to eliminate the frequency dependence.[3-5] The origin of CPE behavior was first attributed to current density inhomogeneities caused by surface roughness, which depend primarily on a geometric roughness factor. However, later it was reported that this view contradicted measurements performed on rough platinum electrodes, and CPE behavior is mainly due to specific ion adsorption, and possibly broad distributions of time constants associated with these processes.[4,5] Replacing the capacitor with a CPE in the equivalent circuit, the complex conductivity can then be written as

$$\sigma^* = \frac{l}{A[R + Q(i\omega)^{-(1-\alpha)}]} \tag{4.3}$$

In this case, the CPE is physically equivalent to an *RC* ladder due to the uneven charging and discharging of the EDLs,[3] and an effective capacitance as defined by eq 4.1 can be calculated from *R* and the fitting parameters:

$$C = (R^{\alpha}Q^{-1})^{1/(1-\alpha)} \tag{4.4}$$

As shown in Figure 4.1, eq 4.3 describes the data better than eq 4.2, especially at low frequencies where the capacitive contribution dominates. Overall, fitting $\sigma^*$ of both SOS and SMS gels with 10 – 50 wt% polymer with eq 4.3 yields $\alpha$ values in the range of 0.10 – 0.25, which are comparable to those reported for stainless steel in contact with aqueous

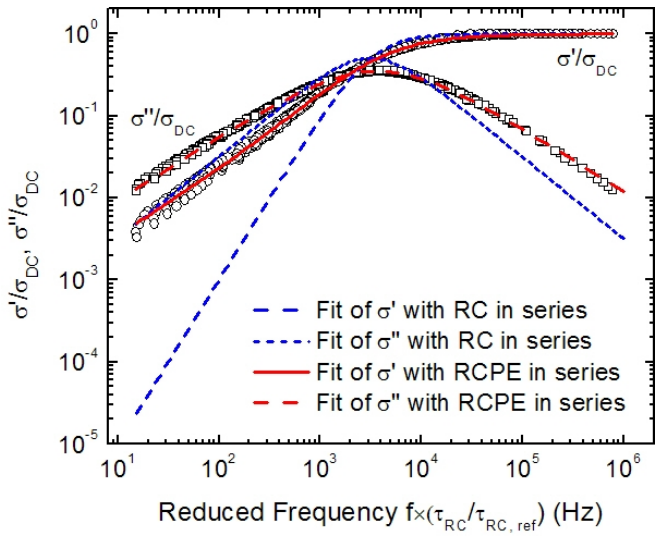


**Figure 4.1** Complex conductivity of SMS/[EMI][TFSA] ion gel with 40 wt% SMS (17-86-17) measured over the temperature range of 30 – 200 °C referenced to 120 °C. The data have been horizontally shifted by $\tau_{RC}/\tau_{RC,\ 120\ °C}$. $\tau_{RC}$ corresponds to the maximum in the $\sigma''$ versus frequency curve. The vertical shifts are the DC conductivities of the gel at different temperatures. Curves include data measured at 12 temperatures.

solutions.[6,7] For both SMS(17-86-17) and SOS(3-35-3) based gels at concentrations below 30 wt% polymer, $\alpha$ decreases with temperature significantly above 40 °C, and tTS fails on the low frequency side of the spectra (not shown).

Clearly, $Q$ and $\alpha$ are related to the phase angle between $Z'$ and $Z''$:

$$\tan\phi = \frac{Z'}{Z''} = \frac{R + \omega^{-(1-\alpha)} Q \sin(\alpha\pi/2)}{\omega^{-(1-\alpha)} Q \cos(\alpha\pi/2)} \tag{4.5}$$

where $\tan\phi$ is the dissipation factor, and $i^{\alpha} = \cos(\alpha\pi/2) + i\sin(\alpha\pi/2)$. In the limit where $\alpha = 0$, $C = 1/Q$ (eq 4.4), and $\tan\phi = \omega RC$ (eq 4.5), which means that the equivalent circuit is $RC$ in series. Figure 4.2 shows the temperature dependence of the dissipation factor at 1 kHz, a diameter of 25 mm, and a thickness of 1 mm, calculated using eq 4.5, for all the ion gels measured. It appears that the dissipation factor for the SMS gels decreases with

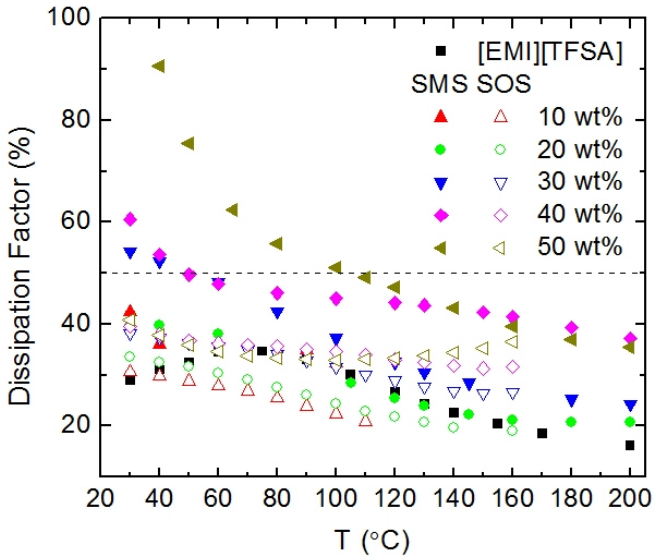


**Figure 4.2** Dissipation factor calculated using an RCPE series circuit (eq 4.5) at 1 kHz, a thickness of 1 mm, and an electrode diameter of 25 mm for [EMI][TFSA] and the ion gels. The dashed line indicates where the electrolyte dissipates half the energy supplied.

increasing temperature, whereas for the SOS gels this trend is less obvious, especially at higher polymer concentrations. Moreover, the dissipation factor tends to be smaller for the SOS gels, due to their higher ionic conductivity and therefore lower resistance (Section 4.3.3). Overall, the dissipation factor values are very large, with most of the gels lying in the region of 15– 35%. Evidently, in actual devices the dielectric would not have such enormous dimensions, and the electrode surface would be smoother and cleaner than the untreated stainless steel ones used here, which would result in lower resistance, lower $\alpha$, and hence smaller dissipation factors. However, this calculation stresses the potential energy loss problem with application of electrolytes as dielectrics.

### 4.3.2 Glass Transition of the Conducting Phase

It has been reported that the temperature dependence of $\sigma$ for both [EMI][TFSA] and ion gels with chemically cross-linked PMMA follows the Vogel-Fulcher-Tammann (VFT) equation:[8]

$$\sigma = \sigma_0 \exp[-B/(T-T_0)] \tag{4.6}$$

where $\sigma_0$ is a prefactor, $B$ is a constant related to the entropic barrier of conduction, and $T_0$ is the Vogel temperature, which is lower than the calorimetric glass transition temperature ($T_g$). Therefore, comparison of ionic conductivity for gels with different mid-blocks would not be meaningful without reference to the $T_g$ of the conducting phase.

Figures 4.3 and 4.4 display the heat flow and derivative of heat flow thermograms for gels with 10 – 50 wt% SMS(17-86-17) and SOS(3-35-3). No transitions of the PS insulating phase were observed, likely due to the small amount of end-blocks present in the samples. For [EMI][TFSA] and the gel with 10 wt% SOS(3-35-3), the samples

display recrystallization and melting peaks. No crystallization was observed for other samples. The steps in the heat flow curves (arrows in Figure 4.3a for clarity) that are associated with the glass transition transform into peaks in the heat flow derivative curves, making it easier to extract the breadth of the transition.[9,10] For gels composed of both polymers, the glass transition is shifted toward higher temperatures with the addition of polymer. For the SMS gels, the glass transition loses its sharpness with the addition of 30 wt% or more SMS(17-86-17), accompanied by broadened transition widths. By 50 wt% SMS(17-86-17), the transition appears to be bimodal (arrows in Figure 4.4a). This effect is much less evident for the SOS(3-35-3) gels.

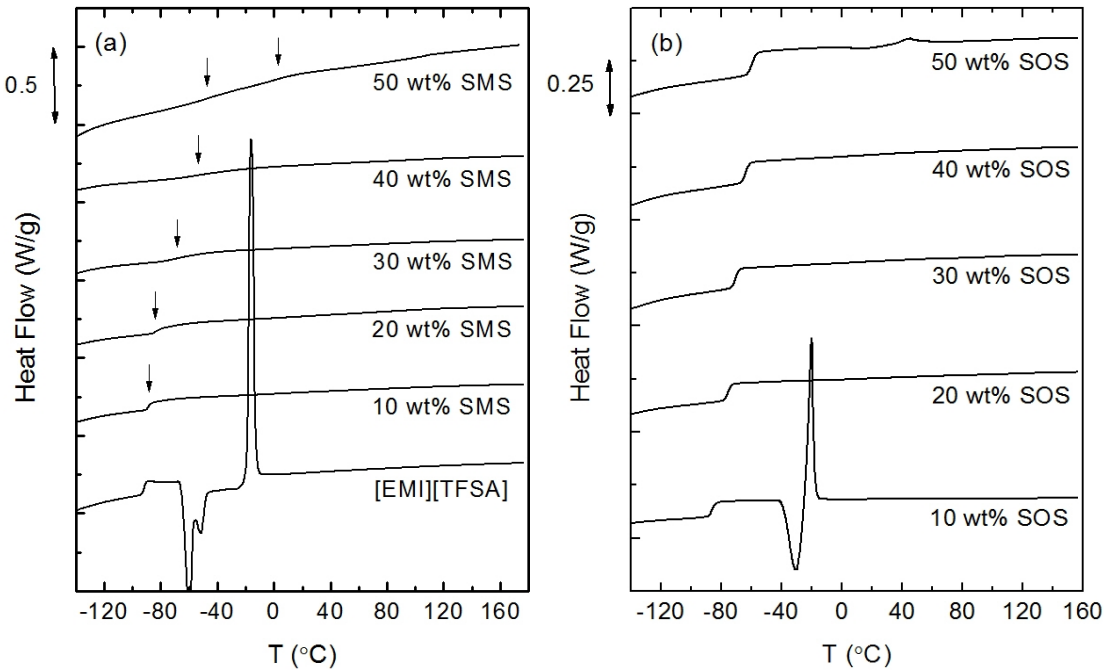


**Figure 4.3** DSC heat flow curves of (a) [EMI][TFSA] and SMS(17-86-17) ion gels and (b) SOS(3-35-3) ion gels with different weight fractions of polymer. Data at different polymer concentrations were shifted vertically for clarity. Arrows in (a) indicate the positions of the steps.

Quantitatively, the $T_g$ values were determined from the peak maxima of the heat flow

derivative curves, and are plotted in Figure 4.5 and listed in Table 4.1. Associated $\Delta T_g$

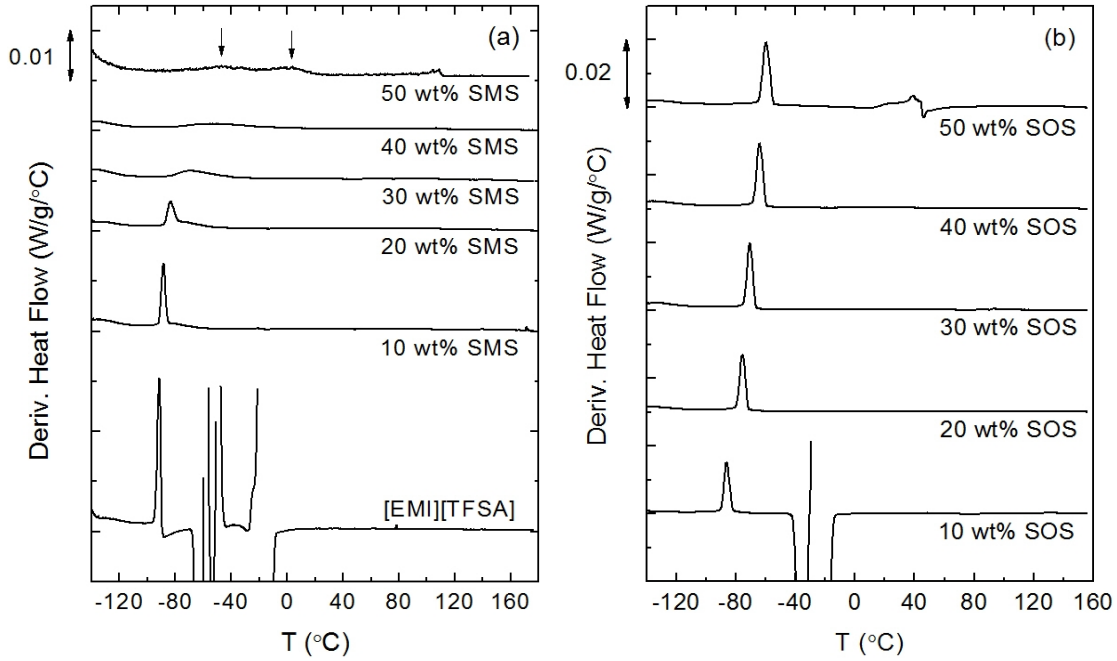


**Figure 4.4** DSC derivative of heat flow curves of (a) [EMI][TFSA] and SMS(17-86-17) ion gels and (b) SOS(3-35-3) ion gels with different weight fractions of polymer. Data at different polymer concentrations were shifted vertically for clarity. Arrows in (a) indicate the positions of the two $T_g$'s for the gel with 50 wt% SMS(17-86-17).

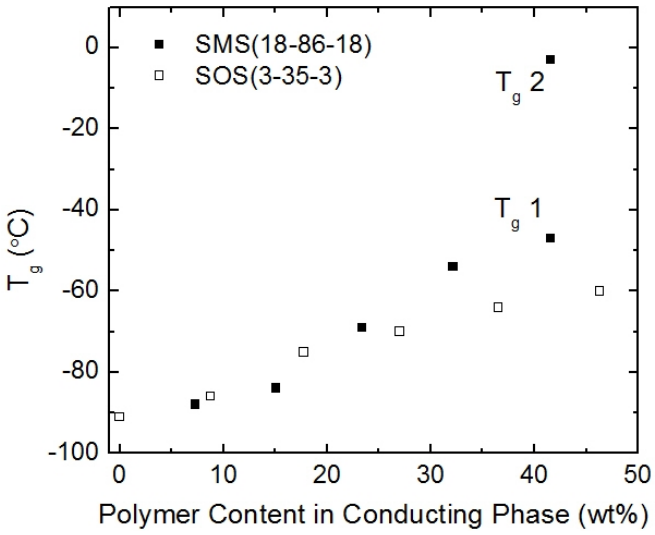


**Figure 4.5** Variation of $T_g$ with polymer fraction for SMS(17-86-17)/[EMI][TFSA] and SOS(3-35-3)/[EMI][TFSA] ion gels.

values were determined from the onsets and ends of deviation from the derivative heat flow curve baselines, and are listed in Table 4.1. The weight fractions of the midblocks in the ionic liquid were used as concentration values to construct Figure 4.5, so as to make a direct comparison with respect to the ionically conducting phase. It is clear from Figure 4.5 that $T_g$ of the ionic liquid phase increases more rapidly with the addition of SMS(17-86-17) than of SOS(3-35-3). This is reasonable since PMMA has a much higher $T_g$ than PEO. Moreover, by 50 wt% SMS(17-86-17), two $T_g$s are present. This is consistent with results reported for PMMA/[EMI][TFSA] solutions[11] and can be attributed to effective PMMA-rich and [EMI][TFSA]-rich local concentrations that arise from chain connectivity and are at length scales relevant to $T_g$ dynamics.[12]

**Table 4.1** Glass Transition Temperatures ($T_g$) and Associated Transition Ranges for [EMI][TFSA] and the Ion Gels.

| Polymer | Polymer Content (wt%) | $T_g$ (±2 °C) | onset (±5 °C) | end (±5 °C) | $\Delta T_g$ |
|---|---|---|---|---|---|
| | 0 | –91 | –96 | –89 | 7 |
| SMS(17-86-17) | 10 | –88 | –95 | –58 | 37 |
| | 20 | –84 | –92 | –40 | 52 |
| | 30 | –69 | –89 | –20 | 69 |
| | 40 | –54 | –83 | –6 | 77 |
| | 50[a] | –47, 3 | –81, –16 | –23, 20 | 51, 36 |
| SOS(3-35-3) | 10 | –86 | –91 | –81 | 10 |
| | 20 | –75 | –88 | –66 | 22 |
| | 30 | –70 | –83 | –63 | 20 |
| | 40 | –64 | –78 | –52 | 26 |
| | 50 | –60 | –79 | –49 | 30 |

[a] Heating rate is 20 °C/min.

### 4.3.3 Ionic Conductivity

Figure 4.6 shows the ionic conductivity as a function of temperature for SMS(17-86-17) and SOS(3-35-3) based gels. The conductivity of bulk [EMI][TFSA] from a previous report[13] is also plotted for comparison. The conductivity data were fit to eq 4.6, as shown by the dashed lines. The fitting parameters are displayed in Tables 4.2. The temperature

dependence of $\sigma$ for both gels with 10 wt% polymer nearly tracks that of the neat ionic liquid, while $\sigma$ becomes more temperature dependent as more polymer is added. This effect is more clearly observed in Figure 4.7, where the conductivity normalized with respect to neat [EMI][TFSA] is plotted versus volume fraction of midblocks within the ionic liquid, at selected reduced temperatures. At a triblock concentration of 10 wt%, the conductivity is reduced by about 30% for the SOS(3-35-3) gel and by about 36% for the SMS(17-86-17) gel from the pure ionic liquid. These values compare well with previously reported conductivities for both physically cross-linked gels with a PEO mid-block (ca. 30% – 40% decrease)[14,15] and the ion gel with chemically cross-linked PMMA (ca. 40% decrease).[8] Moreover, despite the huge difference in $T_g$, differences in molecular weight and volume fraction of the bridging polymers, the conductivity values with addition of 10 wt% SOS(3-35-3) and SMS(17-86-17) are very similar over the temperature range of 25 – 100 °C. These observations are consistent with the expectation that in a moderately dilute polymer solution, the relaxation of the polymer chains scales with the solvent viscosity, while the solvent motion is only weakly affected by polymer. As more SMS(17-86-17) is added, the glassy PMMA block ($T_g$ ~ 110 °C)[16] increases the glass transition temperature and broadens the DSC glass transition widths (Figure 4.5 and Table 4.1). Therefore, at higher SMS(17-86-17) concentrations, the temperature range (starting from 30 °C) where conductivity was measured becomes closer to the glass transition of the conducting PMMA/[EMI][TFSA] phase, with a difference as low as 27 degrees at 50 wt% SMS, leading to a more temperature dependent ionic conductivity. On the other hand, since PEO is very flexible ($T_g$ ~ –60 °C),[16] this effect is much weaker and

the measured temperature range stays well above the glass transition even with 50 wt% addition of SOS(3-35-3) (Figure 4.5 and Table 4.1), which results in much less temperature dependent ionic conductivity of the SOS(3-35-3) based gels than the SMS(17-86-17) based ones. Note that even though the selected reduced temperatures of the SMS and SOS gels are the same in Figure 4.7, the glass transition ranges of the SMS gels are much wider than the SOS gels (Figure 4.4 and Table 4.2). With the glass transition starting at higher temperatures for the SMS gels, a steeper decrease of normalized conductivity versus reduced temperature is not surprising.

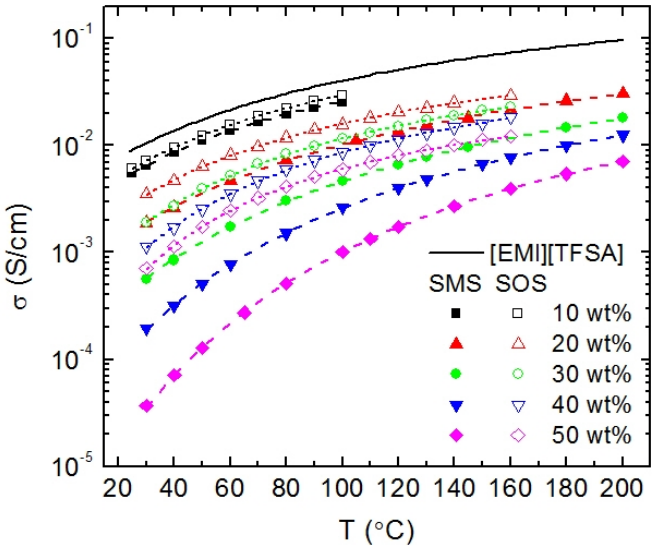


**Figure 4.6** Temperature dependence of ionic conductivity for [EMI][TFSA][13] and the ion gels. Closed and open symbols represent data for the SMS(17-86-17) and SOS(3-35-3) gels, respectively. Dashed lines are best fits using eq 4.6.

**Table 4.2** Vogel-Fulcher-Tammann (VFT) Fitting Parameters of Ionic Conductivity for the Ion Gels.

$$\sigma = \sigma_0 \exp[-B/(T-T_0)]$$

| Polymer | Polymer Content (wt%) | $\sigma_0$ (mS/cm) | $B$ (K) | $T_0$ (K) |
|---|---|---|---|---|
| SMS(17-86-17) | 10 | 246 ± 15 | 416 ± 18 | 189 ± 3 |
| | 20 | 324 ± 32 | 747 ± 45 | 157 ± 6 |
| | 30 | 321 ± 28 | 900 ± 40 | 161 ± 5 |
| | 40 | 258 ± 8 | 888 ± 13 | 180 ± 1 |
| | 50 | 270 ± 7 | 1040 ± 12 | 187 ± 1 |
| SOS(3-35-3) | 10 | 325 ± 31 | 451 ± 28 | 185 ± 4 |
| | 20 | 188 ± 17 | 452 ± 31 | 190 ± 6 |
| | 30 | 164 ± 14 | 458 ± 29 | 200 ± 5 |
| | 40 | 133 ± 11 | 448 ± 27 | 210 ± 4 |
| | 50 | 71 ± 4 | 370 ± 16 | 223 ± 3 |

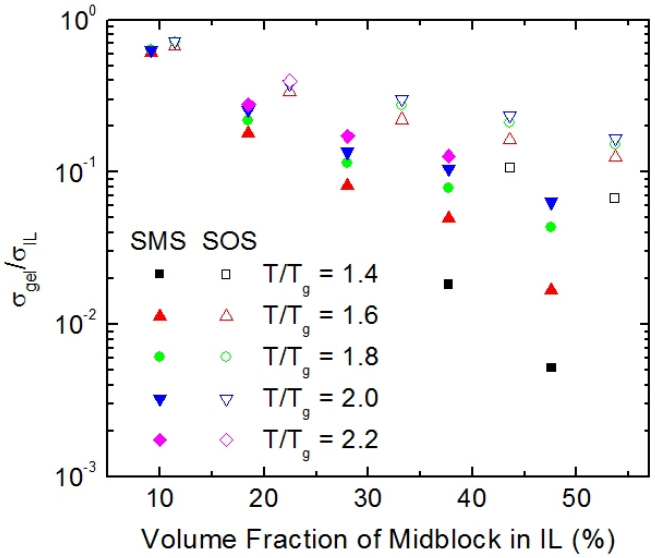


**Figure 4.7** Ionic conductivity normalized with respect to neat [EMI][TFSA] for the SMS(17-86-17) and SOS(3-35-3) based ion gels at selected reduced temperatures ($T/T_g$'s). The lower $T_g$ was chosen for the SMS gel with 50 wt% polymer, which is associated with the ionic liquid rich local concentrations.

Since the PS blocks are introduced mainly to provide mechanical support to the ion gels, it is important to understand the effect they exert on ionic conduction. Figure 4.8 displays the ionic conductivity ratio ($\sigma_{gel}/\sigma_{solution}$) of both the SMS(17-86-17) and SOS(3-35-3) gels to homopolymer solutions having similar PMMA or PEO content, versus the volume fraction of the PS micelles. The total polymer concentrations range from 5 – 50 wt%, and the selected temperatures vary from 25 ºC to 200 ºC. Consequently, the actual conductivities vary by over a factor of 400 (Figures 4.6 and 4.7). However, the reduction of $\sigma$ for the gels with respect to the equivalent solutions is within a factor of 2.1 for both triblocks over the entire composition and temperature ranges investigated, and decreases with increasing volume fraction of PS micelles. This important result highlights the fact that the act of introducing the micellar crosslinks has a negligible effect on conductivity,

while the effect on the low frequency modulus is dramatic, as discussed in Chapters 2 and 3.

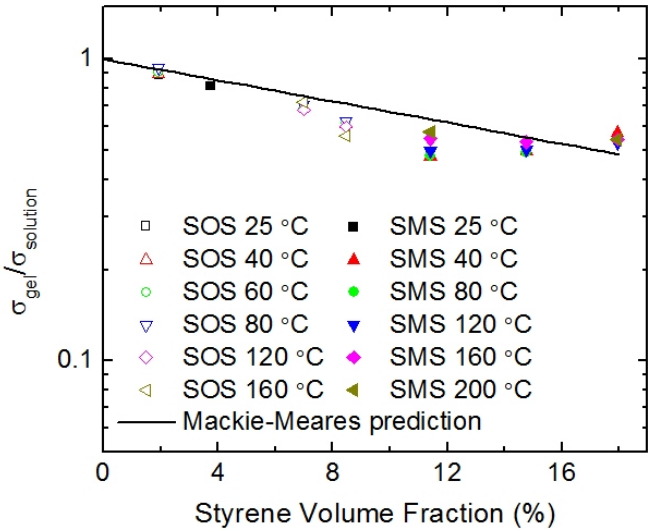


**Figure 4.8** Ionic conductivity ratio of the ion gels to the homopolymer solutions versus volume fraction of styrene in the gels at selected temperatures. The polymer concentrations in the gels and solutions corresponding to the styrene volume fractions from low to high are: 10 wt% SOS(3-35-3) versus 8 wt% PEO(35), 10 wt% SMS(17-86-17) versus 5 wt% PMMA(126), 40 wt% SOS(3-35-3) versus 34 wt% PEO(35), 50 wt% SOS(3-35-3) versus 43 wt% PEO(35), 30 wt% SMS(17-86-17) versus 20 wt% PMMA(126), 40 wt% SMS(17-86-17) versus 30 wt% PMMA(126), and 50 wt% SMS(17-86-17) versus 40 wt% PMMA(126).

The dependence of $\sigma_{gel}/\sigma_{solution}$ on the volume fraction of PS agrees well with the prediction based on an obstruction model developed by Mackie and Meares (solid line in Figure 4.8).[17] In a hypothetical lattice randomly occupied by equally sized polymer chain segments and solvent molecules, assuming that solvent diffusion occurs through lattice sites unoccupied by the polymer, the ratio of diffusion coefficient in the gel ($D_g$) to that of the neat solvent ($D_0$) can be written as[18]

$$\frac{D_g}{D_0} = \left(\frac{1-\phi}{1+\phi}\right)^2 \tag{4.7}$$

where $\phi$ is the polymer volume fraction. For the ion gels, the conducting domain consists of both the mid-blocks and the ionic liquid, and the insulating PS cores obstruct the ion pathways. Therefore, the conducting phase is taken to be the "solvent". Assuming the number density of conducting ions is the same for the gel and the homopolymer solution, the conductivity ratio of the two can be expressed in the same way as the diffusion coefficient:

$$\frac{\sigma_{gel}}{\sigma_{solution}} = \left(\frac{1-\phi}{1+\phi}\right)^2 \tag{4.8}$$

The agreement between theory and experiment is quite remarkable considering the simple assumptions of the Mackie-Meares model, combined with the wide temperature and concentration ranges measured.

### 4.3.4 Double-Layer Capacitance

Figure 4.9 shows the sheet capacitance for [EMI][TFSA], SMS(17-86-17) and SOS(3-35-3) based gels calculated from the fitting parameters, assuming an equivalent RCPE series circuit. The specific capacitance for [EMI][TFSA] can be roughly estimated using the Gouy-Chapman theory:

$$C = \frac{\varepsilon\varepsilon_0}{\lambda} \tag{4.9}$$

where $\varepsilon$ is the relative permittivity, $\varepsilon_0$ is the vacuum permittivity, and $\lambda$ is the Debye length, which is given by[1]

$$\lambda = \sqrt{\frac{\varepsilon\varepsilon_0 k_B T}{e^2 \sum_i z_i^2 n_i}} \tag{4.10}$$

where $k_B$ is Boltzmann constant, $e$ is the magnitude of the charge of an electron, $z_i$ is the charge number of species $i$, and $n_i$ is the number density of species $i$. For [EMI][TFSA] at room temperature, taking $\varepsilon \sim 12$[19,20], $z_{[EMI]} = z_{[TFSA]} = 1$, and $n_{[EMI]} = n_{[TFSA]} \sim 1.5\times10^{21}$ $cm^{-3}$,[8] the calculated Debye length is 0.076 nm and the capacitance is 140 μF/cm$^2$. This calculated Debye length is clearly unphysical since it is smaller than the ionic radii of the component ions. Measurement of forces along ionic liquid/mica interfaces showed that the effective Debye lengths of ionic liquids are on the order of 1 – 4 nm,[21] which agree with other reported EDL thickness values of around 1 nm for ionic liquids.[22] Thus, more meaningful estimated capacitance values should be about 3 – 11 μF/cm$^2$. These are close to those measured at Pt,[23] Au,[24] dropping mercury[25] and glassy carbon electrodes.[24,25] Recently, it has been reported that the capacitance of EDLs formed at metal/ionic conductor interfaces can be even higher than the prediction based on the Gouy-Chapman theory, due to possible binding of the ions to their image charges in the metal.[26] However, the capacitance measured here is smaller (< 1 μF/cm$^2$ at 30 °C) than the Gouy-Chapman prediction. This difference possibly originates from the nature of the stainless steel electrodes, and calculating capacitance from fitting over the entire frequency range (20 Hz – 2 MHz). The possible effect of the roughness of the electrodes is an important point. Measurements of identical gel samples containing 10 wt% SMS(17-86-17) with evaporated platinum contacts on a different impedance apparatus (described in the experimental section) yield $C \sim 6$ μF/cm$^2$ at 1 Hz at 30 °C. Figure 4.10 displays the

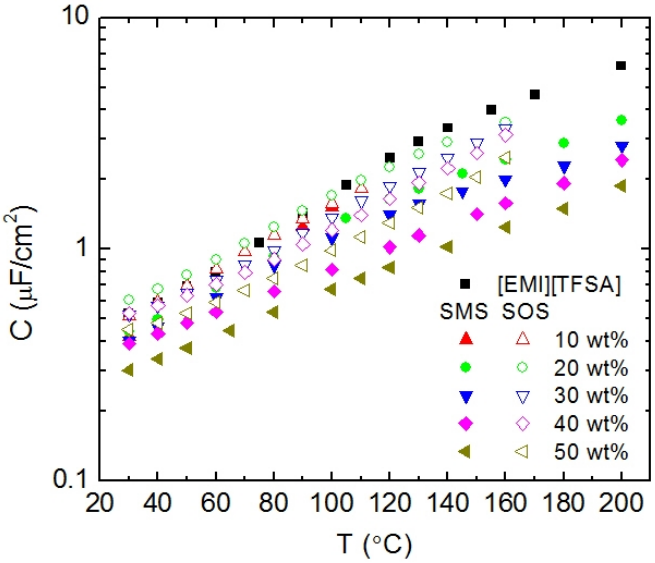


**Figure 4.9** Capacitance calculated from RCPE series circuit fits for [EMI][TFSA], SMS(17-86-17)/[EMI][TFSA] and SOS(3-35-3)/[EMI][TFSA] ion gels. The fits were performed over a frequency range of 20 Hz to 1 MHz.

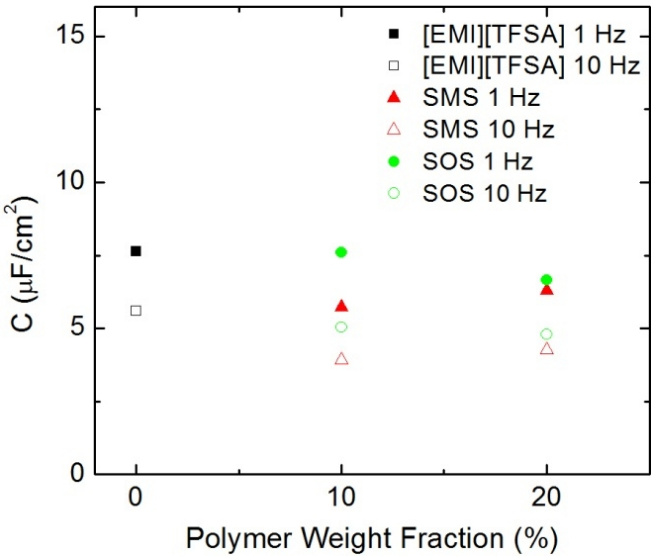


**Figure 4.10** Capacitance calculated from eq 4.1 at 1 and 10 Hz for [EMI][TFSA], SMS(17-86-17)/[EMI][TFSA], and SOS(3-35-3)/[EMI][TFSA] ion gels at room temperature.

capacitance calculated at 1 and 10 Hz for [EMI][TFSA] and ion gels with 10 and 20 wt%

SMS(17-86-17) and SOS(3-35-3) measured at room temperature. It is evident that at 1 Hz, the capacitance values for the ionic liquid and both gels are above 5 $\mu F/cm^2$, much higher than those calculated from fitting with an RCPE equivalent circuit. Thus, the method we have chosen to determine capacitance (namely, by fitting the entire frequency range up to 2 MHz using rough electrodes) has suppressed the values of *C* that one would determine under more "steady state" conditions.

It is evident from Figure 4.9 that capacitance increases with temperature for both [EMI][TFSA] and the ion gels, with the SOS(3-35-3) gels exhibiting slightly higher capacitance than the SMS(17-86-17) gels at the same polymer concentration. The same trend of capacitance versus temperature has been reported for a number of imidazolium based ionic liquids[27–30] and high temperature molten salts.[31,32] This contradicts the predictions of the Gouy-Chapman theory, since capacitance should decrease with increasing temperature as evidenced by equations 4.9 and 4.10 (the dielectric constant decreases slightly[19] and the Debye length increases with increasing temperature). Monte Carlo simulations based on mixtures comprised solely of charged spheres, on the other hand, successfully predict the measured trend at low reduced temperatures.[33] This is because the simulations take into account the strong charge inversion effect caused by closely packed ions. As temperature increases, the EDLs become less closely packed, resulting in an upward shift of the potential profile and a decrease in the magnitude of potential at zero charge. Therefore, at the same extent of surface charge, the ratio of charge to potential, or the capacitance, increases with increasing temperature. Even though these simulations aimed to address high temperature molten salts, they provide

insight into the important role of electrostatic interactions in affecting the temperature dependence of capacitance for ionic liquids. While there is no general agreement on the physical origins that account for this trend, possible explanations include reduced inter-ionic interactions and facilitated ion dissociation with increased temperature.[27,29,34]

The double-layer capacitance decreases with increasing polymer content, as shown in Figures 4.10 and 4.11. This is presumably due to the increased area occupied by polymer chains along the electrode surface and therefore altered structures of the EDLs as more polymers are added. However, this effect does not seem to be very strong, and the reduction in capacitance for a gel with 50 wt% SMS(17-86-17) relative to neat [EMI][TFSA] is within a factor of three. Nor is the reduction very temperature dependent, in contrast to the ionic conductivity. This is likely because capacitance pertains to the

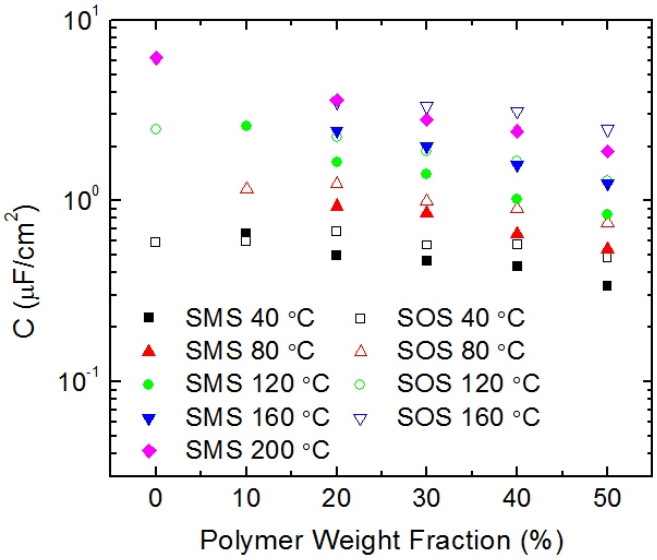


**Figure 4.11** Concentration dependence of capacitance calculated from RCPE series circuit fits for SMS(17-86-17)/[EMI][TFSA] and SOS(3-35-3)/[EMI][TFSA] ion gels at selected temperatures. The fits were performed over a frequency range of 20 Hz to 1 MHz.

property of the established EDLs along the interface, while ionic conductivity is a measure of charge transport in the bulk, which depends on ion mobilities that are strongly affected by temperature.

### 4.3.5 *RC* Time Constant

Shifting $\sigma^*$ along the frequency axis by the ratio of peak positions of $\sigma''$ at different temperatures gives the tTS master curves shown in Figure 4.1. These peak positions correspond to the product of bulk resistance $R$ and double-layer capacitance $C$, indicating that the characteristic time ($\tau_{RC}$) of the ionic motion examined here relates to the establishment of stable EDLs along the electrolyte/electrode interfaces. Therefore, for electrochemical devices where stable EDLs are needed, the operating frequency is potentially limited by the value of $\tau_{RC}$. Figure 4.12 shows $\tau_{RC}$ calculated at a thickness of 1 mm and an electrode diameter of 25 mm. The opposite temperature and concentration dependences of $R$ and $C$ result in an intermediate dependence of $\tau_{RC}$. However, since both

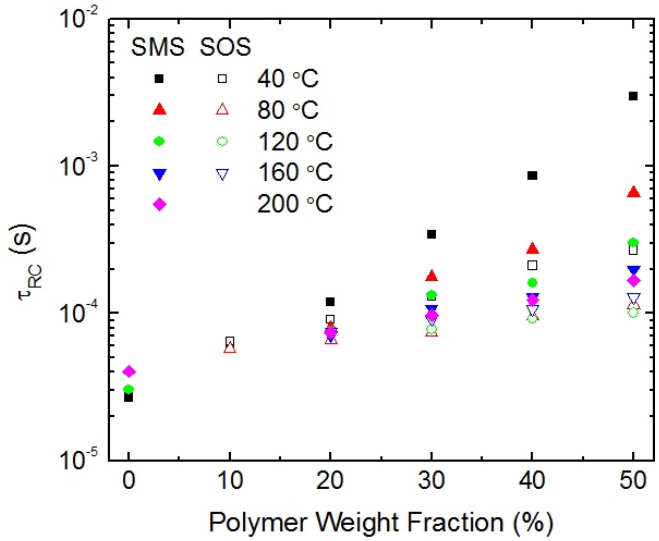


**Figure 4.12** *RC* time constant at a thickness of 1 mm and an electrode diameter of 25 mm for [EMI][TFSA] and the ion gels. *C* was calculated from RCPE series circuit fits.

dependences are stronger for $R$ than for $C$, those of $\tau_{RC}$ resemble $R$ more, as shown by the nearly opposite trends of Figure 4.12 and Figure 4.7. It is worth noting that the value of $R$, and thus $\tau_{RC}$, varies linearly with sample thickness, and that by reducing the sample thickness into the micron range, much smaller relaxation times can be obtained.[35]

### 4.3.6 Materials Design Considerations

Combining the results discussed so far and those reported previously on the ion gels,[36] the concentration and molecular weight of the triblock can be tuned to meet specific property needs. As far as gel modulus is concerned, a higher modulus can be obtained with the addition of more polymer or using a mid-block with a smaller entanglement molecular weight. Nevertheless, as the addition of polymer lowers the ionic conductivity, there is a trade-off that should be balanced. This is shown in Figure 4.13, where the plateau modulus of the gels is plotted versus ionic conductivity at 30 °C. If for

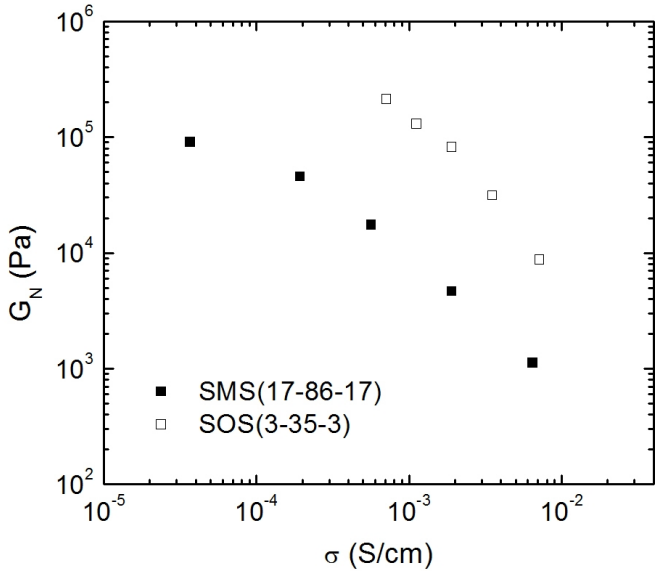


**Figure 4.13** Plateau modulus versus ionic conductivity at 30 °C for SMS(17-86-17)/[EMI][TFSA] and SOS(3-35-3)/[EMI][TFSA] ion gels.

the sake of high modulus 20 wt% or more polymer is needed, it is better to use a flexible mid-block since in this concentration range conductivity is higher for gels with a lower $T_g$ mid-block. Once the mid-block is chosen, the reduction of conductivity for the gels with respect to homopolymer solutions can be minimized by making the PS end-blocks relatively short. However, in order to maintain mechanical integrity at a certain triblock concentration, the end-blocks need to be long enough to obtain a persistent gel at the desired temperature. For the SOS gels, the molecular weight of the end-blocks needs to be at least 3.8 kDa to achieve a melting temperature above 100 °C with 10 wt% SOS.[36] On the other hand, thermoreversible gels can easily be obtained with fine-tuned gelation temperature by varying the molecular weight of the PS block.

## 4.4 Summary

In this chapter, the electrical properties of ion gels based on SMS(17-86-17) and SOS(3-35-3) triblock copolymers and the ionic liquid [EMI][TFSA] were examined over wide temperature and composition ranges. The response of the ion gels to AC electric fields below 1 MHz is similar to an RCPE series circuit, with a characteristic time corresponding to the establishment of stable EDLs. For concentrated SMS gels, the $R$ or $\sigma$ values are strongly affected by the glassy midblocks because they represent ion transport in the bulk. For SOS gels, the $\sigma$ values are higher, and much less dependent on either temperature or concentration. The $\sigma$ ratio of both SOS- and SMS-based gels to homopolymer solutions with the same mid-block content is above 0.5, and depends on PS volume fraction following the Mackie-Meares model. For both gels, $C$ is not affected as

much due to the nature of the gel/electrode interfaces. The opposite temperature and concentration dependences of $R$ and $C$ yield intermediate dependences for $\tau_{RC}$. Combining the considerations on modulus, ionic conductivity, and thermal stability allows rational designs of the triblock in ion gels to meet specific property requirements.

## 4.5 References


(1) Bard, A. J.; Faulkner, L. R. *Electrochemical Methods: Fundamentals and Applications*, 2nd ed.; Wiley: New York, 2001.

(2) De Levie, R. *Electrochim. Acta* **1965**, *10*, 113-130.

(3) Brug, G. J.; Van den Eeden, A. L. G.; Sluyters-Rehbach, M.; Sluyters, J. H. *J. Electroanal. Chem.* **1984**, *176*, 275-295.

(4) Pajkossy, T. *J. Electroanal. Chem.* **1994**, *364*, 111-125.

(5) Pajkossy, T. *Solid State Ionics* **2005**, *176*, 1997-2003.

(6) Huang, V. M.-W.; Vivier, V.; Frateur, I.; Orazem, M. E.; Tribollet, B. *J. Electrochem. Soc.* **2007**, *154*, C89-C98.

(7) Bou-Saleh, Z.; Shahryari, A.; Omanovic, S. *Thin Solid Films* **2007**, *515*, 4727-4737.

(8) Susan, M. A. B. H.; Kaneko, T.; Noda, A.; Watanabe, M. *J. Am. Chem. Soc.* **2005**, *127*, 4976-4983.

(9) Gaikwad, A. N.; Wood, E. R.; Ngai, T.; Lodge, T. P. *Macromolecules* **2008**, *41*, 2502-2508.

(10) Mok, M. M.; Kim, J.; Wong, C. L. H.; Marrou, S. R.; Woo, D. J.; Dettmer, C. M.;

Nguyen, S. T.; Ellison, C. J.; Shull, K. R.; Torkelson, J. M. *Macromolecules* **2009**, *42*, 7863-7876.

(11) Mok, M. M.; Liu, X.; Bai, Z.; Lei, Y.; Lodge, T. P. *Macromolecules* **2011**, *44*, 1016-1025.

(12) Savin, D. A.; Larson, A. M.; Lodge, T. P. *J. Polym. Sci., Part B: Polym. Phys.* **2004**, *42*, 1155-1163.

(13) Tokuda, H.; Ishii, K.; Susan, M. A. B. H.; Watanabe, M. *J. Phys. Chem. B* **2005**, *109*, 6103-6110.

(14) He, Y.; Boswell, P. G.; Buhlmann, P.; Lodge, T. P. *J. Phys. Chem. B* **2007**, *111*, 4645-4652.

(15) He, Y.; Lodge, T. P. *Chem. Commun.* **2007**, 2732-2734.

(16) Brandrup, J.; Immergut, E. H.; Grulke, E. A. *Polymer Handbook*, 4th ed.; Wiley-Interscience: New York, 1999.

(17) Mackie, J. S.; Meares, P. *Proc. R. Soc. London* **1955**, *A232*, 498-509.

(18) Amsden, B. *Macromolecules* **1998**, *31*, 8382-8395.

(19) Krossing, I.; Slattery, J. M.; Daguenet, C.; Dyson, P. J.; Oleinikova, A.; Weingaertner, H. *J. Am. Chem. Soc.* **2006**, *128*, 13427-13434.

(20) Izgorodina, E. I.; Forsyth, M.; MacFarlane, D. R. *Phys. Chem. Chem. Phys.* **2009**, *11*, 2452-2458.

(21) Min, Y.; Akbulut, M.; Sangoro, J. R.; Kremer, F.; Prud'homme, R. K.; Israelachvili, J. *J. Phys. Chem. C* **2009**, *113*, 16445-16449.

(22) Fedorov, M. V.; Kornyshev, A. A. *Electrochim. Acta* **2008**, *53*, 6835-6840.

(23) Drueschler, M.; Huber, B.; Passerini, S.; Roling, B. *J. Phys. Chem. C* **2010**, *114*, 3614-3617.

(24) Alam, M. T.; Islam, Md. M.; Okajima, T.; Ohsaka, T. *J. Phys. Chem. C* **2008**, *112*, 16600-16608.

(25) Nanjundiah, C.; McDevitt, S. F.; Koch, V. R. *J. Electrochem. Soc.* **1997**, *144*, 3392-3397.

(26) Skinner, B.; Loth, M. S.; Shklovskii, B. I. *Phys. Rev. Lett.* **2010**, *104*, 128302/1-128302/4.

(27) Zistler, M.; Wachter, P.; Schreiner, C.; Fleischmann, M.; Gerhard, D.; Wasserscheid, P.; Hinsch, A.; Gores, H. J. *J. Electrochem. Soc.* **2007**, *154*, B925-B930.

(28) Lockett, V.; Sedev, R.; Ralston, J.; Horne, M.; Rodopoulos, T. *J. Phys. Chem. C* **2008**, *112*, 7486-7495.

(29) Silva, F.; Gomes, C.; Figueiredo, M.; Costa, R.; Martins, A.; Pereira, C. M. *J. Electroanal. Chem.* **2008**, *622*, 153-160.

(30) Costa, R,; Pereira, C. M.; Silva, F. *Phys. Chem. Chem. Phys.* **2010**.

(31) Ukshe, E. A.; Bukun, N. G.; Leikis, D. I.; Frumkin, A. N. *Electrochim. Acta* **1964**, *9*, 431-439.

(32) Devanathan, M. A. V.; Tilak, B. V. K. S. R. A. *Chem. Rev.* **1965**, *65*, 635-684.

(33) Boda, D.; Henderson, D.; Chan, K.-Y. *J. Chem. Phys.* **1999**, *110*, 5346-5350.

(34) Holovko, M.; Kapko, V.; Henderson, D.; Boda, D. *Chem. Phys. Lett.* **2001**, *341*, 363-

368.

(35) Lee, K.-H.; Zhang, S.; Lodge, T. P.; Frisbie, C. D. *J. Phys. Chem. B*. **2011**, *115*, 3315-3321.

(36) He, Y.; Lodge, T. P. *Macromolecules* **2008**, *41*, 167-174.

# Chapter 5

# Ion Gels with Chemically Cross-Linkable End-blocks*

## 5.1 Introduction

In this chapter, a novel ion gel composed of poly[(styrene-*r*-vinylbenzyl azide)-*b*-ethylene oxide-*b*-(styrene-*r*-vinylbenzyl azide)] (SOS-$N_3$) and the ionic liquid 1-ethyl-3-methylimidazolium bis(trifluoromethylsulfonyl)amide ([EMI][TFSA]) is introduced. The poly(styrene-*r*-vinylbenzyl azide) (PS-$N_3$) end-blocks associate into micelles, whereas the poly(ethylene oxide) (PEO) mid-blocks are well-solvated by [EMI][TFSA]. Therefore, at lower temperatures, the gel is a physical network with PS-$N_3$ cores and PEO strands. At elevated temperatures, the transient network with 10 wt% polymer becomes liquid-like due to fast end-block chain exchange. Upon further increase in temperature, the azide groups can be chemically cross-linked, thereby locking the PS-$N_3$ blocks in the cores. Thus, as temperature increases, the gel with 10 wt% polymer goes through physical network $\rightarrow$ liquid $\rightarrow$ chemically cross-linked network. Incorporation of azide groups was chosen to realize chemical cross-linking because the cross-linking of PS-$N_3$ has been reported to be a facile process,[1–3] and the synthesis is accessible via reversible addition-fragmentation chain transfer polymerization (RAFT), which can be readily employed to PEO-based triblock copolymer.

This is the first time that both physical and chemical crosslinking have been realized on the same block copolymer-based ion gel. The mechanical properties and ionic

* This work was conducted in collaboration with Yuanyan Gu.

conductivity of the gel are investigated before and after chemical crosslinking. The shear modulus and ionic conductivity with 10 wt% polymer remain the same, whereas the toughness is more than eight times higher after chemical cross-linking. This demonstrates that the simple act of chemically cross-linking the cores yields a much tougher gel without interfering with ion transport.

## 5.2 Experimental

### 5.2.1 Polymer Synthesis and Characterization

All reagents were used as received unless otherwise noted. Styrene and 4-vinylbenzyl chloride (VBC) were passed through activated alumina columns prior to use. Methyl acrylate was passed through a basic alumina column before use. The SOS gel used for extensional rheology was prepared with an SOS(3.4-35-3.4) polymer (Table 5.1) synthesized by Yuanyan Gu. The synthetic procedure was the same with that introduced in Chapter 2.

The SOS-$N_3$ polymer was synthesized as follows (Figure 5.1). In the first step, poly[(styrene-*r*-vinylbenzyl chloride)-*b*-ethylene oxide-*b*-(styrene-*r*-vinylbenzyl chloride)] (SOS-Cl) was synthesized via RAFT from a poly(ethylene glycol) (PEG) precursor. PEG purification and attachment of the chain transfer agent (CTA) was the same as described in Chapter 2. Then, CTA-PEO-CTA was used to copolymerize styrene and VBC. CTA-PEO-CTA (10.01 g, $2.86\times10^{-4}$ mol), styrene (10.98 g, 0.106 mol), and VBC (4.03 g, 0.0264 mol) were mixed in a Schlenk flask, degassed via three freeze-pump-thaw cycles, and heated in an oil bath at 70 °C to obtain a homogeneous solution.

The solution was then heated to 140 °C and polymerization was allowed to proceed for 67 min, followed by quenching with liquid $N_2$. The mixture was dissolved in $CH_2Cl_2$ (ca. 200 mL) and precipitated into *n*-hexane (ca. 3 L) four times. The product was dried in a vacuum oven at ca. 50 °C for two days. In the second step, the CTA was cleaved to prevent reaction of the thiol groups with $NaN_3$ in the next step. SOS-Cl (9.60 g, $2.25\times10^{-4}$ mol) and dry tetrahydrofuran (THF, HPLC grade, ca. 150 mL) were mixed in a Schlenk flask. The mixture was heated to 60 °C and stirred till a homogeneous solution was obtained. The solution was bubbled with Ar for ca. 10 min while *n*-propylamine (4 mL, 0.0485 mol) and tris(2-carboxyethyl)phosphine hydrochloride (TCEP, 150 mg, $5.25\times10^{-4}$ mol) were added. The flask was then sealed and the reaction was allowed to proceed at room temperature for 2 hours, followed by injection of methyl acrylate through the septum. The mixture was stirred overnight for the reaction to complete. The content was precipitated into *n*-hexane. The precipitate was dissolved in $CH_2Cl_2$ and passed through a basic alumina column. Excess $CH_2Cl_2$ was removed using a rotary evaporator, and the concentrated solution (ca. 130 mL) was precipitated in *n*-pentane (ca. 1.5 L) twice. The product was dried in a vacuum oven at ca. 50 °C for two days. In the third step, SOS-Cl with no CTA was reacted with $NaN_3$ to obtain the SOS-$N_3$ triblock. SOS-Cl with no CTA (8.00 g, $1.85\times10^{-4}$ mol) and *N*,*N*-dimethylformamide (DMF, 500 mL) were mixed in a round-bottom flask. A condenser was put on top of the flask, and the mixture was heated to 50 °C and stirred till all polymer was dissolved. $NaN_3$ (1.25 g, 0.0192 mol) was added into the flask, and the reaction was allowed to proceed at 60 °C for 40 hours. Deionized water (ca. 5 mL) was added to quench the reaction, and the mixture was cooled to room

temperature. Most of the DMF was removed using a rotary evaporator, and the content was dissolved in $CH_2Cl_2$ (ca. 300 mL). The mixture was washed with saturated NaCl aqueous solution three times, followed by the addition of $MgSO_4$ to dry the organic phase. Excess $CH_2Cl_2$ was removed with a rotary evaporator. The solution (ca. 100 mL) was then precipitated in diethyl ether (ca. 1 L). The product was redissolved in ca. 200 mL $CH_2Cl_2$ to give a turbid solution, followed by filtering through filter paper. The opaque filtrate was further diluted with ca. 300 mL $CH_2Cl_2$ and filtered with 0.45 μm membrane filters to yield a clear solution. Excess $CH_2Cl_2$ was removed with a rotary evaporator, and the concentrated solution (ca. 60 mL) was precipitated in *n*-pentane (ca. 600 mL) twice. The final product was dried in a vacuum oven at ca. 50 °C for two days. The first and third steps of the synthesis were followed by $^1$H NMR spectroscopy (Figure 5.2). The second step was confirmed via UV-Vis spectroscopy (Figure 5.3a). The dispersity ($Đ$) of the polymers was measured using size exclusion chromatography (SEC, Figure 5.4a). Table 5.1 lists the molecular characteristics of all polymers involved. For simplicity, the SOS-$N_3$ polymer will be denoted as SOS-$N_3$(3.8-35-3.8).

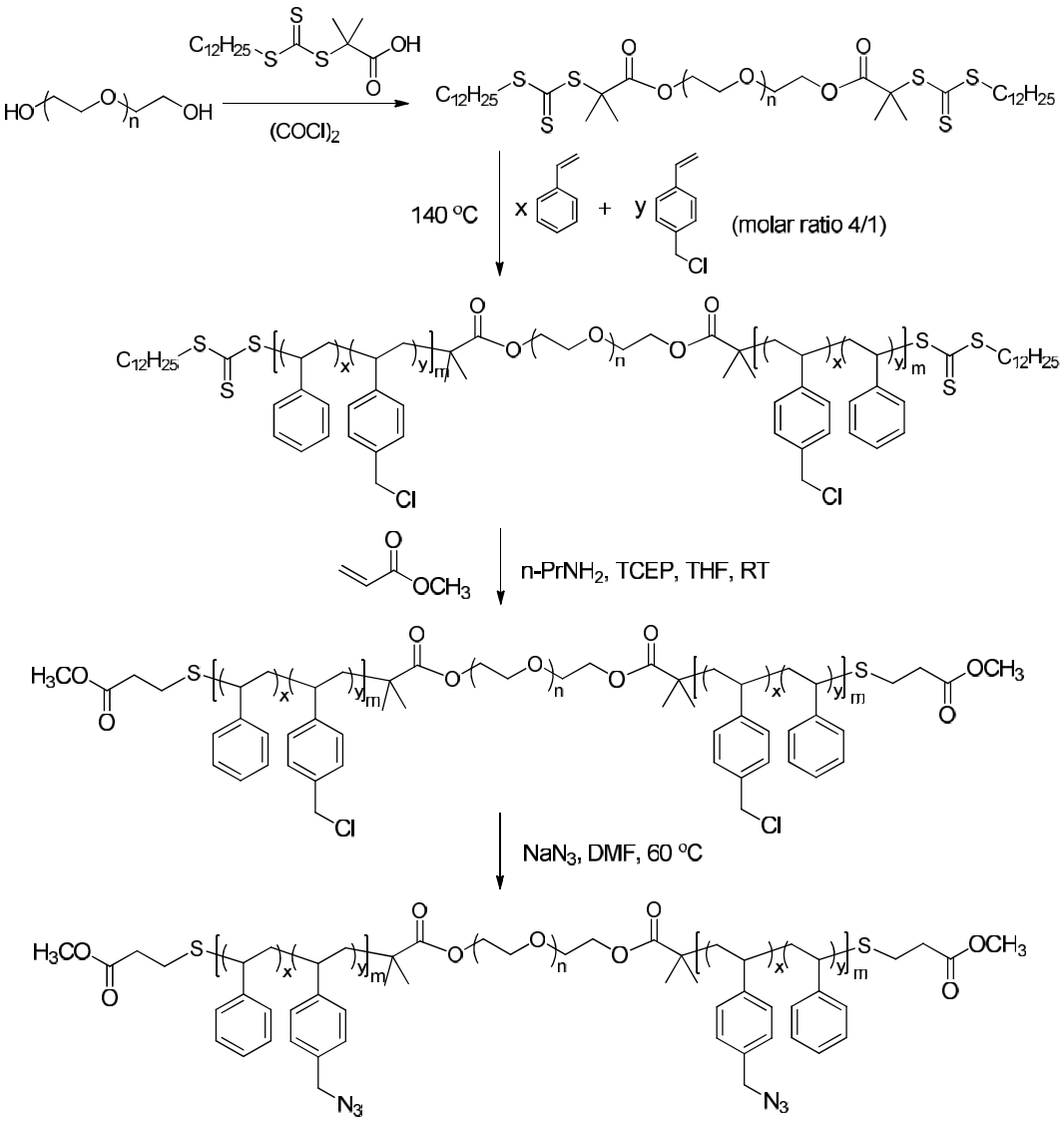


**Figure 5.1** Synthetic scheme of SOS-$N_3$ triblock copolymer.

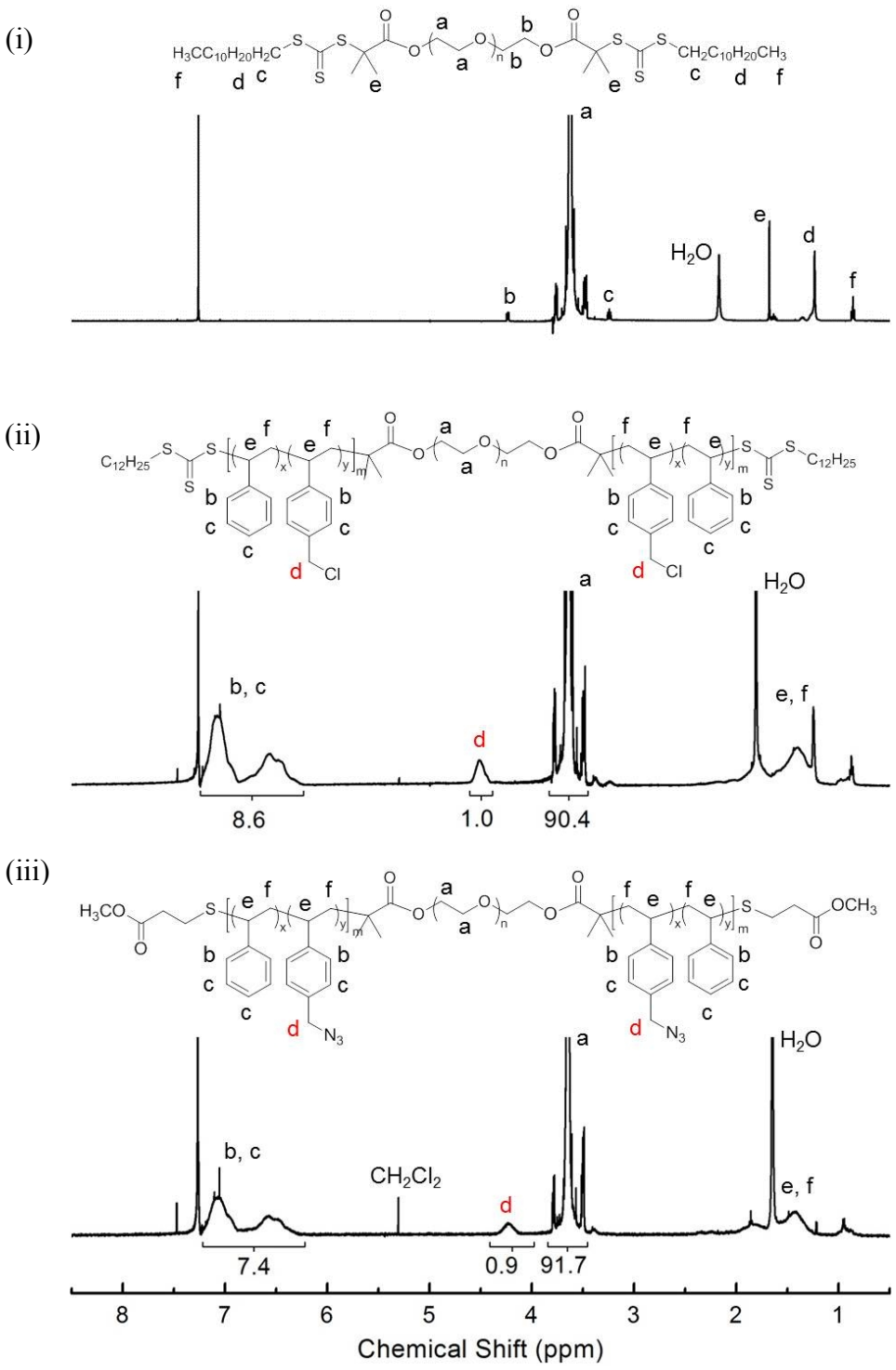


**Figure 5.2** $^{1}$H NMR spectra (500 MHz, in $CDCl_3$) of (i) CTA-PEO-CTA, (ii) SOS-Cl, and (iii) SOS-$N_3$.

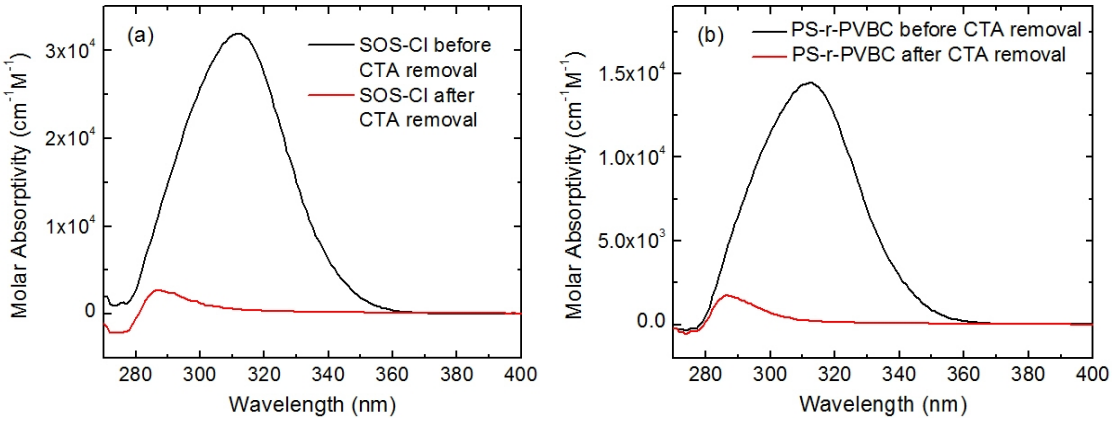


**Figure 5.3** UV-Vis spectra of (a) SOS-Cl and (b) PS-*r*-PVBC before and after CTA removal.

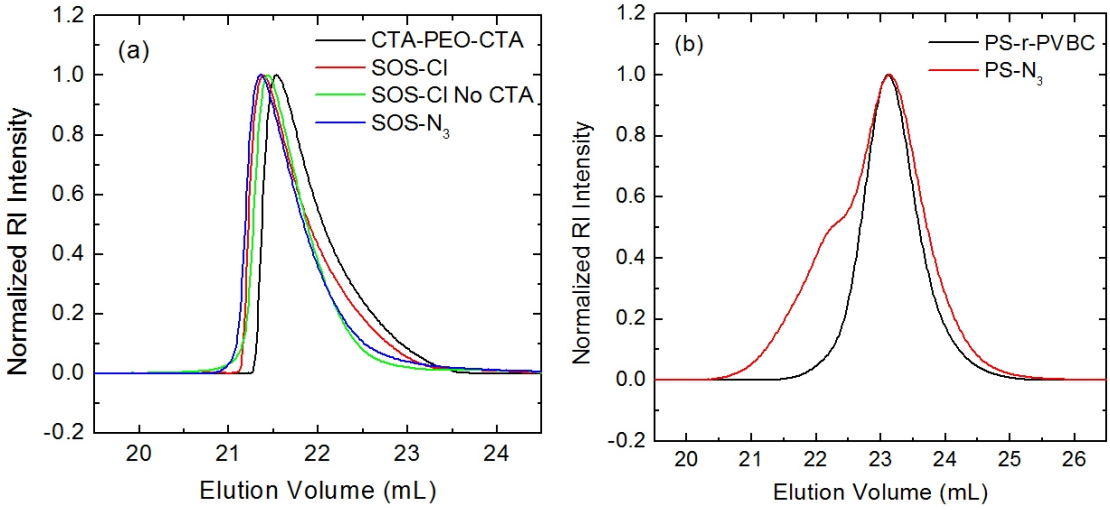


**Figure 5.4** SEC traces of (a) all polymers involved in the synthesis of SOS-$N_3$ and (b) PS-*r*-PVBC and PS-$N_3$.

To study cross-linking kinetics, a poly(styrene-*r*-vinylbenzyl azide) (PS-$N_3$) was synthesized (Figure 5.5). In the first step, poly(styrene-*r*-vinylbenzyl chloride) (PS-*r*-PVBC) was synthesized using RAFT. CTA (0.374 g, $1.03\times10^{-3}$ mol), styrene (6.25 g, 0.041 mol) and VBC (17.04 g, 0.164 mol) were mixed in a Schlenk flask and bubbled with Ar for ca. 30 min. The polymerization then proceeded in bulk at 140 °C for 50 min.

The contents were quenched with liquid $N_2$ and dissolved in $CH_2Cl_2$ (ca. 50 mL). The solution was precipitated with methanol (ca. 500 mL) three times, and the product was dried in a vacuum oven at 70 °C overnight. In the second step, the CTA was removed to prevent reaction of the thiol groups with $NaN_3$ in the subsequent step. PS-*r*-PVBC (4.00 g, $4.44\times10^{-4}$ mol) and dry THF (HPLC grade, ca. 55 mL) were mixed in a round-bottom flask and bubbled with Ar for ca. 10 min, while *n*-propylamine (3.7 mL, 0.0449 mol) and TCEP (150 mg, $5.25\times10^{-4}$ mol) were added. The flask was then sealed and the reaction proceeded at room temperature for 2 hours, followed by injection of methyl acrylate (ca. 8 mL) through the septum. The mixture was stirred overnight for the reaction to complete. The content was precipitated into methanol twice. The product was dried in a vacuum oven at ca. 60 °C for 2 days. In the third step, PS-*r*-PVBC without CTA was reacted with $NaN_3$ to obtain PS-$N_3$. The reaction was completed in two identical batches to limit the addition of $NaN_3$ into each flask to less than 1 g. In each batch, PS-*r*-PVBC (1.40 g, $1.56\times10^{-4}$ mol) and DMF (ca. 150 mL) were mixed in a round-bottom flask and stirred until all polymers were dissolved. Then, $NaN_3$ (0.93 g, 0.0143 mol) was added, and a condenser was put on top of the flask. The reaction was allowed to proceed at 60 °C for 40 h, and quenched by the addition of deionized water (ca. 5 mL). Excess DMF was removed using a rotary evaporator, and the content was dissolved in $CH_2Cl_2$, followed by precipitation into methanol twice. The final product was dried in a vacuum oven at ca. 60 °C for 2 days. The first and third steps were verified with $^1$H-NMR (Figure 5.6). The second step was confirmed with UV-Vis spectroscopy (Figure 5.3b). The dispersity ($Đ$) of the polymers was measured using SEC (Figure 5.4b), and all molecular characteristics

are listed in Table 5.1. The SEC trace of the PS-$N_3$ appears bimodal, which is likely due to coupling resulting from incomplete removal of the CTA. However, this should not have much effect on cross-linking kinetics.

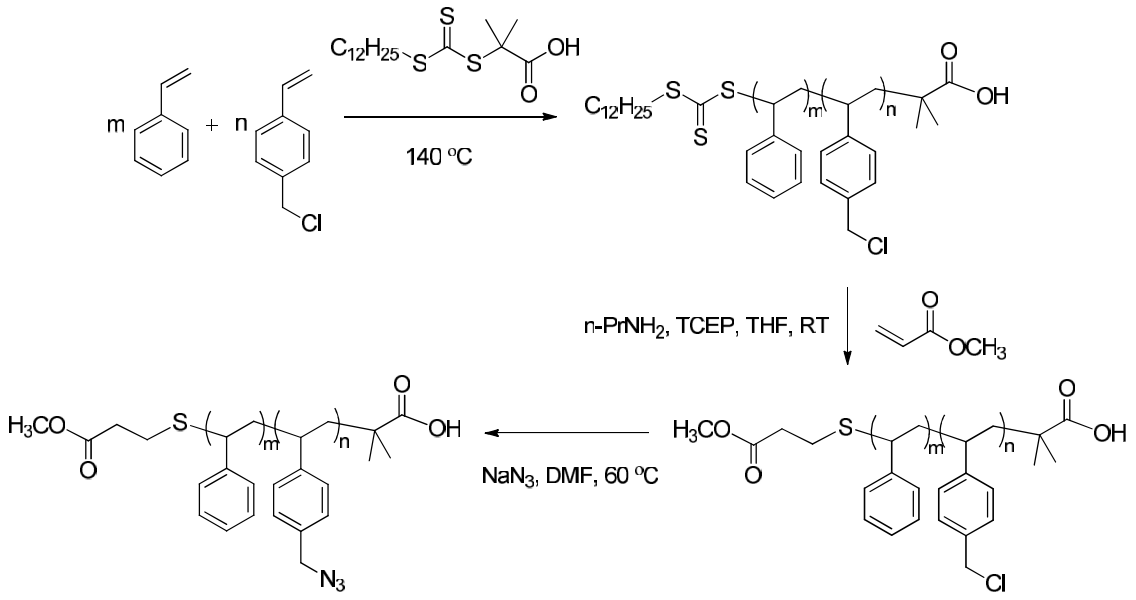


**Figure 5.5** Synthetic scheme of PS-$N_3$ random copolymer.

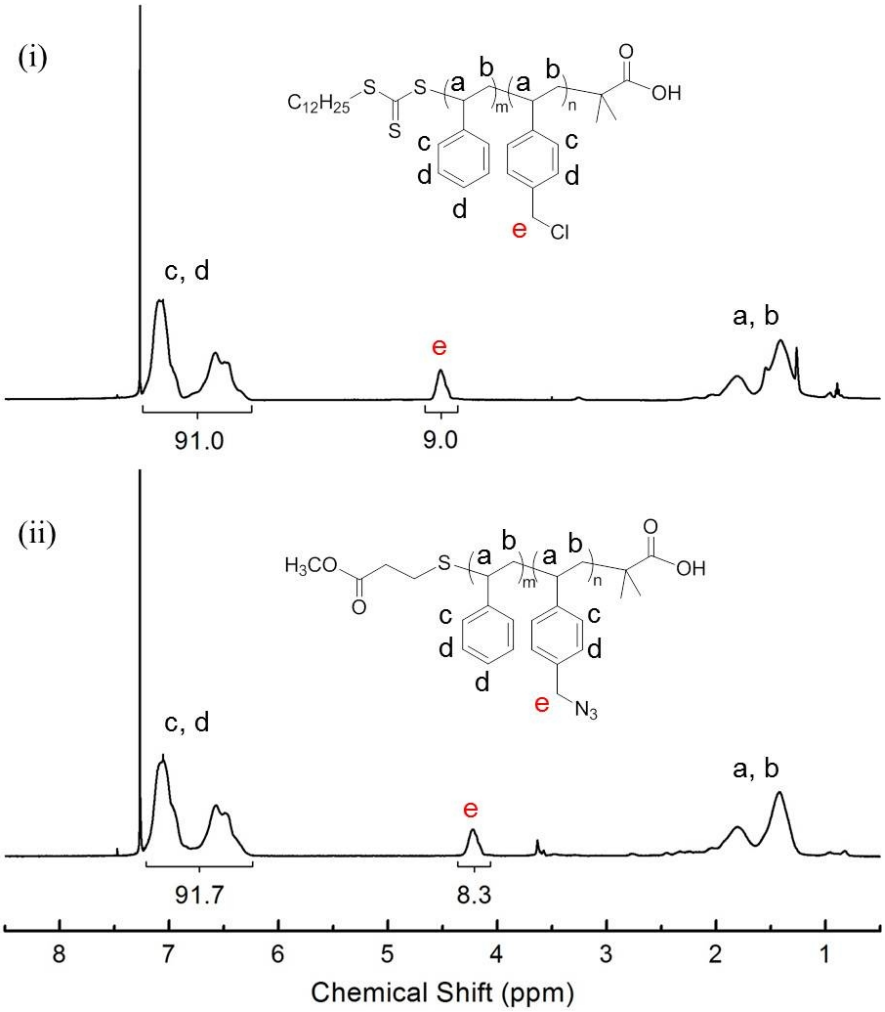


**Figure 5.6** $^{1}H$ NMR spectra (500 MHz, in $CDCl_3$) of (i) PS-*r*-PVBC and (ii) PS-$N_3$ random copolymers.

**Table 5.1** Molecular Characteristics of Polymers used in this Chapter.

| polymer | $M_{n,\ PVBC/PVBA}$ (kDa)[a] | $N_{PVBC/PVBA}$ | $M_{n,\ PS}$ (kDa)[a] | $N_{PS}$ | $M_{n,\ PEO}$ (kDa) | $Đ$ |
|---|---|---|---|---|---|---|
| SOS-$N_3$ | 1.4 | 9 | 2.4 | 23 | 35 | 1.12 |
| SOS-Cl no CTA | 1.4 | 9 | 2.4 | 23 | 35 | 1.11 |
| SOS-Cl | 1.4 | 9 | 2.4 | 23 | 35 | 1.07 |
| SOS[1] | | | 2.8 | 27 | 35 | 1.05 |
| SOS[2] | | | 3.4 | 33 | 35 | 1.08 |
| CTA-PEO-CTA | | | | | 35 | 1.10 |
| PS-$N_3$ | 2.9 | 18 | 6.2 | 60 | | 1.43 |
| PS-*r*-PVBC | 2.7 | 18 | 6.2 | 60 | | 1.15 |

[1] Introduced in Chapter 2, used in ion gels for comparison of shear rheology and ionic conductivity. [2] Used in ion gels for comparison of extensional rheology. [a] Block $M_n$ determined by $^1$H-NMR. PVBA: poly(vinylbenzyl azide). For the two random copolymers, $M_n$ of each component was calculated from $^1$H-NMR peak integration based on the overall $M_n$ of PS-*r*-PVBC determined by SEC (PS standards). PVBC/PVBA and PS are randomly distributed through the end-blocks in SOS-Cl and SOS-$N_3$.

### 5.2.2 Ionic Liquid and Ion Gel Preparation

The [EMI][TFSA] ionic liquid was synthesized through an anion exchange reaction following a previously reported protocol as described in Chapter 2,[4] and was stored in a glovebox to avoid water absorption. The ion gels were prepared by mixing weighed amounts of the respective polymer and the ionic liquid in $CH_2Cl_2$ cosolvent. After stirring

for 2 hours, the mixtures were purged with nitrogen gas overnight to evaporate most of the cosolvent. Finally, the samples were placed in a vacuum oven at ca. 45 °C for 2 days to completely remove the cosolvent. Samples for extensional rheology were dissolved using $CH_2Cl_2$ the same as above, cast into petri dishes, purged with nitrogen gas overnight, and annealed in a vacuum oven at ca. 100 °C for several hours to obtain smooth films. To avoid any effects of moisture, all samples were kept in a vacuum desiccator.

For the cross-linking kinetics study, PS-$N_3$ polymer was put in 1 mL ampules, and active vacuum was applied at least 3 hours before the ampules were flame-sealed. They were heated on a pre-heated heating block at different temperatures for different amounts of time. After air-cooling to room temperature, the ampules were smashed and the polymer within was put in $CH_2Cl_2$ and vigorously stirred for at least 6 hours to determine whether the sample had chemically cross-linked.

### 5.2.3 Rheology

Shear measurements were conducted on an ARES rheometer (Rheometric Scientific) using parallel plate geometry. Depending on the modulus, both 50 and 25 mm diameter plates were employed, with a gap spacing of ca. 1 mm. For temperature ramps, the sample was equilibrated at 100 °C to remove any prior thermal history, and cooled down to 25 °C to start the measurement. It was then heated to 100 °C at 1 °C/min with a shear rate of 0.3 rad/s and a strain of 5%. After holding at 100 °C for 10 min, it was cooled back to 30 °C under the same conditions as heating. To obtain time temperature superposition (tTS) master curves before chemical cross-linking, the sample was

thermally equilibrated for 15 – 20 min at each temperature, and the gap was adjusted to compensate for the thermal expansion of the tool set. Then, strain sweeps were conducted to determine the linear viscoelastic regime, followed by measurements of the dynamic shear moduli. Temperatures were controlled to within 0.2 °C of the set points with an environmental control circulator under a nitrogen atmosphere. Measurements were taken at a series of decreasing temperatures. For strain sweeps, the shear rate was set at 10 rad/s. For cross-linking kinetic studies, one set of experiments were frequency sweeps performed at 100 °C after holding at a higher temperature for a certain amount of time. Specifically, the sample was heated up to the desired temperatures using a temperature ramp, with a heating rate of 10 °C/min, strain of 0.1% and shear rate of 0.3 rad/s. It was then held at that temperature for 10 min and cooled down to 100 °C with the same ramp parameters. Then, frequency sweeps were conducted at the same conditions described above. Another experiment involves heating the sample to 200 °C using a temperature ramp, with a heating rate of 10 °C/min, strain of 3% and shear rate of 0.3 rad/s. Then, a time sweep was conducted immediately afterwards with the same strain and a shear rate of 10 rad/s to determine the time it takes for the gel modulus to reach a plateau.

Extensional measurements were performed by Luca Martinetti on an ARES-G2 rheometer (TA Instruments) using an extensional viscosity fixture (Figure 5.7). Samples were shaped with a rectangular punch (width = 4.5 mm) and carefully lifted out of the petri dish. They were then loaded onto the fixture in between the drums (length = 13 mm). The thickness of each sample was measured using a caliper, and on average is approximately 0.7 mm. Tests were conducted at 40 °C, and the temperature was

controlled to within 0.2 °C of the set point with an environmental control circulator under a nitrogen atmosphere. Unlike standard tensile tests where the ends of the sample are pulled at a constant velocity, in this case the sample was pulled at a constant deformation rate, and the instrument measures the resulting extensional stress/viscosity until the sample breaks.

**Figure 5.7** Photograph of extensional viscosity fixture. The loaded sample is an SOS/[EMI][TFSA] ion gel with 10 wt% SOS(3.4-35-3.4). Taken by Luca Martinetti.

### 5.2.4 Impedance Spectrocopy

Impedance measurements were performed with a homemade cell using a Solartron 1255B frequency response analyzer connected to a Solartron SI 1287 electrochemical interface. Frequency sweeps were conducted from 1 – $10^6$ Hz with an AC amplitude of 10 mV. The cell is composed of a Teflon spacer with an inner diameter of 4 mm and a thickness of 2 mm sandwiched between two platinum coated stainless steel electrodes. Temperatures were controlled to within 0.5 °C of the set points with a thermostated water bath. The samples were thermally equilibrated for 30 min prior to the measurements. Measurements were performed at a series of increasing temperatures. Ionic conductivity

was determined from the high frequency plateau of the real part of complex conductivity (not shown). The shapes of the complex conductivity versus frequency curves are similar to the ones shown in Chapter 4.

## 5.3 Results and Discussion

### 5.3.1 Viscoelastic Properties before Chemical Cross-linking

The dynamic storage ($G'$) and loss ($G''$) moduli for the ion gel with 10 wt% SOS-$N_3$(3.8-35-3.8) were measured over the temperature range from 30 °C to 100 °C. Over this temperature range, the gel is a physically cross-linked transient network. The loss tangent (tan $\delta$) spectra were shifted horizontally using tTS, and the same shift factors were applied to the dynamic moduli to obtain master curves as a function of reduced

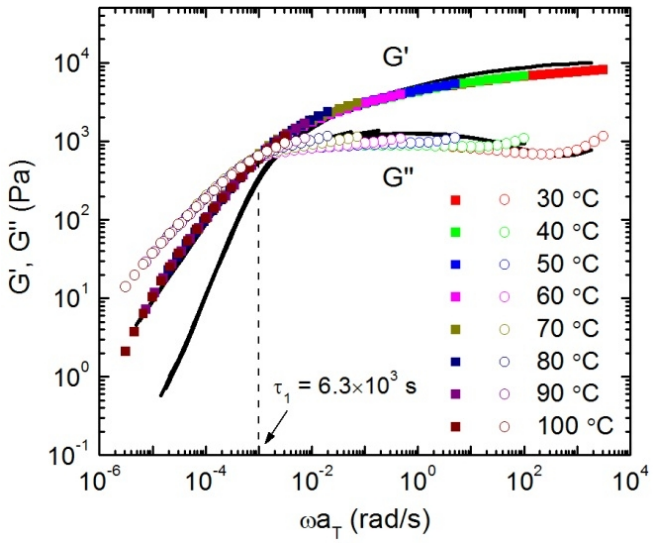


**Figure 5.8** tTS master curves of dynamic storage and loss moduli referenced to 40 °C for ion gels with 10 wt% SOS-$N_3$(3.8-35-3.8) and 10 wt% SOS(2.8-35-2.8). Colored symbols and black lines represent moduli for the SOS-$N_3$(3.8-35-3.8) and SOS(2.8-35-2.8) gel, respectively.

frequency, as shown in Figure 5.8 (colored symbols). The tTS master curves for an SOS/[EMI][TFSA] ion gel with 10 wt% SOS(2.8-35-2.8) described in Chapter 2 are also shown in comparison (solid black lines). Curves for both gels are shifted to a reference temperature of 40 °C.

For the SOS-$N_3$ gel, a liquid-like behavior is observed at temperatures above 70 °C, as evidenced by the crossover between $G'$ and $G''$. The longest relaxation time, $\tau_{1,\text{gel}}$, at 40 °C is $6.3\times10^3$ s, as determined by the crossover frequency at which $G'$ and $G''$ values are equal. Applying the horizontal shift factors, the temperature dependence of $\tau_{1,\text{gel}}$ can be obtained, as displayed in Figure 5.9. The plateau modulus of the SOS-$N_3$(3.8-35-3.8) gel ($G_N$) is 6600 Pa, determined as the value of $G'$ at the frequency where the corresponding curve of tan $\delta$ has a minimum. According to linear viscoelastic theory, the plateau modulus can be expressed as[5]

$$G_N = \frac{cfRT}{M_x} \tag{2.4}$$

where $c$ is the concentration of the block copolymer in w/v, $f$ is the fraction of bridging or effective mid-blocks inside the copolymer, $R$ is the ideal gas constant, and $M_x$ is the molecular weight between cross-links. Here, we estimate $M_x = M_{e,\,PEO}/w_{PEO}$, where $M_{e,\,PEO}$ is the entanglement molecular weight of melt PEO, which is 1.6 kDa at 140 °C,[6] and $w_{PEO}$ is the weight fraction of PEO in the gel. Assuming all PEO chains bridge two cross-linking cores instead of looping back to the same one ($f$ = 1), the value of $G_N$ at 30 °C (the temperature at which the measured plateau modulus was extracted) was calculated to be $2.5\times10^4$ Pa. Therefore, the bridging fraction is 26%, which is very similar to that

calculated for the SOS(2.8-35-2.8) gel (29%), and agrees with previously reported gels.[7–9]

Since both the mid- and end-block degree of polymerizations are similar for the two polymers, the modulus of the two gels with 10 wt% polymer are very similar as well, as shown by the near overlap of the master curves. This similarity was also observed for the longest relaxation times, as displayed in Figure 5.9. The small difference is likely due to the presence of azide groups in the SOS-$N_3$ polymer, and thus a slightly different interaction parameter ($\chi$) between the end-blocks and the ionic liquid.

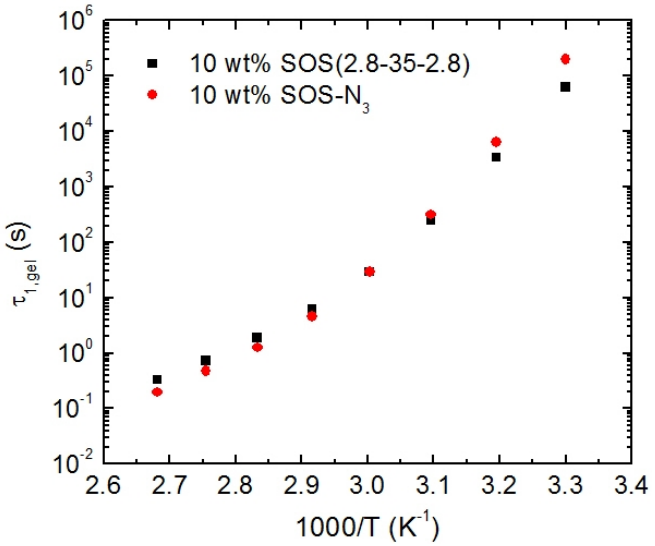


**Figure 5.9** Temperature dependent terminal relaxation times ($\tau_{1,gel}$) of ion gels with 10 wt% SOS-$N_3$(3.8-35-3.8) and 10 wt% SOS(2.8-35-2.8).

To confirm that no chemical cross-linking happens below 100 °C, temperature ramps were conducted on the gel with 10 wt% SOS-$N_3$(3.8-35-3.8), as shown in Figure 5.10. It is obvious from the plot that the heating and cooling traces overlap well, suggesting that the gel is fully thermoreversible in the temperature range of 30 – 100 °C. A gel

temperature of 62 °C was extracted, as indicated by the crossover at which $G'$ and $G''$ values are equal. This is slightly higher than that of the SOS(2.8-35-2.8) gel, for which $T_{gel}$ = 54 °C under the same conditions, likely due to the slightly higher end-block degree of polymerization for the SOS-$N_3$ polymer (Table 5.1).

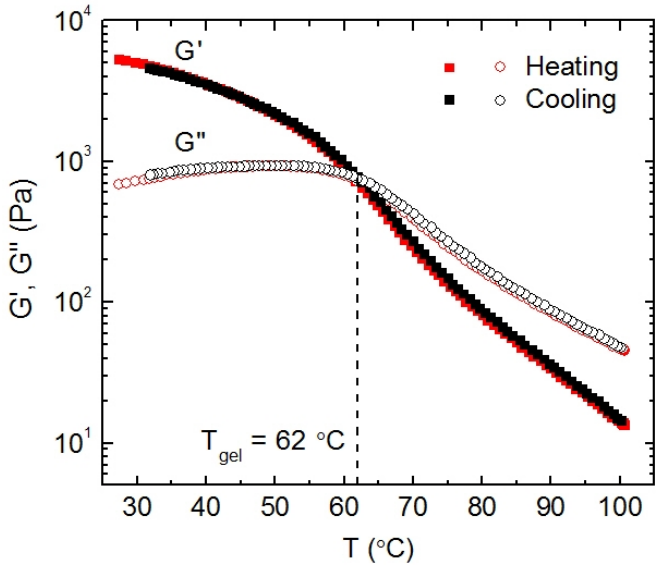


**Figure 5.10** Temperature ramps of ion gel with 10 wt% SOS-$N_3$(3.8-35-3.8).

### 5.3.2 Cross-linking Kinetics

It has been reported that the cross-linking reaction of the azide group can be achieved via either UV irradiation (254 nm) or heating (250 °C).[1–3] However, no detailed information on the kinetics has been reported in the case of heating. Table 5.2 summarizes the results for cross-linking kinetic studies performed on PS-$N_3$ random copolymer samples sealed under vacuum. The times shown are heating times at the respective temperatures. At 140 °C, the sample heated for 10 min appeared to be completely insoluble in $CH_2Cl_2$, a good solvent for all components of the gel before chemical cross-linking, indicating that it had been chemically cross-linked. The same

happened to the samples heated for 5 and 10 min at 160 °C, and all three samples at 180 °C. Based on this study, the cross-linking process is fairly quickly and happens at a temperature as low as 140 °C.

**Table 5.2** Cross-linking Kinetic Results on PS-$N_3$.

| $T$ (°C) | 2 min | 5 min | 10 min |
|---|---|---|---|
| 140 | - | SS | I |
| 160 | SS | I | I |
| 180 | I | I | I |

SS: slightly soluble. I: insoluble.

Intuitively, one would expect that the kinetics of chemical cross-linking for the random copolymer is similar to the gel, since the local concentration of azide groups should be similar in the copolymer and the micelle cores of the gel. However, this turned out to be not the case, as holding a 10 wt% SOS-$N_3$ gel at 140 °C and then 160 °C for 10 min still yielded a liquid-like material ($G'' > G'$). Not until the same sample was held at 180 °C for 10 min did it show solid-like behavior over the frequency range measured, indicating that chemical cross-linking has proceeded to a measurable extent. Figure 5.11 displays $G'$ and $G''$ versus frequency measured at 100 °C after holding the sample at 180 °C for 10 min, another 10 min, 200 °C for 10 min, and another 10 min. The curves before chemical cross-linking showing a liquid-like material were also presented as a comparison. Overall, $G'$ of the sample keeps increasing while $G''$ keeps decreasing. By holding at 200 °C for 10 + 10 min, $G'$ is independent of frequency, and $G''$ is too small to

be measured below 20 rad/s. This suggests that the gel is fully chemically cross-linked.

In another experiment, a sample was rapidly heated from 110 °C to 200 °C, and held at 200 °C to determine the time it takes for chemical cross-linking to complete, *i.e.*, when the storage modulus becomes time/frequency independent. Figure 5.12 shows the results

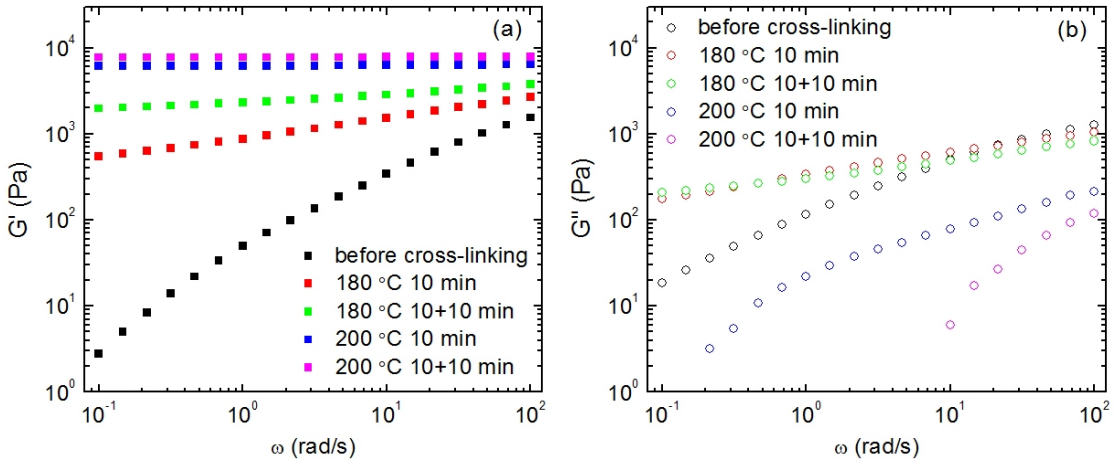


**Figure 5.11** Dynamic (a) storage and (b) loss moduli of ion gel with 10 wt% SOS-$N_3$(3.8-35-3.8) before chemical cross-linking and after holding at the 180 °C and 200 °C for certain amounts of time.

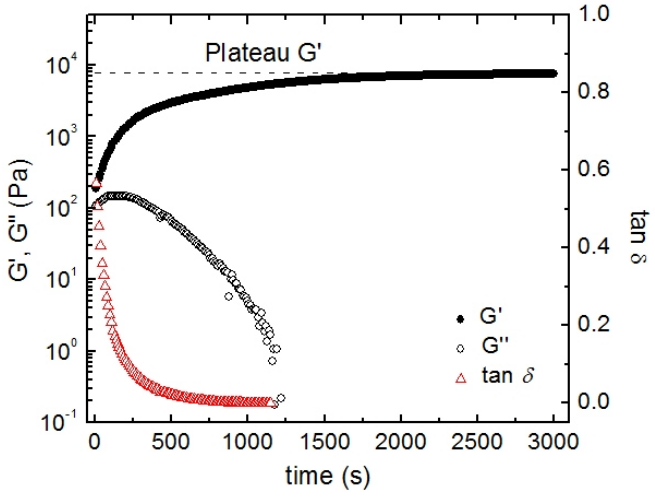


**Figure 5.12** Dynamic storage and loss moduli of ion gel with 10 wt% SOS-$N_3$(3.8-35-3.8) as a function of time at 200 °C.

of the time sweep at 200 °C. The storage modulus reached a plateau after ca. 45 min, indicating that chemical cross-linking is complete. Both of these experiments suggest that the cross-linking time for the gel is much longer than that for a pure PS-$N_3$ copolymer. A possible cause is solvent penetration into the micelle cores at elevated temperatures. Additionally, in the case of the gel, end-block chain exchange between different micelle cores happen constantly at 200 °C, making it different from the scenario of the random copolymer, where the only diffusive contribution comes from the motion of the PS-$N_3$ chains. Given the elusive mechanism of the azide cross-linking reaction by itself,[2] this process is even more complicated in an originally physically cross-linked gel.

### 5.3.3 Mechanical Properties after Chemical Cross-linking

Figure 5.13 displays $G'$ and $G''$ as a function of shear strain for a 10 wt% SOS-$N_3$ gel before and after chemical cross-linking. The storage modulus increases slightly, while the loss modulus drops significantly after chemical cross-linking, suggesting that the gel does not change much in terms of stiffness, but it becomes more elastic after cross-linking. The fluctuation in $G''$ versus shear rate after cross-linking is likely because $G''$ is too much smaller than $G'$ for the instrument to yield a reliable measurement. Such changes in $G''$ and $G''$ are reasonable, since the modulus is mainly determined by the number density of elastically effective mid-blocks, which is not expected to vary significantly upon chemical cross-linking. On the other hand, the act of chemical cross-linking locks the PS-$N_3$ end-blocks within the cores, thereby eliminating chain pull-out, leading to a more elastic network. It is also noteworthy that the linear region of the gel both before and after cross-linking is very large (> 100% strain). After chemical cross-linking, $G'$ and $G''$

deviate from the values in the linear region very drastically as strain is increased to more than 300%, suggesting that the network starts to break down.

While there is not much change in stiffness of the gel after chemical cross-linking,

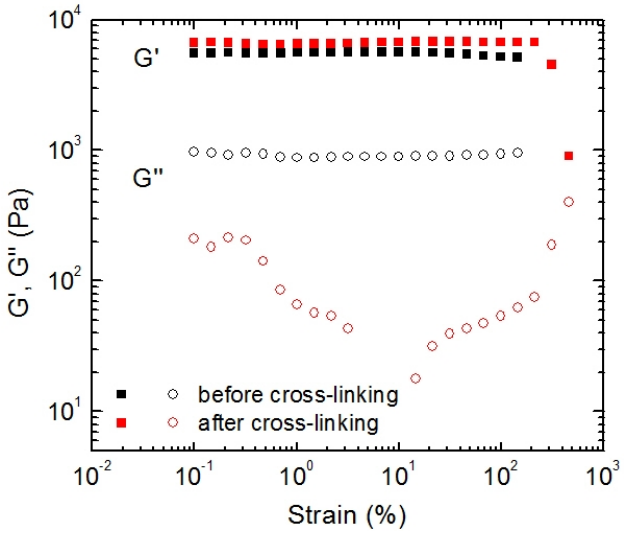


**Figure 5.13** Dynamic storage and loss moduli of ion gel with 10 wt% SOS-$N_3$(3.8-35-3.8) as a function of shear strain at 40 °C.

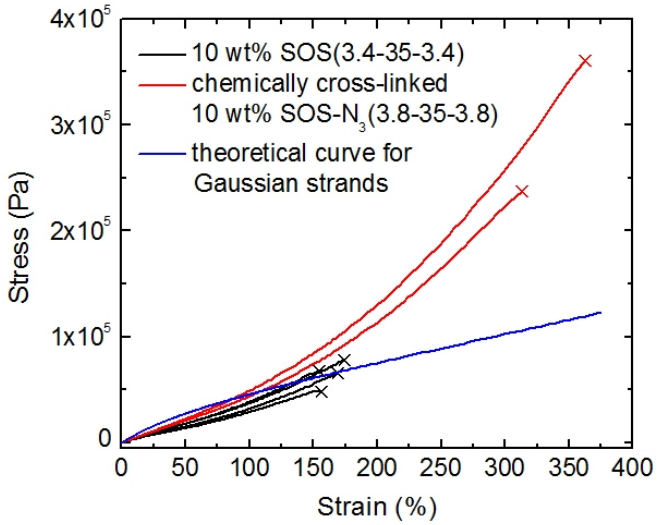


**Figure 5.14** Stress-strain relationships for ion gels with 10 wt% SOS(3.4-35-3.4) and 10 wt% SOS-$N_3$ after chemical cross-linking measured at 40 °C.

other mechanical properties in regions of large strain are improved significantly. Figure 5.14 compares the stress-strain relationships of gels with 10 wt% SOS(3.4-35-3.4) and 10 wt% SOS-$N_3$ after chemical cross-linking. The gel with 10 wt% SOS-$N_3$ before chemical cross-linking is too tacky to be picked up from the petri dish without damage or deformation. Figures 5.15 and 5.16 summarize the extracted average values of percent elongation, tensile strength, and toughness of the two gels showed in Figure 5.14. Clearly, the mechanical properties for the gel with 10 wt% SOS-$N_3$ are improved substantially, with a toughness value more than eight times higher than the gel with 10 wt% SOS(3.4-35-3.4). This considerable difference in toughness is likely because the failure mechanism changed from pulling out the end-blocks in a physical network to breaking the mid-blocks in a chemical network. The collective results on extensional rheology highlight the dramatic effect of chemically cross-linking the cores on mechanical

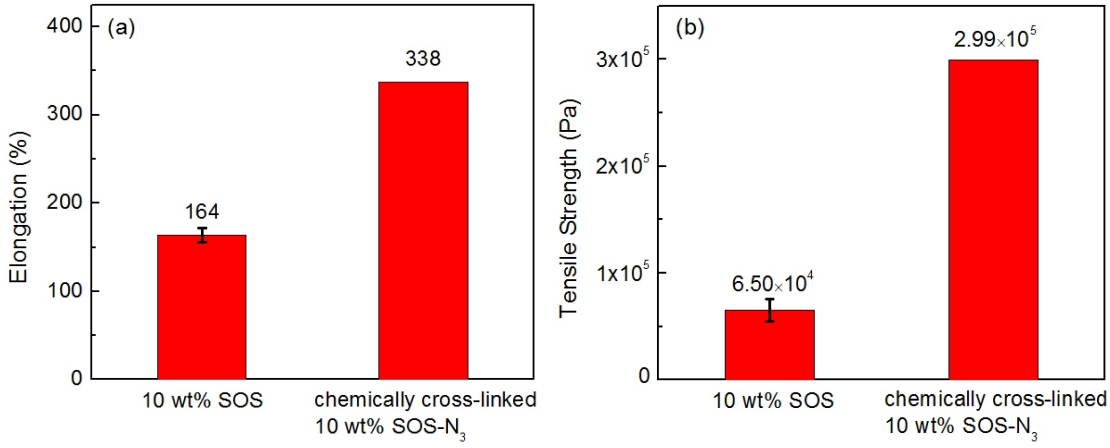


**Figure 5.15** Average (a) percent elongation and (b) tensile strength of ion gels with 10 wt% SOS(3.4-35-3.4) and 10 wt% SOS-$N_3$ after chemical cross-linking measured at 40 °C.

properties of the gel.

The tensile stress of the two gels can be compared to that predicted from rubber

elasticity assuming the mid-blocks are Gaussian strands:[5]

$$\sigma_e = \frac{\nu k_B T}{V}\left(\lambda - \frac{1}{\lambda^2}\right) = \frac{cfRT}{M_x}\left(\lambda - \frac{1}{\lambda^2}\right) \tag{5.2}$$

where $\nu$ is the number density of elastically effective mid-blocks, $k_B$ is Boltzmann's constant, $V$ is the volume of the gel, and $\lambda$ is the extension ratio ($\lambda = \varepsilon + 1$, where $\varepsilon$ is strain). Assuming a bridging fraction of 100%, the calculated values of tensile stress are plotted as a blue line in Figure 5.14. It can be seen that for the gel with 10 wt% SOS(3.4-35-3.4), the theoretical values are higher than those measured, mainly because in the actual gel, the bridging fraction is less than 100%. The same trend can be observed for the gel with 10 wt% SOS-$N_3$ at lower strains (< 100%), because the actual bridging fraction in the gel is 26%, as calculated in section 5.3.1. At strains greater than 150%, where the gels with 10 wt% SOS(3.4-35-3.4) start to break, the measured stress of the gel with 10 wt% SOS-$N_3$ deviates significantly from that of a Gaussian coil. In fact, such a

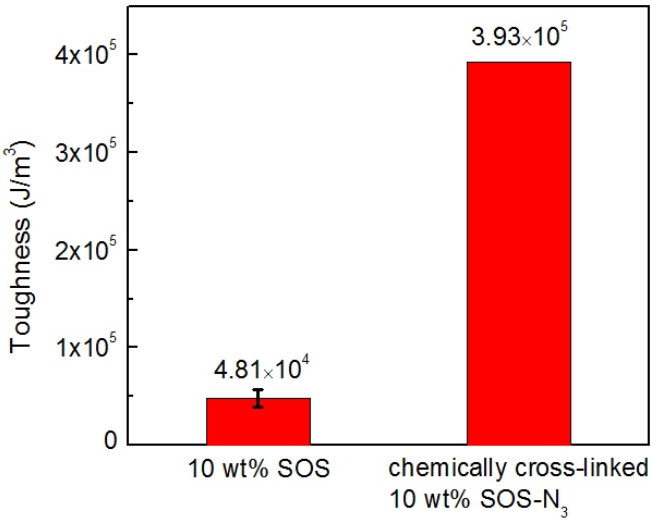


**Figure 5.16** Average toughness of ion gels with 10 wt% SOS(3.4-35-3.4) and 10 wt% SOS-$N_3$ after chemical cross-linking measured at 40 °C.

deviation is reasonable. Since the failure of the gel is most likely caused by breaking the mid-blocks, it is expected that the chains are stretched to a significant extent at the break point. Additionally, [EMI][TFSA] is a good solvent for PEO, and the mid-blocks are "anchored" by the end-blocks after chemical cross-linking, so they would not assume a Gaussian conformation even without external forces.

### 5.3.4 Ionic Conductivity

Figure 5.17 displays the ionic conductivity of the ion gel with 10 wt% SOS-$N_3$ measured over a temperature range of 25 – 100 °C before and after chemical cross-linking. The conductivities of [EMI][TFSA] taken from ref. 10 and the gel with 10 wt% SOS(2.8-35-2.8) (discussed in Chapter 4) are also plotted for comparison. It is evident that the ionic conductivities of the two gels are almost the same over the temperature range measured, and the act of chemical cross-linking does not have any measurable

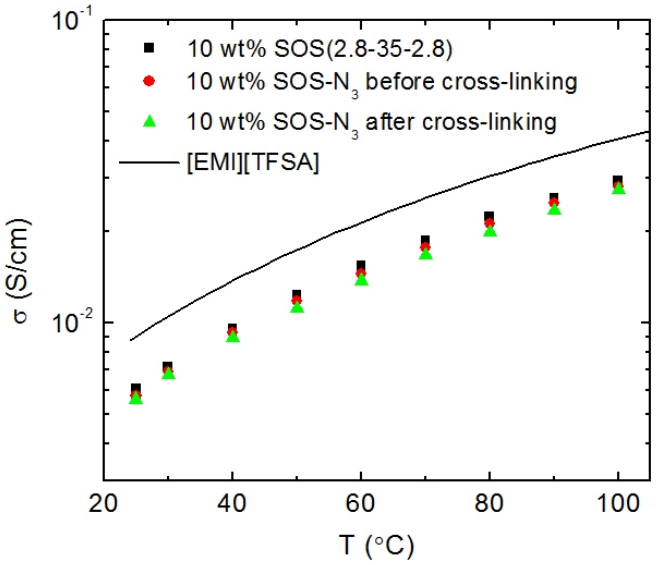


**Figure 5.17** Temperature dependence of ionic conductivity for [EMI][TFSA][10] and ion gels with 10 wt% SOS(2.8-35-2.8) and 10 wt% SOS-$N_3$(3.8-35-3.8).

effect on ion transport. This agrees with the observation in Chapter 4 that at a polymer concentration of 10 wt%, the ionic conductivity is reduced to very similar extent even with very different polymers, because in this moderately dilute regime, $T_g$ of the conducting phase remains very low, and ion transport is dominated by the ionic liquid. Additionally, this agrees with the conclusion in Chapter 4 that the cross-links only act as obstructions to ion paths. Therefore, ionic conductivity should be independent of whether the cores are physically or chemically cross-linked, since the volume fraction of end-blocks remains the same.

## 5.4 Summary

In this chapter, a novel SOS-$N_3$/[EMI][TFSA] ion gel with 10 wt% polymer was studied. The azide groups can be chemically cross-linked at elevated temperatures, thereby realizing physical and chemical crosslinking on the same gel. The mechanical properties and ionic conductivity of the gel were investigated before and after chemical crosslinking. Before cross-linking, the viscoelastic properties of the gel are qualitatively very similar to the gel with 10 wt% SOS(2.8-35-2.8). The cross-linking reaction takes longer to complete in the gel than a pure PS-$N_3$ random copolymer. After cross-linking, the shear modulus and ionic conductivity with 10 wt% polymer remain the same, whereas the ductility, tensile strength, and toughness are substantially improved. Since chemically cross-linking the cores yields a much tougher gel without interfering with ion transport, the gel could potentially be employed in applications requiring more robust materials such as stretchable circuits and actuators.

## 5.5 References

(1) Lee, S.; Lee, B.; Kim, B. J.; Park, J.; Yoo, M.; Bae, W. Ki; Char, K.; Hawker, C. J.; Bang, J.; Cho, J. *J. Am. Chem. Soc.* **2009**, *131*, 2579-2587.

(2) Yoo, M.; Kim, S.; Lim, J.; Kramer, E. J.; Hawker, C. J.; Kim, B. J.; Bang, J. *Macromolecules* **2010**, *43*, 3570-3575.

(3) Bang, J.; Bae, J.; Lowenhielm, P.; Spiessberger, C.; Given-Beck, S. A.; Russell, T. P.; Hawker, C. J. *Adv. Mater.* **2007**, *19*, 4552-4557.

(4) Susan, M. A. B. H.; Kaneko, T.; Noda, A.; Watanabe, M. *J. Am. Chem. Soc.* **2005**, *127*, 4976-4983.

(5) Hiemenz, P. C.; Lodge, T. P. *Polymer Chemistry*, 2nd ed.; CRC Press: New York, 2007.

(6) Fetters, L. J.; Lohse, D. J.; Richter, D.; Witten, T. A.; Zirkel, A. *Macromolecules* **1994**, *27*, 4639-4647.

(7) Tae, G.; Kornfield, J. A.; Hubbell, J. A.; Lal, J. *Macromolecules* **2002**, *35*, 4448-4457.

(8) He, Y.; Boswell, P. G.; Buhlmann, P.; Lodge, T. P. *J. Phys. Chem. B* **2007**, *111*, 4645-4652.

(9) Annable, T.; Buscall, R.; Ettelaie, R.; Whittlestone, D. *J. Rheol.* **1993**, *37*, 695-726.

(10) Tokuda, H.; Ishii, K.; Susan, M. A. B. H.; Watanabe, M. *J. Phys. Chem. B* **2005**, *109*, 6103-6110.

# Chapter 6

# Summary and Outlook

## 6.1 Summary

The goal of this thesis project is to systematically study the mechanical and electrical properties of block copolymer (BCP)-based ion gel electrolytes, and find ways to enhance the properties of the gels, in order to formulate optimal designs in terms of the triblock for applications to electrochemical devices. Of particular interest are organic transistors and electrochemical capacitors, due to the very large specific capacitance of these electrolytes and therefore low voltage operation and potentially desirable energy storage. Ionic liquids exhibit a unique combination of properties such as negligible volatility, exceptional thermal, chemical and electrochemical stability, as well as relatively high ionic conductivity, which make them promising candidates in electrochemical applications.[1−3] The role of the BCP is mainly to provide mechanical support without too much sacrifice on the desirable electrical properties.[4]

In terms of the viscoelastic properties, the effect of polymer concentration, mid-block identity and end-block lengths have been examined over wide temperature ranges. The most important factor with respect to stiffness is polymer concentration. The plateau modulus spans nearly two orders of magnitude over a polymer content range of 10 – 50 wt%. The other factor that influences the stiffness is the entanglement molecular weight ($M_e$) of the mid-block. A smaller effective $M_e$ leads to higher plateau modulus at the same polymer concentration, and hence a stiffer gel. In the case where no entanglements are

present, a mid-block with smaller molecular weight would be preferable to obtain a higher modulus. Thermoreversibility is mainly controlled by the length of the end-blocks. Short end-blocks exhibit small incompatibility with the ionic liquid (small $\chi N$, where $\chi$ is the Flory-Huggins interaction parameter and $N$ is the end-block degree of polymerization), making chain exchange facile at elevated temperatures and thus resulting in a thermoreversible gel. For long end-blocks, relaxations of both the mid-block and end-block have been observed under shear. The temperature range where mid-block relaxation can be observed clearly depends on how flexible the mid-block is. For a glassy polymer such as poly(methyl methacrylate) (PMMA), the relaxation can be captured in the temperature range of 30 – 140 °C, whereas for a flexible polymer like poly(ethylene oxide) (PEO), the fast relaxation only starts to reveal itself below 70 °C.

In terms of the electrical properties, it was found that polymer concentration does not have much effect on specific capacitance. Even with 50 wt% polymer, the reduction in capacitance is only within a factor of 3. However, the effect of polymer content on ionic conductivity, and in turn on response time and dissipation factor, is more significant. The drop in conductivity for the gels with PMMA mid-blocks over the concentration range of 10 – 50 wt% can be as high as nearly two orders of magnitude. Therefore, a trade-off exists between large modulus and high ionic conductivity. Conductivity is also affected greatly by mid-block identity, especially at polymer concentrations above 20 wt%. A gel with 50 wt% addition of a flexible mid-block like PEO exhibit similar conductivity as a gel with 30 wt% addition of a glassy mid-block like PMMA over the same temperature range, due to the larger increase in glass transition temperature of the conducting phase

induced by a glassy mid-block. Thus, a flexible mid-block is more desirable to obtain a higher conductivity. At 10 wt% polymer, however, conductivity is nearly independent of polymer identity. It was also found that the role of the end-blocks is obstructing the ion paths, and ionic conductivity is really only affected by the volume fraction of end-blocks present in the gel.

For applications requiring fast response times, such as fast switching circuits, it is desirable to enhance the mechanical properties of the gel especially at the low polymer concentration end, since the ionic conductivity is not sacrificed much in this region. Generally, enhancing the mechanical properties for ion gels is beneficial. To this end, a novel ion gel composed of chemically cross-linkable end-blocks has been developed. The kinetics of chemical cross-linking via heating have been investigated. Upon chemical cross-linking, there are 2-, 4-, and 8-fold increases in percent elongation, tensile strength, and toughness of the gel with 10 wt% polymer, respectively, while the ionic conductivity remains the same. Therefore, this serves both as an interesting system for further explorations and as an excellent example of improving the mechanical properties without sacrificing ionic conductivity.

## 6.2 Outlook

On the basis of the results presented in this thesis, many opportunities remain for future research. The following discussions will be focused on two specific areas that are of most relevance.

### 6.2.1 Further Investigations of Gels with Chemically Cross-linkable End-blocks

We have demonstrated that incorporating chemically cross-linkable end-blocks into BCP-based ion gels enhances the mechanical properties substantially without diminishing ionic conductivity, proving that it is a promising approach worthy of further investigation.

One of the fundamental questions of interest is why it takes such longer time to cross-link the cores in a gel with 10 wt% polymer than a pure poly(styrene-*r*-vinylbenzyl azide) (PS-$N_3$) random copolymer. One possibility is that the time it takes to fully cross-link the gel depends on the total number of bridging mid-blocks locked between two different micelle cores, which in turn depends on the aggregation number of the micelle cores. This can be examined versus polymer concentration via small angle X-ray scattering (SAXS). Another possibility is ionic liquid penetration into the micelle cores at elevated temperatures, which can be evaluated by whether there is any shift in glass transitions observed through differential scanning calorimetry (DSC) on mixtures of PS-$N_3$ and 1-ethyl-3-methylimidazolium bis(trifluoromethylsulfonyl)amide ([EMI][TFSA]). Additionally, it would be fundamentally interesting to explore the onset of plastic deformation, as there is no yielding observed in the gel. This can be determined by the onset of birefringence (refractive index anisotropy) when a piece of gel under tension is subject to a monochromic laser beam. Another interesting question is how different the gel performs mechanically in the form of thin films before and after chemical cross-linking. This can be examined by measuring thickness variations of spun-coat gel patches on polyimide substrates that are rolled up (with a specific radius) for different lengths of time using optical profilometry. Other common ways of measuring the mechanical

properties of thin films include nanoindentation, microbeam cantilever deflection, and direct tensile testing. Nanoindentation involves forcing a sharp diamond indenter into the film while measuring the force and indentation depth. This technique does not require special sample preparation and therefore is fairly straightforward. Microbeam cantilever deflection is performed by deflecting one end of a cantilever fabricated using the testing material and measuring the amount of deflection versus applied pressure.[5] This technique requires that the sample be made into a well-defined shape. For direct tensile testing, one potential challenge is that if the gel is composed mostly of the ionic liquid, *e.g.* 90%, the applied force in a test may be below the instrument limit.

Practically, annealing 45 min at 200 °C under an inert atmosphere or vacuum can be a harsh condition in terms of processing. One possibility is to increase the density of azide groups in the end-block, and examine whether this yields faster kinetics. A potential concern is that the increased amount of azide groups would require an increased amount of the explosive $NaN_3$ to complete the reaction. Therefore, large amounts of polymers may have to be synthesized in several small batches for safety reasons.

Another possibility is to explore UV cross-linking. Although photo-patternable transistors have already been reported for other directly chemically cross-linked ion gels,[6] our system allows a physical gel to be deposited onto the semiconductor instead of casting a liquid layer with cross-linking precursors. Therefore, the thickness of the gel can be tuned easily via spin coating,[7] providing the potential of fabricating fast-switching, photo-patternable devices and circuits. Chemical cross-linking of the azide groups via UV irradiation has been reported for PS-$N_3$ and PMMA-*r*-(PS-$N_3$) random copolymers at

254 nm.[8–10] One potential challenge in applying this condition to the gels lies in the fact that the imidazolium ring of [EMI][TFSA] absorbs strongly near 229 nm (Figure 6.1). Therefore, the wavelength of the light source needs to be controlled very precisely to avoid absorption by the ionic liquid, and efforts need to be devoted to explore the optimal conditions (intensity and time) where cross-linking can be completed without damaging the gel.

With respect to processing, it is often preferable to use a hydrophobic mid-block to avoid the effect of moisture coming from subsequent deposition of the gate electrode from aqueous solutions.[11] Based on the results from Chapter 4, it would also be desirable to select a polymer with low glass transition temperature ($T_g$) in case more than 10 wt% polymer is needed. Acrylates would be a good choice in both respects.[12] It has been reported that triblock copolymers with poly(*n*-butyl acrylate) ($T_g$ = −54 °C)[11] as mid-block and PS as end-blocks can be readily synthesized through reversible addition fragmentation chain transfer polymerization (RAFT) using a bis-trithiocarbonate chain transfer agent.[13] Therefore, copolymerizing 4-vinylbenzyl chloride with styrene to form the cross-linkable end-block via RAFT should be feasible. Another possibility is to employ atom transfer radical polymerization (ATRP) to incorporate benzylcyclobutene (BCB) monomers into the end-block.[14] One potential challenge with this approach, however, is that the monomer is not commercially available and thus will need to be synthesized in the lab, adding difficulty to making the triblock copolymer.

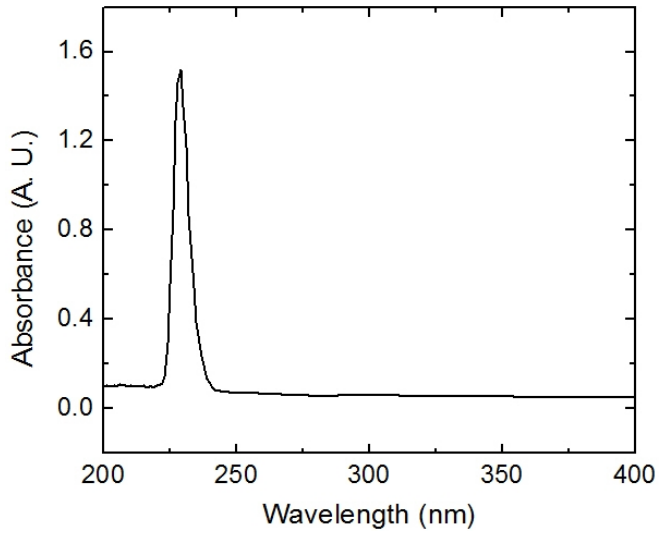


**Figure 6.1** UV-Vis spectrum of [EMI][TFSA].

### 6.2.2 Electrochemical Capacitors based on Ion Gel Electrolytes

It has been well-established that electrochemical capacitors (ECs, often referred to as supercapacitors or ultracapacitors) offer an attractive alternative to batteries when high power densities (rates of electrical charging or discharging) are desired.[15] Charge storage can be realized both through electrical double-layers (EDLs) and fast redox reactions at electrode/electrolyte interfaces (pseudocapacitance). High capacitance is achieved by using nanoporous electrodes with very high surface area, such as activated carbon, graphene, or carbon nanotubes (CNTs).[16] Typical organic electrolyte for ECs are based on solvents such as acetonitrile and propylene carbonate, which are flammable materials. Ionic liquids and ion gels are potentially advantageous in this area because of their negligible volatility and large electrochemical window, which offer improved electrolyte stability and enable higher energy storage ($U = CV^2/2$).[17–19] However, the development of ionic liquid-based ECs is still in a preliminary stage, and one of the most important challenges is choosing the appropriate ionic liquid with a combined wide electrochemical

window and a high ionic conductivity.

Robust and thin ion gel films employed as the separator (electrolyte) would be desirable as they eliminate the need for a support material and offer the potential of high charge-discharge rates (controlled by electrolyte resistance and hence thickness). Ion gels formed with poly(vinylidene fluoride-*co*-hexafluoropropylene) (P(VDF-HFP)) and several ionic liquids have been utilized as separators for ECs, which exhibited better performance than ECs having separators based on a support membrane filled with ionic liquid.[20,21] However, the polymer concentrations reported were at least 28 wt%, which increases the electrolyte resistance and thus limits the charge-discharge rate. In this regard, a gel with chemically cross-linkable end-block would be advantageous if a thin separator can be made with 10 wt% polymer.

In terms of processing, it would be desirable to fabricate printable ECs using ion gel electrolytes on flexible substrates. Our group has reported all-printed fast digital circuits based on CNTs and ion gel dielectrics.[22] Therefore, producing printable ECs with CNTs electrodes, thin ion gel electrolyte films, and possibly gold current collectors seem to be both feasible and fascinating.

Another interesting area of future research is combining pseudocapacitance and double-layer capacitance in a single device to achieve both high power and energy density.[18,23] If pseudocapacitance is realized by employing an electronically conducting polymer electrode,[24] an electrochromic supercapacitor can be obtained, with different colors indicating the capacitor's different charge conditions. Ultimately, it would be a state-of-the-art development if such devices can be fabricated via printing and integrated

into a flexible digital circuit.

### 6.3 References

(1) Welton, T.; *Chem. Rev.* **1999**, *99*, 2071-2083.

(2) Galinski, M.; Lewandowski, A.; Stepniak, I. *Electrochim. Acta* **2006**, *51*, 5567-5580.

(3) MacFarlane, D. R.; Forsyth, M.; Howlett, P. C.; Pringle, J. M.; Sun, J.; Annat, G.; Neil, W.; Izgorodina, E. I. *Acc. Chem. Res.* **2007**, *40*, 1165-1173.

(4) Lodge, T. P. *Science* **2008**, *321*, 50-51.

(5) Weihs, T. P.; Hong, S.; Bravman, J. C.; Nix, W. D. *J. Mater. Res.* **1988**, *3*, 931.

(6) Lee, S. W.; Lee, H. J.; Choi, J. H.; Koh, W. G.; Myoung, J. M.; Hur, J. H.; Park, J. J.; Cho, J. H.; Jeong, U. *Nano Lett.* **2010**, *10*, 347-351.

(7) Lee, K. H.; Zhang, S.; Lodge, T. P.; Frisbie, C. D. *J. Phys. Chem. B* **2011**, *115*, 3315-3321.

(8) Lee, S.; Lee, B.; Kim, B. J.; Park, J.; Yoo, M.; Bae, W. Ki; Char, K.; Hawker, C. J.; Bang, J.; Cho, J. *J. Am. Chem. Soc.* **2009**, *131*, 2579-2587.

(9) Yoo, M.; Kim, S.; Lim, J.; Kramer, E. J.; Hawker, C. J.; Kim, B. J.; Bang, J. *Macromolecules* **2010**, *43*, 3570-3575.

(10) Bang, J.; Bae, J.; Lowenhielm, P.; Spiessberger, C.; Given-Beck, S. A.; Russell, T. P.; Hawker, C. J. *Adv. Mater.* **2007**, *19*, 4552-4557.

(11) Cho, J. H.; Lee, J.; Xia, Y.; Kim, B.; He, Y.; Renn, M. J.; Lodge, T. P.; Frisbie, C. D. *Nat. Mater.* **2008**, *7*, 900-906.

(12) Brandrup, J.; Immergut, E. H.; Grulke, E. A. *Polymer Handbook*, 4th ed.; Wiley-

Interscience: New York, 1999.

(13) Moad, G.; Mayadunne, R. T. A.; Rizzardo, E.; Skidmore, M.; Thang, S. H. *Macromol. Symp.* **2003**, *192*, 1-12.

(14) Drockenmuller, E.; Li, L. Y. T.; Ryu, D. Y.; Harth, E.; Russell, T. P.; Kim, H.-C.; Hawker, C. J. *J. Polym. Sci., Part A: Polym. Chem.* **2005**, *43*, 1028-1037.

(15) Conway, B. E. *Electrochemical Supercapacitors*; Kluwer Academic Pub.: Norwell, 1999.

(16) Frackowiak, E. *Phys. Chem. Chem. Phys.* **2007**, *9*, 1774-1785.

(17) Largeot, C.; Portet, C.; Chmiola, J.; Taberna, P.-L.; Gogotsi, Y.; Simon, P. *J. Am. Chem. Soc.* **2008**, *130*, 2730-2731.

(18) Simon, P.; Gogotsi,Y. *Nat. Mater.* **2008**, *7*, 845-854.

(19) Armand, M.; Endres, F.; MacFarlane, D. R.; Ohno, H.; Scrosati, B. *Nat. Mater.* **2009**, *8*, 621-629.

(20) Lu, W.; Henry, K.; Turchi, C.; Pellegrino, J. *J. Electrochem. Soc.* **2008**, *155*, A361-A367.

(21) Lewandowski, A.; Galinski, M. *J. Phys. Chem. Solids* **2004**, *65*, 281-286.

(22) Ha, M.; Xia, Y.; Green, A. A.; Zhang, W.; Renn, M. J.; Kim, Ch. H.; Hersam, M. C.; Frisbie, C. D. *ACS Nano* **2010**, *4*, 4388-4395.

(23) Wei, D.; Scherer, M. R. J.; Bower, C.; Andrew, P.; Ryhanen, T.; Steiner, U. *Nano Lett.* **2012**, *12*, 1857-1862.

(24) Rudge, A., Raistrick, I., Gottesfeld, S. & Ferraris, J. P. *J. Power Sources* **1994**, *47*,

89-107.

# Bibliography

Adebahr, J.; Best, A. S.; Byrne, N.; Jacobsson, P.; MacFarlane, D. R.; Forsyth, M. *Phys. Chem. Chem. Phys.* **2003**, *5*, 720.

Alam, M. T.; Islam, M. M.; Okajima, T.; Ohsaka, T. *J. Phys. Chem. C* **2007**, *111*, 18326-18333.

Alam, M. T.; Islam, M. M.; Okajima, T.; Ohsaka, T. *J. Phys. Chem. C* **2008**, *112*, 2601-2606.

Alam, M. T.; Islam, Md. M.; Okajima, T.; Ohsaka, T. *J. Phys. Chem. C* **2008**, *112*, 16600-16608.

Aliaga, C.; Baldelli, S. *J. Phys. Chem. B* **2006**, *110*, 18481-18491.

Amsden, B. *Macromolecules* **1998**, *31*, 8382-8395.

Annable, T.; Buscall, R.; Ettelaie, R.; Whittlestone, D. *J. Rheol.* **1993**, *37*, 695-726.

Armand, M.; Endres, F.; MacFarlane, D. R.; Ohno, H.; Scrosati, B. *Nat. Mater.* **2009**, *8*, 621-629.

Baldelli, S. *J. Phys. Chem. B* **2005**, *109*, 13049-13051.

Balducci, A.; Henderson, W. A.; Mastragostino, M.; Passerini, S.; Simon, P.; Soavi, F. *Electrochim. Acta* **2005**, *50*, 2233-2237.

Bang, J.; Bae, J.; Lowenhielm, P.; Spiessberger, C.; Given-Beck, S. A.; Russell, T. P.; Hawker, C. J. *Adv. Mater.* **2007**, *19*, 4552-4557.

Bard, A. J.; Faulkner, L. R. *Electrochemical Methods: Fundamentals and Applications*, 2nd ed.; Wiley: New York, 2001.

Bazant, M. Z.; Storey, B. D.; Kornyshev, A. A. *Physical Rev. Lett.* **2011**, *106*, 046102/1-046102/4.

Boda, D.; Henderson, D.; Chan, K.-Y. *J. Chem. Phys.* **1999**, *110*, 5346-5350.

Bonhote, P.; Dias, A.-P.; Papageorgiou, N.; Kalyanasundaram, K.; Graetzel, M. *Inorg. Chem.* **1996**, *35*, 1168-1178.

Bou-Saleh, Z.; Shahryari, A.; Omanovic, S. *Thin Solid Films* **2007**, *515*, 4727-4737.

Brandrup, J.; Immergut, E. H.; Grulke, E. A. *Polymer Handbook*, 4th ed.; Wiley-Interscience: New York, 1999.

Brug, G. J.; Van den Eeden, A. L. G.; Sluyters-Rehbach, M.; Sluyters, J. H. *J. Electroanal. Chem.* **1984**, *176*, 275-295.

Buzzeo, M. C; Evans, R. G; Compton, R. G. *Chem. Phys. Chem.* **2004**, *5*, 1106-20.

Cavicchi, K. A.; Lodge, T. P. *Macromolecules* **2003**, *36*, 7158-7164.

Chapman, B. R.; Hamersky, M. W.; Milhaupt, J. M.; Kostelecky, C.; Lodge, T. P.; von Meerwall, E. D.; Smith, S. D. *Macromolecules* **1998**, *31*, 4562-4573.

Chen, F.; Qing, Q.; Xia, J.; Li, J.; Tao, N. *J. Am. Chem. Soc.* **2009**, *131*, 9908-9909.

Chen, H.; Choi, J.-H.; Salas-de la Cruz, D.; Winey, K. I.; Elabd, Y. A. *Macromolecules* **2009**, *42*, 4809-4816.

Cheung, I. W.; Chin, K. B.; Greene, E. R.; Smart, M. C.; Abbrent, S.; Greenbaum, S. G.; Prakash, G. K. S.; Surampudi, S. *Electrochim. Acta* **2003**, *48*, 2149-2154.

Cho, J. H.; Lee, J.; Xia, Y.; Kim, B.; He, Y.; Renn, M. J.; Lodge, T. P.; Frisbie, C. D. *Nat. Mater.* **2008**, *7*, 900-906.

Choi, S.-H.; Bates, F. S.; Lodge, T. P. *J. Phys. Chem. B* **2009**, *113*, 13840-13848.

Choi, S.-H.; Bates, F. S.; Lodge, T. P. *Macromolecules* **2011**, *44*, 3594-3604.

Choi, S.-H.; Lodge, T. P.; Bates, F. S. *Phys. Rev. Lett.* **2010**, *104*, 047802/1-047802/4.

Colby, R. H. *Rheol. Acta* **2010**, *49*, 425-442.

Conway, B. E. *Electrochemical Supercapacitors*; Kluwer Academic Pub.: Norwell, 1999.

Costa, R.; Pereira, C. M.; Silva, F. *Phys. Chem. Chem. Phys.* **2010**, *12*, 11125-11132.

Daniel, V. V. *Dielectric Relaxation*; Academic Press: London and New York, 1965.

De Levie, R. *Electrochim. Acta* **1965**, *10*, 113-130.

Devanathan, M. A. V.; Tilak, B. V. K. S. R. A. *Chem. Rev.* **1965**, *65*, 635-684.

Drockenmuller, E.; Li, L. Y. T.; Ryu, D. Y.; Harth, E.; Russell, T. P.; Kim, H.-C.; Hawker, C. J. *J. Polym. Sci., Part A: Polym. Chem.* **2005**, *43*, 1028-1037.

Drueschler, M.; Huber, B.; Passerini, S.; Roling, B. *J. Phys. Chem. C* **2010**, *114*, 3614-3617.

Dyson, P. J.; Geldbach, T. J. *Electrochem. Soc. Interface* **2007**, *16*, 50-53.

Fedorov, M. V.; Kornyshev, A. A. *Electrochim. Acta* **2008**, *53*, 6835-6840.

Feng, G.; Huang, J.; Sumpter, B. G.; Meunier, V.; Qiao, R. *Phys. Chem. Chem. Phys.* **2011**, *13*, 14723-14734.

Fenton, D. E.; Parker, J. M.; Wright, P. V. *Polymer* **1973**, *14*, 589-589.

Fetters, L. J.; Lohse, D. J.; Richter, D.; Witten, T. A.; Zirkel, A. *Macromolecules* **1994**, *27*, 4639-4647.

Frackowiak, E. *Phys. Chem. Chem. Phys.* **2007**, *9*, 1774-1785.

Fuller, J.; Carlin, R. T.; De Long, H. C.; Haworth, D. *J Chem. Soc. Chem.Commun.* **1994**, 299-300.

Gaikwad, A. N.; Wood, E. R.; Ngai, T.; Lodge, T. P. *Macromolecules* **2008**, *41*, 2502-2508.

Gale, R. J.; Gilbert, B.; Osteryoung, R. A. *Inorg. Chem.* **1978**, *17*, 2728-2729.

Gale, R. J.; Osteryoung, R. A. *Electrochim. Acta* **1980**, *25*, 1527-1529.

Galinski, M.; Lewandowski, A.; Stepniak, I. *Electrochim. Acta* **2006**, *51*, 5567-5580.

Gavelin, P.; Jannasch, P.; Wesslen, B. *J. Polym. Sci., Part A: Polym. Chem.* **2001**, *39*, 2223-2232.

Georgi, N.; Kornyshev, A. A.; Fedorov, M. V. *J. Electroanal. Chem.* **2010**, *649*, 261-267.

Gorlov, M.; Kloo, L. *Dalton Trans.* **2008**, 2655-2666.

Graessley, W. W. *Adv. Polym. Sci.* **1974**, *16*, 1-179.

Grahame, D. C. *Chem. Rev.* **1947**, *41*, 441-501.

Guilherme, L. A.; Borges, R. S.; Moraes, E. Mara S.; Silva, G. Goulart; Pimenta, M. A.; Marletta, A.; Silva, R. A. *Electrochim. Acta* **2007**, *53*, 1503-1511.

Ha, M.; Xia, Y.; Green, A. A.; Zhang, W.; Renn, M. J.; Kim, Ch. H.; Hersam, M. C.; Frisbie, C. D. *ACS Nano* **2010**, *4*, 4388-4395.

Hamley, I. W. *Phil. Trans. R. Soc. A* **2001**, *359*, 1017-1044.

Hanabusa, K.; Fukui, H.; Suzuki, M.; Shirai, H. Langmuir 2005, 21, 10383-10390.

He, Y.; Boswell, P. G.; Buhlmann, P.; Lodge, T. P. *J. Phys. Chem. B* **2007**, *111*, 4645-4652.

He, Y.; Lodge, T. P. *Chem. Commun.* **2007**, 2732-2734.

He, Y.; Lodge, T. P. *Macromolecules* **2008**, *41*, 167-174.

He, Y.; Lutz, T. R.; Ediger, M. D.; Ayyagari, C.; Bedrov, D.; Smith, G. D.

*Macromolecules* **2004**, *37*, 5032-5039.

Herlogsson, L.; Crispin, X.; Robinson, N. D.; Sandberg, M.; Hagel, O.-J.; Gustafsson, G.; Berggren, M. *Adv. Mater.* **2007**, *19*, 97-101.

Hermann, W.; *Angew. Chem.* **2008**, *47*, 654-670.

Hiemenz, P. C.; Lodge, T. P. *Polymer Chemistry*, 2nd ed.; CRC Press: New York, 2007.

Holovko, M.; Kapko, V.; Henderson, D.; Boda, D. *Chem. Phys. Lett.* **2001**, *341*, 363-368.

Huang, V. M.-W.; Vivier, V.; Frateur, I.; Orazem, M. E.; Tribollet, B. *J. Electrochem. Soc.* **2007**, *154*, C89-C98.

Hurley, F. H. US2446331, 1948.

Hussey, C. L. *Pure Appl. Chem.* **1988**, *60*, 1763-1772.

Ignat'ev, N. V.; Welz-Biermann, U.; Kucheryna, A.; Bissky, G.; Willner, H. *J. Fluorine Chem.* **2005**, *126*, 1150-1159.

Inomata, K.; Nakanishi, D.; Banno, A.; Nakanishi, E.; Abe, Y.; Kurihara, R.; Fujimoto, K.; Nose, T. *Polymer* **2003**, *44*, 5303-5310.

Ishikawa, M.; Sugimoto, T.; Kikuta, M.; Ishiko, E.; Kono, M. *J. Power Sources* **2006**, *162*, 658.

Izgorodina, E. I.; Forsyth, M.; MacFarlane, D. R. *Phys. Chem. Chem. Phys.* **2009**, *11*, 2452-2458.

Ding, J.; Zhou, D.; Spinks, G.; Wallace, G.; Forsyth, S.; Forsyth, M.; MacFarlane, D. *Chem. Mater.* **2003**, *15*, 2392.

Jackson, N. F. *Phys. Educ.* **1968**, *3*, 253-259.

Jana, S.; Parthiban, A.; Chai, C. L. L. *Chem. Commun.* **2010**, *46*, 1488-1490.

Jiang, D.; Meng, D.; Wu, J. *Chem. Phys. Lett.* **2011**, *504*, 153-158.

Kaskhedikar, N.; Burjanadze, M.; Karatas, Y.; Wiemhoefer, H.-D. *Solid State Ionics* **2006**, *177*, 3129-3134.

Katakabe, T.; Kaneko, T.; Watanabe, M.; Fukushima, T.; Aida, T. *J. Electrochem. Soc.* **2005**, *152*, A1913-A1916.

Kim, G. T.; Jeong, S. S.; Joost, M.; Rocca, E.; Winter, M.; Passerini, S.; Balducci, A. *J. Power Sources* **2011**, *196*, 2187-2194.

Kim, S. H.; Hong, K.; Xie, W.; Lee, K. H.; Zhang, S.; Lodge, T. P.; Frisbie, C. D. *Adv. Mater.*, accepted.

Kimizuka, N.; Nakashima, T. *Langmuir* **2001**, *17*, 6759-6761.

Klingshirn, M. A.; Spear, S. K.; Subramanian, R.; Holbrey, J. D.; Huddleston, J. G.; Rogers, Robin, D. *Chem. Mater.* **2004**, *16*, 3091-3097.

Kossuth, M. B.; Morse, D. C.; Bates, F. S. *J. Rheol.* **1999**, *43*, 167-196.

Krossing, I.; Slattery, J. M.; Daguenet, C.; Dyson, P. J.; Oleinikova, A.; Weingaertner, H. *J. Am. Chem. Soc.* **2006**, *128*, 13427-13434.

Lai, C.; Russel, W. B.; Register, R. A. *Macromolecules* **2002**, *35*, 841-849.

Lai, J. T.; Filla, D.; Shea, R. *Macromolecules* **2002**, *35*, 6754-6756.

Largeot, C.; Portet, C.; Chmiola, J.; Taberna, P.-L.; Gogotsi, Y.; Simon, P. *J. Am. Chem. Soc.* **2008**, *130*, 2730-2731.

Lauw, Y.; Horne, M. D.; Rodopoulos, T.; Nelson, A.; Leermakers, F. A. M. *J. Phys. Chem. B* **2010**, *114*, 11149-11154.

Lee, J.; Panzer, M. J.; He, Y.; Lodge, T. P.; Frisbie, C. D. *J. Am. Chem.*

*Soc.* **2007**, *129*, 4532-4533.

Lee, K. H.; Kang, M. Sung; Zhang, S.; Gu, Y.; Lodge, T. P.; Frisbie, C. D. *Adv. Mater.* **2012**, *24*, 4457-4462.

Lee, K. H.; Zhang, S.; Lodge, T. P.; Frisbie, C. D. *J. Phys. Chem. B* **2011**, *115*, 3315-3321.

Lee, S. W.; Lee, H. J.; Choi, J. H.; Koh, W. G.; Myoung, J. M.; Hur, J. H.; Park, J. J.; Cho, J. H.; Jeong, U. *Nano Lett.* **2010**, *10*, 347-351.

Lee, S.; Lee, B.; Kim, B. J.; Park, J.; Yoo, M.; Bae, W. Ki; Char, K.; Hawker, C. J.; Bang, J.; Cho, J. *J. Am. Chem. Soc.* **2009**, *131*, 2579-2587.

Levie, R. D. *Electrochim. Acta* **1965**, *10*, 113-130.

Lewandowski, A.; Galinski, M. *J. Phys. Chem. Solids* **2004**, *65*, 281-286.

Lewandowski, A.; Swiderska-Mocek, A. *J. Power Sources* **2009**, *194*, 601-609.

Liu, X.; Osaka, T. *J. Electrochem. Soc.* **1996**, *143*, 3982-3986.

Lockett, V.; Horne, M.; Sedev, R.; Rodopoulos, T.; Ralston, J. *Phys. Chem. Chem. Phys.* **2010**, *12*, 12499-12512.

Lockett, V.; Sedev, R.; Ralston, J.; Horne, M.; Rodopoulos, T. *J. Phys. Chem. C* **2008**, *112*, 7486-7495.

Lodge, T. P. *Science* **2008**, *321*, 50-51.

Loth, M. S.; Skinner, Brian; Shklovskii, B. I. *Phys. Rev. E* **2010**, *82*, 056102/1-056102/7.

Lu, J.; Yan, F.; Texter, J. *Prog. Polym. Sci.* **2009**, *34*, 431-448.

Lu, W.; Fadeev, A. G.; Qi, B.; Smela, E.; Mattes, B. R.; Ding, J.; Spinks, G. M.; Mazurkiewicz, J.; Zhou, D.; Wallace, G. G.; MacFarlane, D. R.; Forsyth, S. A.; Forsyth,

M. *Science* **2002**, *297*, 983-987.

Lu, W.; Henry, K.; Turchi, C.; Pellegrino, J. *J. Electrochem. Soc.* **2008**, *155*, A361-A367.

MacFarlane, D. R.; Forsyth, M.; Howlett, P. C.; Pringle, J. M.; Sun, J.; Annat, G.; Neil, W.; Izgorodina, E. I. *Acc. Chem. Res.* **2007**, *40*, 1165-1173.

MacFarlane, D. R.; Forsyth, M.; Howlett, P. C.; Pringle, J. M.; Sun, J.; Annat, G.; Neil, W.; Izgorodina, E. I. *Acc. Chem. Res.* **2007**, *40*, 1165-1173.

Mackie, J. S.; Meares, P. *Proc. R. Soc. London* **1955**, *A232*, 498-509.

Matsumoto, K.; Endo, T. *Macromolecules* **2008**, *41*, 6981-6986.

Matsumoto, K.; Endo, T. *Macromolecules* **2009**, *42*, 4580-4584.

Matsumoto, K.; Hagiwara, R.; Ito, Y. *Electrochem. Solid-State Lett.* **2004**, *7*, E41-E44.

Matyjaszewski, K.; Xia, J. *Chem. Rev.* **2001**, *101*, 2921-2990.

McConnell, G. A.; Gast, A. P.; Huang, J. S.; Smith, S. D. *Phys. Rev. Lett.* **1993**, *71*, 2102-2105.

McEwen, Alan B.; Ngo, Elen L.; LeCompte, Karen; Goldman, Jay L. *J. Electrochem. Soc.* **1999**, *146*, 1687-1695.

Mecerreyes, D. *Prog. Polym. Sci.* **2011**, *36*, 1629-1648.

Meyer, W. H. *Adv. Mater.* **1998**, *10*, 439-448.

Min, Y.; Akbulut, M.; Sangoro, J. R.; Kremer, F.; Prud'homme, R. K.; Israelachvili, J. *J. Phys. Chem. C* **2009**, *113*, 16445-16449.

Moad, G.; Mayadunne, R. T. A.; Rizzardo, E.; Skidmore, M.; Thang, S. H. *Macromol. Symp.* **2003**, *192*, 1-12.

Mohmeyer, N.; Kuang, D.; Wang, P.; Schmidt, H.-W.; Zakeeruddin, S. M.; Graetzel, M.

*J. Mater. Chem.* **2006**, *16*, 2978-2983.

Mok, M. M.; Kim, J.; Wong, C. L. H.; Marrou, S. R.; Woo, D. J.; Dettmer, C. M.; Nguyen, S. T.; Ellison, C. J.; Shull, K. R.; Torkelson, J. M. *Macromolecules* **2009**, *42*, 7863-7876.

Mok, M. M.; Liu, X.; Bai, Z.; Lei, Y.; Lodge, T. P. *Macromolecules* **2011**, *44*, 1016-1025.

Nanjundiah, C.; McDevitt, S. F.; Koch, V. R. *J. Electrochem. Soc.* **1997**, *144*, 3392-3397.

Neouze, M.-A.; Le Bideau, J.; Gaveau, P.; Bellayer, S.; Vioux, A. *Chem. Mater.* **2006**, *18*, 3931-3936.

Noda, A.; Hayamizu, K.; Watanabe, M. *J. Phys. Chem. B* **2001**, *105*, 4603-4610.

Noro, A.; Matsushita, Y.; Lodge, T. P. *Macromolecules* **2008**, *41*, 5839-5844.

Ohno, H. *Electrochemical Aspects of Ionic Liquids*; John Wiley & Sons, Inc., 2005.

Ono, S.; Seki, S.; Hirahara, R.; Tominari, Y.; Takeya, J. *Appl. Phys. Lett.* **2008**, *92*, 103313/1-103313/3.

Opekar, F.; Stulik, K. *Anal. Chim. Acta* **1999**, *385*, 151-162.

Pajkossy, T. *J. Electroanal. Chem.* **1994**, *364*, 111-125.

Pajkossy, T. *Solid State Ionics* **2005**, *176*, 1997-2003.

Pandey, S. *Anal. Chim. Acta* **2006**, *556*, 38-45.

Panzer, M. J.; Newman, C. R.; Frisbie, C. D. *Appl. Phys. Lett.* **2005**, *86*, 103503/1-103503/3.

Papageorgiou, N.; Athanassov, Y.; Armand, M.; Bonhote, P.; Pettersson, H.; Azam, A.; Grätzel, M. *J. Electrochem. Soc.* **1996**, *143*, 3099-3108.

Parashkov, R.; Becker, E.; Ginev, G.; Riedl, T.; Johannes, H.-H.; Kowalsky, W. *J. Appl.*

*Phys.* **2004**, *95*, 1594-1596.

Patten, T. E.; Xia, J.; Abernathy, T.; Matyjaszewski, K. *Science* **1996**, *272*, 866-868.

Phillips, D. M.; Drummy, L. F.; Conrady, D. G.; Fox, D. M.; Naik, R. R.; Stone, M. O.; Trulove, P. C.; De Long, H. C.; Mantz, R. A. *J. Am. Chem. Soc.* **2004**, *126*, 14350-14351.

Plazek, D. J.; O'Rourke, V. M. *J. Polym. Sci., Polym. Phys. Ed.* **1971**, *9*, 209-243.

Randstroem, S.; Appetecchi, G. B.; Lagergren, C.; Moreno, A.; Passerini, S. *Electrochim. Acta* **2007**, *53*, 1837-1842.

Renou, F.; Nicolai, T.; Benyahia, L.; Nicol, E. *J. Phys. Chem. B* **2009**, *113*, 3000-3007.

Roth, C. B.; Dutcher, J. R. *J. Electroanal. Chem.* **2005**, *584*, 13-22.

Rudge, A., Raistrick, I., Gottesfeld, S. & Ferraris, J. P. *J. Power Sources* **1994**, *47*, 89-107.

Sandi, G.; Carrado, K. A.; Joachin, H.; Lu, W.; Prakash, J. *J. Power Sources* **2003**, *119-121*, 492-496.

Sangoro, J. R.; Iacob, C.; Naumov, S.; Valiullin, R.; Rexhausen, H.; Hunger, J.; Buchner, R.; Strehmel, V.; Kaerger, J.; Kremer, F. *Soft Matter* **2011**, *7*, 1678-1681.

Sangoro, J. R.; Iacob, C.; Serghei, A.; Friedrich, C.; Kremer, F. *Phys. Chem. Chem. Phys.* **2009**, *11*, 913-916.

Sangoro, J. R.; Serghei, A.; Naumov, S.; Galvosas, P.; Karger, J.; Wespe, C.; Bordusa, F.; Kremer, F. *Phys. Rev. E* **2008**, *77*, 051202.

Sangoro, J.; Iacob, C.; Serghei, A.; Naumov, S.; Galvosas, P.; Karger, J.; Wespe, C.; Bordusa, F.; Stoppa, A.; Hunger, J.; Buchner, R.; Kremer, F. *J. Chem. Phys.* **2008**, *128*, 214509/1-214509/5.

Sarjeant, W. J.; Zirnheld, J.; MacDougall, F. W. *IEEE Trans. Plasma Sci.* **1998**, *26*, 1368-

1392.

Sato, T.; Masuda, G.; Takagi, K. *Electrochim. Acta* **2004**, *49*, 3603-3611.

Sato, T.; Watanabe, H.; Osaki, K. *Macromolecules* **2000**, *33*, 1686-1691.

Savin, D. A.; Larson, A. M.; Lodge, T. P. *J. Polym. Sci., Part B: Polym. Phys.* **2004**, *42*, 1155-1163.

Schroder, U.; Wadhawan, J. D.; Compton, R. G.; Marken, F.; Suarez, P. A. Z.; Consorti, C. S.; de Souza, R. F.; Dupont, J. *New J. Chem.* **2000**, *24*, 1009-1015.

Scrosati, B.; Croce, F. *Polym. Adv. Technol.* **1993**, *4*, 198-204.

Sebastian, J. M.; Lai, C.; Graessley, W. W.; Register, R. A. *Macromolecules* **2002**, *35*, 2707-2713.

Seddon, K. R.; Stark, A.; Torres, M.-J. *Pure Appl. Chem.* **2000**, *72*, 2275-2287.

Seitz, M. E.; Burghardt, W. R.; Faber, K. T.; Shull, K. R. *Macromolecules* **2007**, *40*, 1218-1226.

Shipp, D. A.; Wang, J.-L.; Matyjaszewski, K. *Macromolecules* **1998**, *31*, 8005-8008.

Si, X.; Li, S.; Wang, Y.; Ye, S.; Yan, T. *Chem. Phys. Chem.* **2012**, *13*, 1671-1676.

Silva, F.; Gomes, C.; Figueiredo, M.; Costa, R.; Martins, A.; Pereira, C. M. *J. Electroanal. Chem.* **2008**, *622*, 153-160.

Simon, P.; Gogotsi,Y. *Nat. Mater.* **2008**, *7*, 845-854.

Singh, K. P.; Gupta, P. N. *Eur. Polym. J.* **1998**, *34*, 1023-1029.

Skinner, B.; Loth, M. S.; Shklovskii, B. I. *Phys. Rev. Lett.* **2010**, *104*, 128302/1-128302/4.

Smitha, B.; Sridhar, S.; Khan, A. A. *J. Membr. Sci.* **2005**, *259*, 10-26.

Susan, M. A. B. H.; Kaneko, T.; Noda, A.; Watanabe, M. *J. Am. Chem. Soc.* **2005**, *127*,

4976-4983.

Tae, G.; Kornfield, J. A.; Hubbell, J. A.; Lal, J. *Macromolecules* **2002**, *35*, 4448-4457.

Tanaka, F.; Edwards, S. F. *Macromolecules* **1992**, *25*, 1516-1523.

Tao, H.; Huang, C.; Lodge, T. P. *Macromolecules* **1999**, *32*, 1212-1217.

Tokuda, H.; Ishii, K.; Susan, M. A. B. H.; Watanabe, M. *J. Phys. Chem. B* **2005**, *109*, 6103-6110.

Tokuda, H.; Tsuzuki, S.; Susan, M. A. B. H.; Hayamizu, K.; Watanabe, M. *J. Phys. Chem. B* **2006**, *110*, 19593-19600.

Ue, M.; Takeda, M.; Toriumi, A.; Kominato, A.; Hagiwara, R.; Ito, Y. *J Electrochem. Soc.* **2003**, *150*, A499-A502.

Ueki, T.; Watanabe, M. *Macromolecules* **2008**, *41*, 3739-3749.

Ueno, K.; Hata, K.; Katakabe, T.; Kondoh, M.; Watanabe, M. *J. Phys. Chem. B* **2008**, *112*, 9013-9019.

Ukshe, E. A.; Bukun, N. G.; Leikis, D. I.; Frumkin, A. N. *Electrochim. Acta* **1964**, *9*, 431-439.

Uno, T.; Kawaguchi, S.; Kubo, M.; Itoh, T. *J. Power Sources* **2008**, *178*, 716-722.

Vatamanu, J.; Cao, L.-L.; Borodin, O.; Bedrov, D.; Smith, G. D. *J. Phys. Chem. Lett.* **2011**, *2*, 2267-2272.

Vega, D. A.; Sebastian, J. M.; Loo, Y.-L.; Register, R. A. *J. Polym. Sci., Part B: Polym. Phys.* **2001**, *39*, 2183-2197.

Vijayakrishna, K.; Jewrajka, S. K.; Ruiz, A.; Marcilla, R.; Pomposo, J. A.; Mecerreyes, D.; Taton, D.; Gnanou, Y. *Macromolecules* **2008**, *41*, 6299-6308.

Walden, P. *Bull. Sci. Acad. Imp. Sci. St. Petersb.* **1914**, 405-422.

Wasserscheid, P.; Welton, T. *Ionic Liquids in Synthesis*, 2nd ed.; Wiley-VCH, 2008.

Wei, D.; Scherer, M. R. J.; Bower, C.; Andrew, P.; Ryhanen, T.; Steiner, U. *Nano Lett.* **2012**, *12*, 1857-1862.

Weihs, T. P.; Hong, S.; Bravman, J. C.; Nix, W. D. *J. Mater. Res.* **1988**, *3*, 931.

Welton, T.; *Chem. Rev.* **1999**, *99*, 2071-2083.

Weston, J. E.; Steele, B. C. H. *Solid State Ionics* **1982**, *7*, 75-79.

Wier, T. P., Jr. US2446350, 1948.

Wier, T. P., Jr.; Hurley, F. H. US2446349, 1948.

Wilkes, J. S. *Green Chem.* **2002**, *4*, 73-80.

Wilkes, J. S.; Zaworotko, M. J. *J Chem. Soc.,Chem.Commun.* **1992**, 965-967.

Winterton, N. *J. Mater. Chem.* **2006**, *16*, 4281-4293.

Xia, J.; Matyjaszewski, K. *Macromolecules* **1997**, *30*, 7697-7700.

Xie, H.; Zhang, S.; Li, S. *Green Chem.* **2006**, *8*, 630-633.

Yan, H.; Chen, Z.; Zheng, Y.; Newman, C.; Quinn, J. R.; Dotz, F.; Kastler, M.; Facchetti, A. *Nature* **2009**, *457*, 679-686.

Ye, J. T.; Inoue, S.; Kobayashi, K.; Kasahara, Y.; Yuan, H. T.; Shimotani, H.; Iwasa, Y. *Nat. Mater.* **2010**, *9*, 125-128.

Yokoyama, H.; Kramer, E. J. *Macromolecules* **1998**, *31*, 7871-7876.

Yoo, M.; Kim, S.; Lim, J.; Kramer, E. J.; Hawker, C. J.; Kim, B. J.; Bang, J. *Macromolecules* **2010**, *43*, 3570-3575.

Yuan, H.; Shimotani, H.; Tsukazaki, A.; Ohtomo, A.; Kawasaki, M.; Iwasa, Y. *Adv. Funct.*

*Mater.* **2009**, *19*, 1046-1053.

Zakeeruddin, S. M.; Graetzel, M. *Adv. Funct. Mater.* **2009**, *19*, 2187-2202.

Zeroni, I.; Ozair, S.; Lodge, T. P. *Macromolecules* **2008**, *41*, 5033-5041.

Zhou, D.; Spinks, G. M.; Wallace, G. G.; Tiyapiboonchaiya, C.; MacFarlane, D. R.; Forsyth, M.; Sun, J. *Electrochim. Acta* **2003**, *48*, 2355-2359.

Zistler, M.; Wachter, P.; Schreiner, C.; Fleischmann, M.; Gerhard, D.; Wasserscheid, P.; Hinsch, A.; Gores, H. J. *J. Electrochem. Soc.* **2007**, *154*, B925-B930.

# Appendix A

## Glass Transition and Ionic Conductivity of Ionic Liquid Mixtures

From a materials point of view, since the major component that provides desirable electrical properties is the ionic liquid, it would be beneficial to utilize ionic liquids with higher conductivities than [EMI][TFSA], while satisfying the criteria of wide electrochemical window and high specific capacitance. Attempts to explore ionic liquid mixtures in the hope of obtaining ionic conductivity higher than the pure components are described herein. Glass transitions and ionic conductivity were measured for the combination of 1-ethyl-3-methylimidazolium bis(trifluoromethylsulfonyl)amide ([EMI][TFSA]) and five other ionic liquids over the whole composition range. Unfortunately, no single mixture exhibited higher conductivity than the more conductive component.

[EMI][TFSA] was synthesized as described in Chapter 2. All other ionic liquids were used as received without further purification. For [EMI] tetracyanoborate ([TCB]), 1-butyl-1-methylpyrrolidinium ([BMPL]) [TFSA], and *N*-butylpyridinium ([BP]) [TFSA], mixtures were prepared by mixing weighed amounts of the respective components followed by vigorous stirring overnight. None of the mixtures showed macrophase separation. For [EMI][Br] and [EMI][I], mixtures were prepared by mixing weighed amounts of the components in $CH_2Cl_2$. After vigorous stirring for ca. 2 hours, the cosolvent was evaporated by purging with $N_2$ gas overnight. All mixtures were further dried in a vacuum oven at 70 °C for 2 days.

Thermal transitions were measured using a TA Instruments Q1000 Differential Scanning Calorimeter (DSC) with liquid $N_2$ cooling capability. Samples weighing ca. 5 – 10 mg were sealed in hermetic aluminum pans, heated up to 120 °C, and equilibrated for 3 min to remove prior thermal history. They were then cooled rapidly to –150 °C, and heated back up to 120 °C at 10 °C/min. Thermograms shown are second heating traces.

Impedance measurements were performed with a homemade cell using a Solartron 1255B frequency response analyzer connected to a Solartron SI 1287 electrochemical interface. Frequency sweeps were conducted from 1 – $10^6$ Hz with an AC amplitude of 10 mV. The cell is composed of a Teflon spacer with an inner diameter of 4 mm and a thickness of 2 mm sandwiched between two platinum coated stainless steel electrodes. All measurements were performed at room temperature. Ionic conductivity was determined from the high frequency plateau of the real part of complex conductivity.

Figures A.1 through A.5 show heat flow and derivative heat flow curves for the 5 mixtures. The steps and peaks in heat flow and derivative heat flow curves indicate the glass transition, respectively. Figure A.6 summarizes the glass transition temperature ($T_g$) of the mixtures. Figure A.7 displays the ionic conductivity ($\sigma$) of the mixtures. Clearly, both $T_g$ and $\sigma$ are monotonic versus composition. The exceptions are the mixtures with [EMI][I] and [EMI][Br], where the $T_g$ increases and drops with [EMI][TFSA] concentration. This might be due to crystallization. The only report that could be found on conductivity for a eutectic mixture of two ionic liquids is shown in Figure A.8.[1] Unfortunately, the conductivity of the eutectic mixture is still lower than the more conducting pure component.

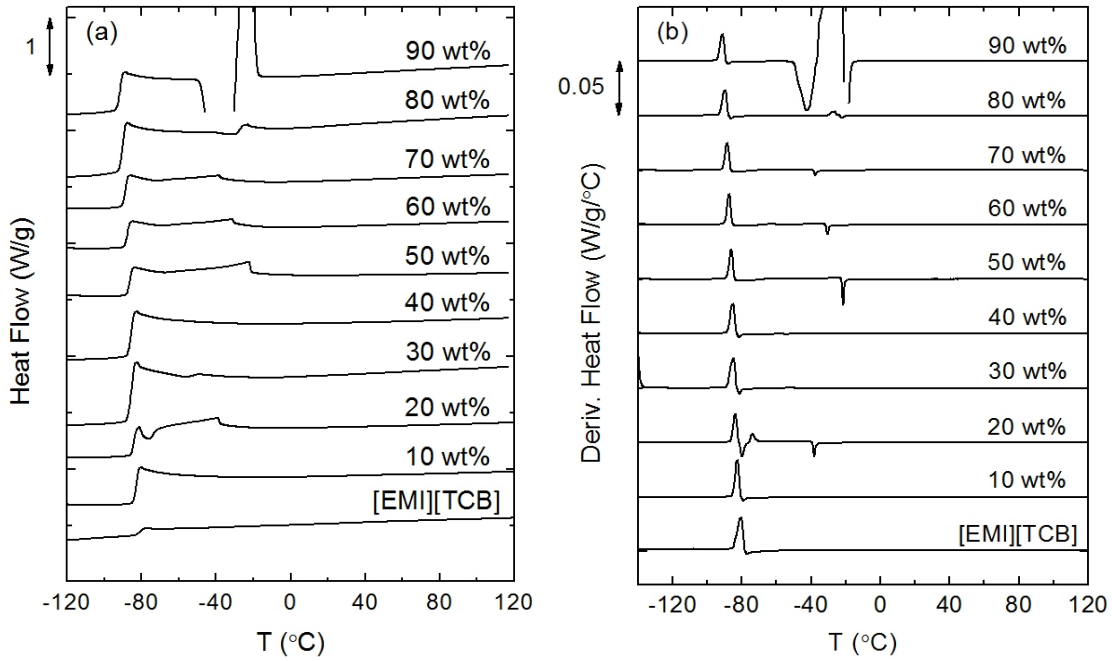


**Figure A.1** DSC (a) heat flow and (b) derivative heat flow curves of [EMI][TFSA]/[EMI][TCB] mixtures. Percentages are [EMI][TFSA] weight fractions. Data at different concentrations were shifted vertically for clarity.

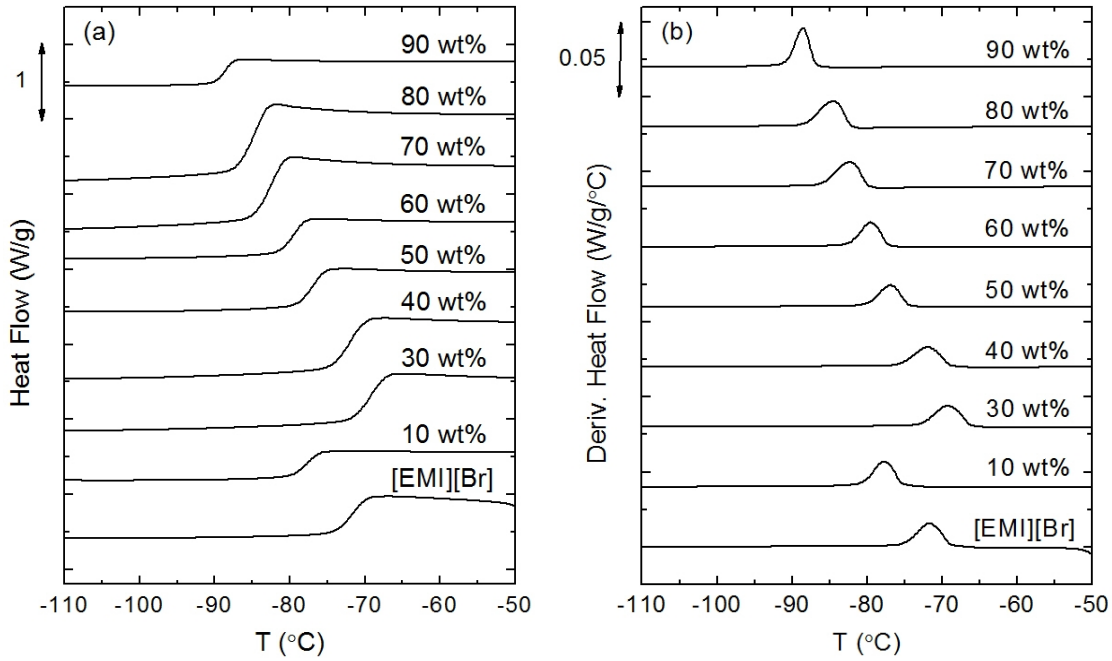


**Figure A.2** DSC (a) heat flow and (b) derivative heat flow curves of [EMI][TFSA]/[EMI][Br] mixtures. Percentages are [EMI][TFSA] weight fractions. Data at different concentrations were shifted vertically for clarity.

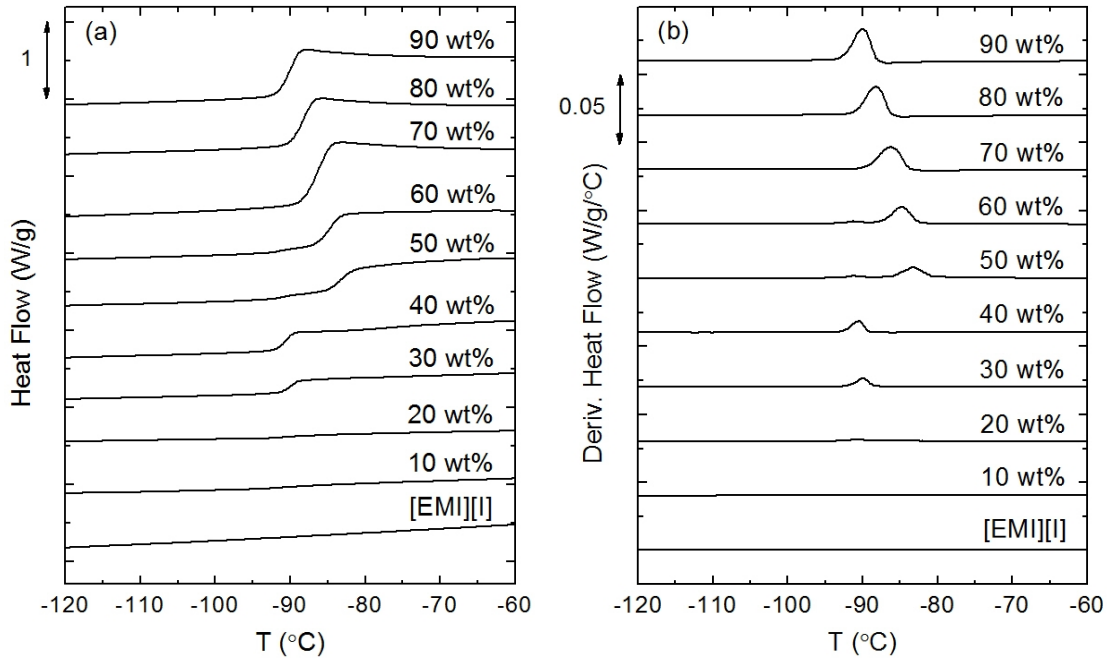


**Figure A.3** DSC (a) heat flow and (b) derivative heat flow curves of [EMI][TFSA]/[EMI][I] mixtures. Percentages are [EMI][TFSA] weight fractions. Data at different concentrations were shifted vertically for clarity.

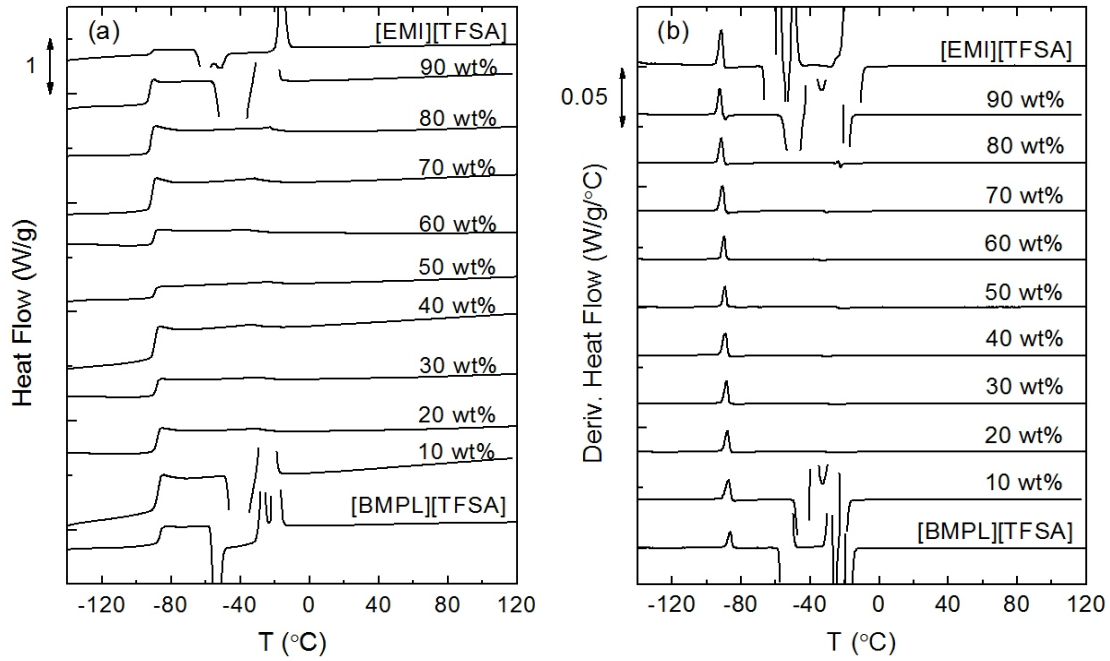


**Figure A.4** DSC (a) heat flow and (b) derivative heat flow curves of [EMI][TFSA]/[BMPL][TFSA] mixtures. Percentages are [EMI][TFSA] weight fractions. Data at different concentrations were shifted vertically for clarity.

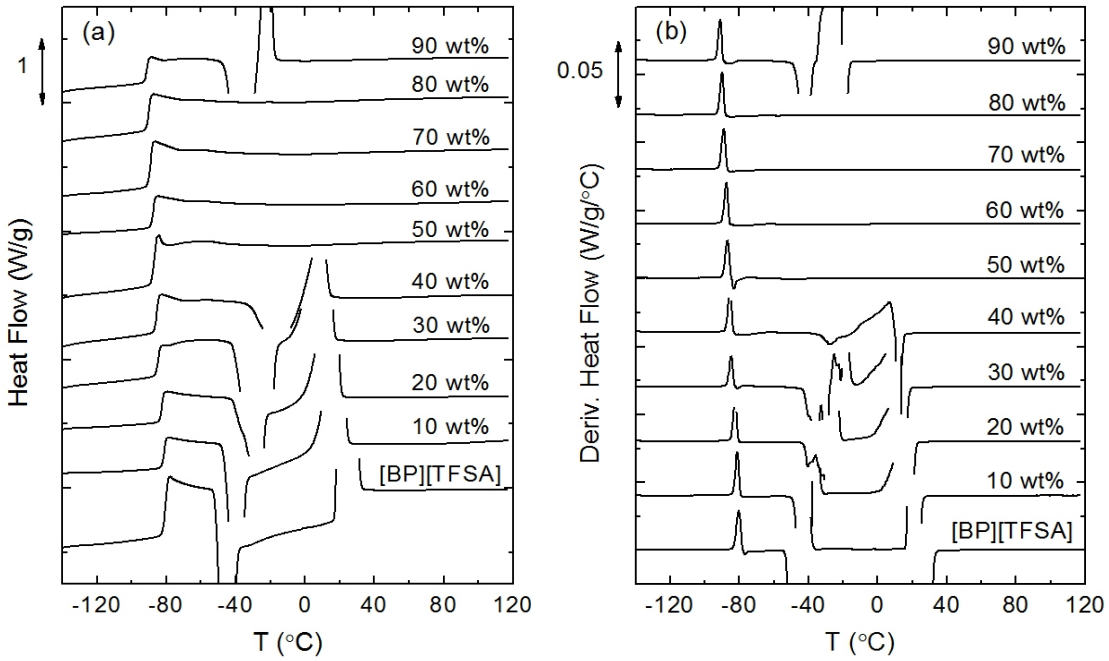


**Figure A.5** DSC (a) heat flow and (b) derivative heat flow curves of [EMI][TFSA]/[BP][TFSA] mixtures. Percentages are [EMI][TFSA] weight fractions. Data at different concentrations were shifted vertically for clarity.

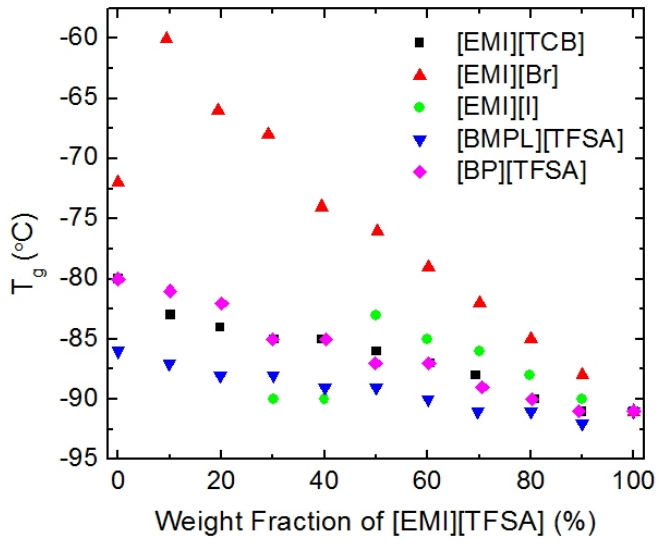


**Figure A.6** $T_g$ of ionic liquid mixtures versus [EMI][TFSA] concentration.

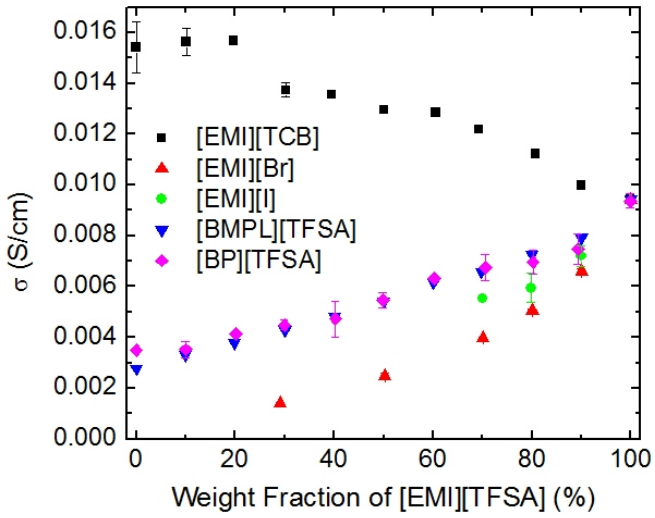


**Figure A.7** Conductivity of ionic liquid mixtures versus [EMI][TFSA] concentration at room temperature. Error bars are based on 3 to 5 samples. Compositions not shown indicate a melting temperature above 25 °C.

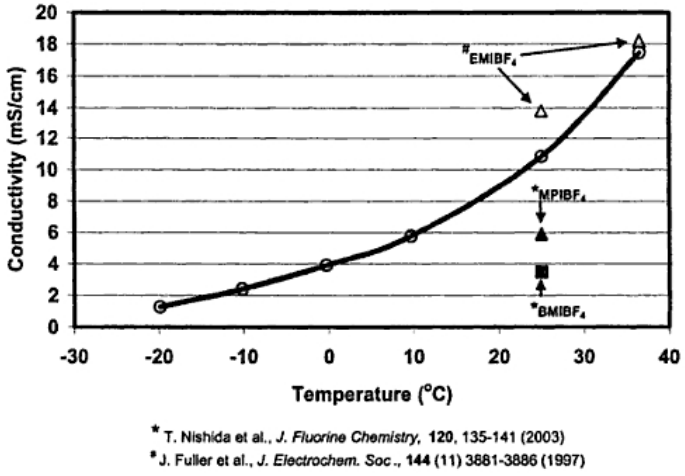


**Figure A.8** Temperature dependence of ionic conductivity for an equimolar eutectic mixture ($T_m$ = −16 °C) of [EMI][$BF_4$] ($T_m$ = 48 °C)/1-ethyl-2-methylpyrazolium ([EMP]) [$BF_4$] ($T_m$ = 13 °C).[1] As can be seen from the plot, the conductivity of the mixture is still lower than [EMI][$BF_4$] at room temperature.

**Reference**

(1) Dunstan, T. D. J.; Caja, J.; Katovic, V. *Proc. Electrochem. Soc.* **2006**, *2004-24*, 312-325.

# Appendix B

# Electrochemical Capacitors based on an Ionic Liquid/Ion Gel

Initial efforts to fabricate high capacitance electrochemical capacitors (ECs) based on an ionic liquid and an ion gel formed with a commercial copolymer are described here.

The ionic liquid 1-ethyl-3-methylimidazolium bis(trifluoromethylsulfonyl)amide ([EMI][TFSA]) was synthesized as described in Chapter 2. Poly(vinylidene fluoride-*co*-hexafluoropropylene) (P(VDF-HFP), $M_n$ = 130 kg/mol and $M_w$ = 400 kg/mol, Aldrich) was used as received.

The porous carbon electrode was purchased from Y-Carbon (average thickness = 0.26 mm) and used as received. The volume fraction of the pores was measured by filling with [EMI][TFSA]. After soaking a piece of pre-weighed electrode in the ionic liquid at ambient conditions or in a vacuum oven at 70 °C for a day, the electrode was taken out of the ionic liquid, and weighed again after the ionic liquid on the surface was blotted away. Assuming the pores are completely filled with the ionic liquid, the volume fraction of pores can be calculated from the weight difference and the densities of the electrode (0.7 g/cm$^3$ as specified by manufacturer) and [EMI][TFSA] (1.52 g/cm$^3$).[1] The average values obtained for immersing at ambient conditions and under vacuum at 70 °C are both 36% (based on 14 and 6 electrodes, respectively), suggesting that immersing at ambient conditions is sufficient to fill the pores.

The pore characteristics of the electrodes were also measured using nitrogen sorption. The carbon material was put in a 6 mm diameter glass stem, degassed for 24 hours, and

the measurement was carried out at 77 K on an Autosorb $IQ_2$ Sorption Instrument. Figure B.1 displays the nitrogen sorption isotherm and pore size distribution calculated by the Barret-Joymer-Halenda (BJH) method.[2] It can be seen that the majority of pores have a radius below 2 nm. The BET specific area calculated from the adsorption curve in the low range of relative pressure (below 0.35 $p/p_0$) is 1013 $m^2/g$.

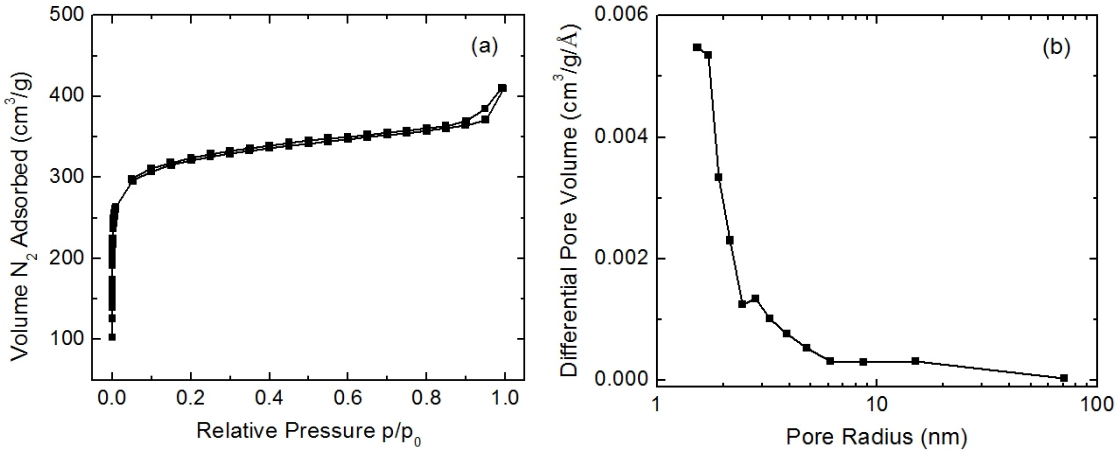


**Figure B.1** (a) Nitrogen sorption isotherm of the nanoporous carbon electrode. (b) Resultant pore size distribution calculated from the desorption isotherm by the BJH method.

The separator material used was either a PVDF membrane (Millipore, average thickness = 0.1 mm, pore diameter = 0.45 μm, porosity = 75%) filled with [EMI][TFSA] or a P(VDF-HFP) gel with 20 wt% polymer. The PVDF membrane was filled by dipping in the ionic liquid for ca. 5 min. Because the refractive indices of the two materials are almost the same (1.42 for PVDF as specified by manufacturer and 1.42 for [EMI][TFSA] at 30 °C and a wavelength of 589.3 nm),[3] the white membrane turns transparent the instant it gets in contact with [EMI][TFSA]. The P(VDF-HFP) gel was prepared by mixing weighed amounts of the components in $CH_2Cl_2$. After stirring vigorously for 2

hours, the solution was cast onto a glass petri-dish. Most of the cosolvent was removed by purging with $N_2$ gas overnight. The gel was further dried in a vacuum oven at 70 °C for a day.

The devices were fabricated by pressing together five layers consisting of bottom current collector (aluminum foil coated with 3 nm gold, fabricated by Bryan Paulsen), bottom electrode (filled with ionic liquid), separator, top electrode (same with the bottom), and top current collector (same with the other one). Figure B.2 shows a cross-sectional schematic of a typical device. All layers except the separator with PVDF support were shaped with a punch with a diameter of 1.43 cm. The PVDF separator was cut into a 1.6 by 1.6 cm square to prevent contact of the electrodes. The thickness of the P(VDF-HFP) separator was 0.3 mm. It was made thick also to prevent contact of the electrodes. Bottom contact was made by applying silver paint onto a glass slide and putting the device on top. Top contact was made by connecting a silver wire to the top electrode and the glass slide with Ag paint. Capacitance was measured by a Keithley 2612 unit in a Lakeshore vacuum probe station under $10^{-6}$ Torr at room temperature.

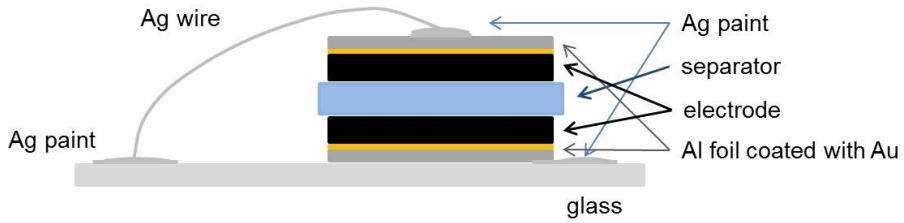


**Figure B.2** Cross-sectional schematic of a typical electrochemical capacitor based on [EMI][TFSA]/PVDF separator (not drawn to scale).

Figures B.3 and B.4 show the current-voltage (*I-V*) characteristics of the capacitors and computed capacitance of the electrodes based on [EMI][TFSA] with PVDF support

and the P(VDF-HFP) ion gel. The capacitance is calculated using

$$C = \frac{2I}{m(dV/dt)} \tag{B.1}$$

where $I$ is current, $m$ is the mass of a single electrode, and d$V$/d$t$ is sweep rate. Nice capacitive behavior is observed with the slower sweep rates of 2 and 5 mV/s. At higher sweep rates, the shape of the $C$-$V$ curves becomes distorted. This has been observed for ionic liquid-based ECs, and can be attributed to slow mass transport processes of ions at/inside the porous electrodes.[4,5] The capacitance of the electrodes for both devices exceeds 100 F/g, which is very reasonable compared with other reported values based on activated carbon devices with ionic liquid electrolytes.[4–7]

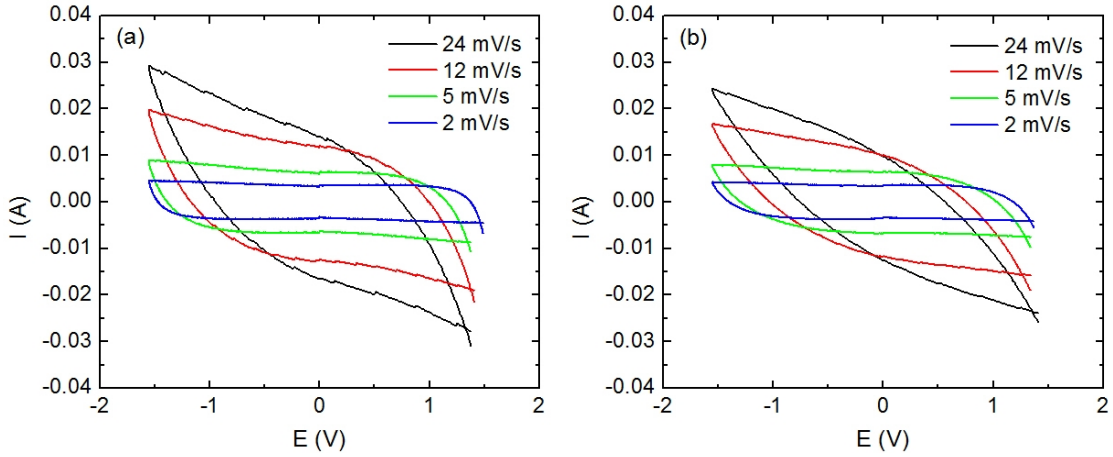


**Figure B.3** *I*-*V* characteristics of ECs based on (a) [EMI][TFSA] with PVDF support and (b) PVDF-HFP/[EMI][TFSA] with 20 wt% polymer.

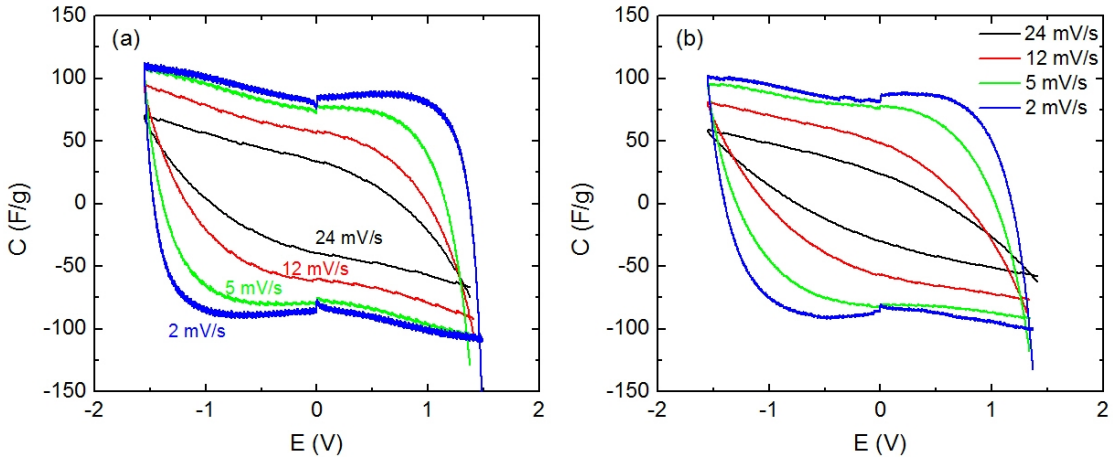


**Figure B.4** *C-V* characteristics of the electrodes for ECs based on (a) [EMI][TFSA] with PVDF support and (b) PVDF-HFP/[EMI][TFSA] with 20 wt% polymer.

## References

(1) Wasserscheid, P.; Welton, T. *Ionic Liquids in Synthesis*, 2nd ed.; Wiley-VCH, 2008.

(2) Barrett, E. P.; Joyner, L. G.; Halenda, P. P. *J. Am. Chem. Soc.* **1951**, *73*, 373-380.

(3) Froeba, A. P.; Kremer, H.; Leipertz, A. *J. Phys. Chem. B* **2008**, *112*, 12420-12430.

(4) Kurig, H.; Vestli, M.; Janes, A.; Lust, E. *Electrochem. Solid-State Lett.* **2011**, *14*, A120-A122.

(5) Kurig, H.; Janes, A.; Lust, E. *J. Electrochem. Soc.* **2010**, *157*, A272-A279.

(6) Lu, W.; Qu, L.; Henry, K.; Dai, L. *J. Power Sources* **2009**, *189*, 1270-1277.

(7) Largeot, C.; Portet, C.; Chmiola, J.; Taberna, P.-L.; Gogotsi, Y.; Simon, P. *J. Am. Chem. Soc.* **2008**, *130*, 2730-2731.